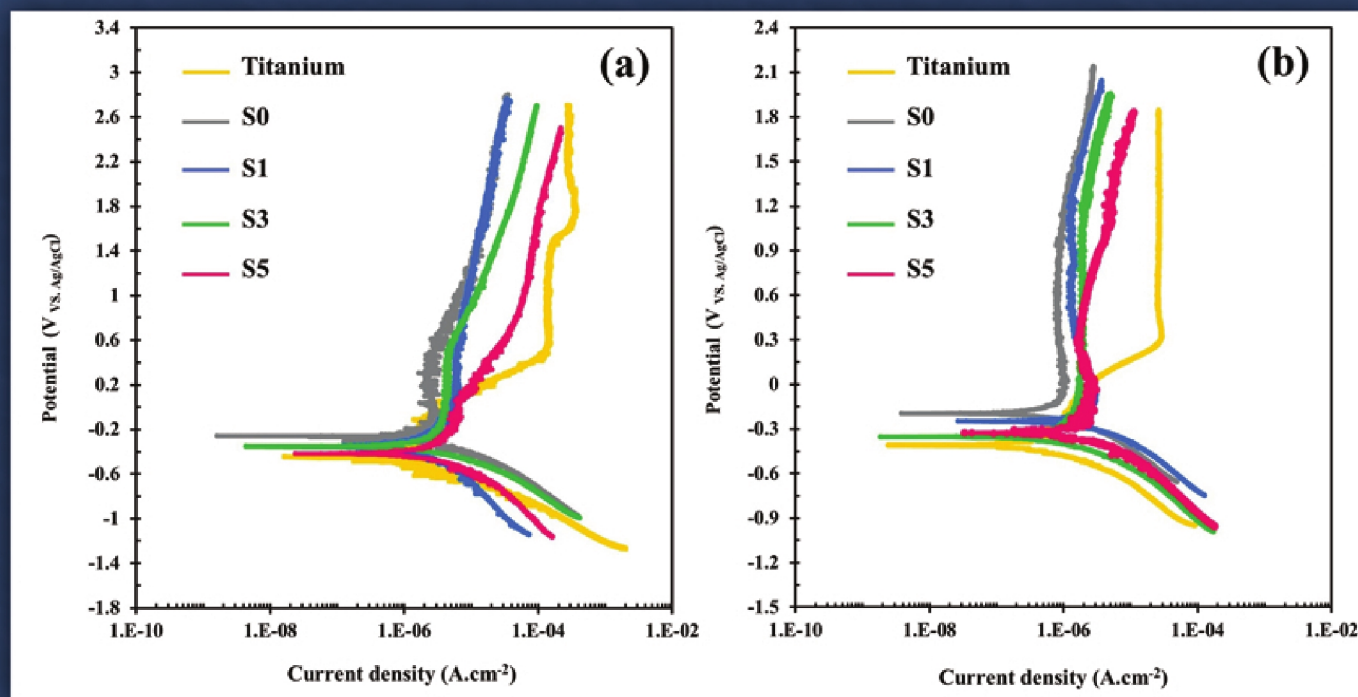


Advanced Ceramics Progress



Materials and Energy
Research Center



Iranian Ceramic Society

In The name of God

Advanced Ceramics Progress

DIRECTOR-IN-CHARGE

H. Omidvar

EDITOR-IN-CHIEF

M. R. Rahimipour

EXECUTIVE MANAGER

M. Razavi

EDITORIAL BOARD

- | | |
|---|--|
| A. R. Aghaei, Materials and Energy Research Center | H. Omidvar, Amirkabir University of Technology |
| P. Alizadeh, Tarbiat Modares University | M. R. Rahimipour, Materials and Energy Research Center |
| T. Ebadzadeh, Materials and Energy Research Center | M. Razavi, Materials and Energy Research Center |
| M. A. Faghihi Sani, Sharif University of Technology | E. Salahi, Materials and Energy Research Center |
| M. Ghassemi Kakroudi, University of Tabriz | M. Salehi, Isfahan University of Technology |
| A. R. Khavandi, Iran University of Science and Technology | Ş. Țălu, Technical University of Cluj-Napoca |
| M. M. Mohebi, Imam Khomeini University | |

EDITORIAL ADVISORY BOARD

P. Feng, F.S. Torknik

ENGLISH LANGUAGE EDITOR

M. Sabzevari

TECHNICAL STAFF

E. Pouladi, V. Hajabdolali, R. Chaluei

DISCLAIMER

The publication of articles in *Advanced Ceramics Progress* does not imply that the editorial board, editorial advisory board, reviewers or the publisher accept, approve or endorse the data and conclusions of authors.

Advanced Ceramics Progress (ISSN 2423-7477) (e-ISSN 2423-7485)

Web Site: www.acerp.ir, E-mail: office@acerp.ir

Tel: +98 (0) 26 36280040-7 ext.: 382, Fax: +98 (0) 26 36201888

Tel:+98 (0)21 88771626-7 ext.: 8931, Fax: +98 (0)21 88773352

Materials and Energy Research Center (MERC); Iranian Ceramic Society (ICERS)

CONTENTS

Solmaz Moniri Javadhesari Mohaddeseh Koochi Masoud Jabraili	Nanomaterials: Applications in Regeneration of Damaged Tissues	1-14
Nazli Aharipour Ali Nemati Adrine Malek Khachatourian	Green Synthesis of Silica Extracted from Rice Husk Ash	15-20
Behnaz Hamrahi Benyamin Yarmand Abouzar Massoudi	Tailoring Bioactivity and Corrosion Properties of Plasma Electrolytic Oxidized Titanium Using GO-Silane Particles	21-31
Behnam Doudkanlouy Milan Hurieh Mohammadzadeh Robabeh Jafari Mohammad Soltani	Investigation of the Coating Methods and Types of Coatings Containing Hydroxyapatite for Applications in Tissue Engineering	32-41
Kazem Jeddi Farhad Sattari Seyedeh Zahra Mortazavi Soghra Mirershadi	Investigation of the Impact of Graphene Nanostructure on the Mechanical Properties of Tires Compounds	42-47
Komeil Azadikhah Mehran Davallo Vahid Kiarostami Saeid Mortazavi Nik	Characterization and Stability Study of Polyurethane / Magnetic Strontium Hexaferrite / Clinoptilolite Nanocomposite	48-56



Materials and Energy Research Center

MERC

Contents lists available at [ACERP](#)

Advanced Ceramics Progress

Journal Homepage: www.acerp.ir



Advanced Ceramics Progress

Review Article

Nanomaterials: Applications in Regeneration of Damaged Tissues

Solmaz Moniri Javadhesari ^{a, *}, Mohaddeseh Koohi ^b, Masoud Jabraili ^c

^a Assistant Professor, Department of Cellular and Molecular Biology, Faculty of Basic Sciences, Azarbaijan Shahid Madani University, Tabriz, East Azerbaijan, Iran

^b MSc, Department of Cellular and Molecular Biology, Faculty of Basic Sciences, Azarbaijan Shahid Madani University, Tabriz, East Azerbaijan, Iran

^c MSc Student, Department of Cellular and Molecular Biology, Faculty of Basic Sciences, Azarbaijan Shahid Madani University, Tabriz, East Azerbaijan, Iran

* Corresponding Author Email: solmazmoniri@gmail.com (S. Moniri Javadhesari)

URL: https://www.acerp.ir/article_161837.html

ARTICLE INFO

ABSTRACT

Article History:

Received 15 August 2022
Received in revised form 3 November 2022
Accepted 29 November 2022

Keywords:

Nanoparticles
Scaffolds
Tissue Regeneration
Biomedical Engineering
Replacement Therapy

Biomedical engineering has been developed to be applied in repairing/regenerating the damaged tissues or organs to facilitate restoration of the lost biological function. Regenerative medicine has been frequently investigated over years to promote the methodology of the replacement of the injured cells and tissues and improve the life quality of the affected individuals. In this regard, the current study examined the application of various ceramic and metal nanoparticles and polymers in treatment of several tissue/organ damages. It was revealed that application of nanotechnology in tissue regeneration could remarkably improve these approaches and succeed in obtaining low-cost, long-lasting, nanoscale scaffolds to be used in clinical practice where nanomaterial-based tissue regeneration showed greater efficacy than the conventional artificial or animal-derived grafts. In addition, nanomaterials with antibacterial or anti-inflammatory properties may be able to overcome some challenges such as infections, inflammations, and immune responses. With the knowledge of regenerating the damaged tissues using nanomaterials, it is possible to combine the nanomaterials strength or antimicrobial properties with the biological properties, such as tissue-specific growth factors, and create new alternatives that are similar to the original tissues of the human body in terms of their preferred properties and characteristics. Different nanomaterials and their applications in the regeneration of bone, tooth, skin, heart, neurons, and bladder tissues were studied in this review. Despite great promise that these approaches have brought into the replacement of damaged organs, many challenging issues still remain unresolved.



<https://doi.org/10.30501/acp.2022.356039.1100>

1. INTRODUCTION

Nanomaterials (NMs) are defined as materials whose size ranges from about 1 to 100 nanometers that are available in different types including nanopatterns, nanofibers, nanotubes, nanoparticles, nanospheres as well as nanopores and nanocomposites with nanometer size [1,2].

With the recent development of nanoparticles, their clinical applications have been extended, and they have been used, for instance, to overcome the restrictions of free therapeutics and crossing biological (microenvironmental, systemic, and cellular) barriers (which differ among the populations of patients and different diseases), thus facilitating the emergence of regenerative medicine (a technique used for tissue

Please cite this article as: Moniri Javadhesari, S., Koohi, M., Jabraili, M., "Nanomaterials: Applications in Regeneration of Damaged Tissues", *Advanced Ceramics Progress*, Vol. 8, No. 4, (2022), 1-14. <https://doi.org/10.30501/acp.2022.356039.1100>

2423-7485/© 2022 The Author(s). Published by MERC.

This is an open access article under the CC BY license (<https://creativecommons.org/licenses/by/4.0/>).



regeneration based on the replacement or renovation of the damaged tissues or organs to reconstitute the function of lost, defective, and aged cells in the body). In 2000, National Nanotechnology Initiative (NNI) was established by National Science and Technology Council (NSTC) of the United States to facilitate the appreciation and clinical applications of nanotechnologies. The main challenges in this field were the toxicity of NMs, development of guidelines for safety assessment, industrialization, and affordability, to name a few [3-5].

Nanotechnology aims to design and employ systems and structures in the range of 1-500 nm. NMs are at least one-dimensional particles of about 1-100 nm in length characterized by unique features that, compared to conventional materials, facilitate distinct interactions with the environment. The characteristics of these materials are as follows: (A) they have a higher surface-to-volume ratio than that of bulk materials which in turn provides a higher degree of reactivity; (B) their length is highly suited for effective interaction with cells, particularly in the cases of entrance to cells; and (C) the presence of some dominant physical phenomena such as surface tension in NMs rather than in macroscopic materials while this feature is unexpected or negligible in bulk materials. These features bring about advantageous properties for drug delivery purposes [3,6].

The present study intended to summarize the existing knowledge about the applications of NMs in the reconstruction of damaged tissues of various origins. In addition, efforts were made in this study to discuss the advantages and disadvantages of these approaches compared to the conventional tissue regeneration approaches.

2. APPLICATION OF NANOMATERIALS IN REGENERATIVE MEDICINE

Regenerative medicine, first proposed by Alexis Carrel in 1902, is a method for tissues regeneration that can replace or repair the injured tissues/organs to reconstitute the function of damaged, lost, or aging cells through replacing them with new healthy cells. Some necessary components for tissue regeneration include cells, growth factors, and scaffolding materials. Application of nanotechnology to each of the essential components of tissue regeneration assists the regenerative medicine in improving the life quality of patients who have not received appropriate medical treatments. Recent advances in the application of nanotechnology in tissue regeneration have focused on applying new functionalized inorganic NMs to tissues and delivering cells, real-time tracking of the process of tissue regeneration, and improving the therapeutic efficiency [5].

The following methods are used mainly in manufacturing NMs that can be used in regenerative

medicine. Bottom-up techniques benefit nanotechnology knowledge as an efficient method for the fabrication of new nanoscale materials with different behavior than that of their bulk versions. Polymeric nanoparticles, inorganic nanoparticles, self-assembled NMs, Quantum Dots (QDs), dendrimers, Carbon Nanotubes (CNTs), and Layer-by-Layer (LbL) nanostructures are examples of such materials. It can be anticipated that in the future, nano-based regenerative medicine can develop a new approach to healthcare by designing effective targeting systems for stem cell-based therapies [3].

A multidisciplinary method facilitates the production of unique "smart" materials capable of mimicking the extracellular environment that can result in the triggering of cellular responses. Improving the diagnosis process of diseases at the early stages plays a vital role as the sensitivity and precision of diagnostics tests increased. To date, many nanotechnology applications are at the concept level, thus requiring much more basic studies to achieve commercial exploitation. There are numerous reports on the acceleration of treatments based on tissue regeneration, e.g., for skin, bone, teeth, blood vessels, heart, brain, and bladder tissue (Figure 1). In this regard, biocompatibility and cytocompatibility of various nanoparticles and alloys were evaluated in this research [3,7].



Figure 1. Application of nanomaterials in regenerative medicine for several diseases with no definite treatment

3. BONE REGENERATION

Nanoparticles are commonly used in bone tissue regeneration strategies by conducting the fate of cells into osteogenesis and regenerating remarkable bone deficiencies. Nanoparticles, as multi-purpose compounds, can be used in scaffold-based and scaffold-free approaches of Tissue Engineering (TE) to promote the

osteogenesis and regenerate the bone tissues. These particles can provide an osteogenic niche by regulating the inflammatory reactions and osteo/angio/osteoclastic signaling pathways such as FAK/RhoA/YAP1 pathway which regulates the signaling between stress fibers and osteogenesis, MAPK pathway that connects the cell surface to the nucleus to receive extracellular signals, especially osteoblast signals, BMP/Smad pathway that promotes osteogenesis and upregulates the transcription of osteogenic marker genes such as Runx2, and Wnt/ β -catenin pathway that modulates the osteoblast lineage cells and affect various stages of bone formation [8,9]. In addition, the interaction of nanoparticles with biomolecules can improve the bioavailability and half-life of that molecules. Although nanoparticles are relatively ideal candidates for improvement of the osteogenesis processes, the interaction between the nanoparticles and biological environments has its complications, especially the cytotoxicity of the NPs regarding their clinical utilization [8].

Topography is another essential factor in the cellular behavior of NMs that modulates the adhesion, migration, differentiation, and biological function of the cells and tissues. Scaffolds are mostly produced with different topologies including nanoparticles, nanotubes, and nanofibers to better mimic the nano-scale structure of Extracellular Matrix (ECM) for regeneration of bone tissue [10,11].

Earlier research revealed the improved function of osteoblasts on the surface of different NMs, e.g., Black Phosphorous (BP), nano-hydroxyapatite (HA), anodized titanium (Ti), electrospun silk, and nano-structured Ti, compared to the common materials of an orthopedic implant. One of the challenges in this field is identification of the mechanisms that enhance the function of osteoblast cells on these NMs. In this respect, several studies confirmed that high surface energy of NMs would make some alterations in the amount and biological activity of the absorbed proteins (e.g., fibronectin, vitronectin, and collagen), which in turn increased the function of the bone cells [12-14].

Along with the enhanced responses of the bone cells in the presence of NMs, the improved functions of osteoblasts, such as deposition of phosphate and calcium minerals, can last for a more extended period of time on the nanostructural materials. These functions are essential for the osseointegration of implants under orthopedic conditions [12].

BP Quantum Dots (BPQDs) and BP nanosheets, as the emerging layered metal-free two-dimensional materials, were proved beneficial to the bone tissue regeneration. These NMs are characterized by many superior properties such as adjustable direct band gap, distinct pleated structures in layers, great carrier capacity, and several attractive in-layer anisotropies. Moreover, BP NMs show great biodegradability, biocompatibility, PTT

and PDT effects, and excellent drug-loading capacity [13].

Ti is another attractive material with good biocompatibility, load-bearing capability, corrosion resistance, and machinability that is commonly used in dental and orthopedic implants [15]. This element is also used in the form of nanostructures. Ti nanostructures provide a large surface area, improved antibacterial properties, bone integrity, and protein interactions, which are advantages for an implant with clinical use [2]. The relevant conducted studies have highlighted that despite the minimal difference between the size of Ti surfaces on a sub-micron and nanometer scale, bone cells behave differently on these surfaces. In other words, one can state that small changes in the characteristics of these materials can have significant effects on the process of bone regeneration. Likewise, the nanophase structures of Ti, CoCrMo, and Ti_6AlV_4 significantly advanced the crystallization of calcium compared to their microphase structures [12].

A novel flax/silk protein-based nanofibrous scaffold has been recently developed for bone regeneration. This scaffold showed biocompatibility in the MG-63 osteoblast cells and long-term antibacterial activity against *E. coli* and *S. aureus*. Flax holds bioactive peptides, which can promote the antioxidant activity, antibacterial performance, and anti-inflammation capacity [16].

Webster TJ's reported the first evidence of the improved osteoblast adhesion on nanophase, compared to the conventional metals in 2004 [12,17].

Another parameter that is considered in the design of NMs is the application of aligned nanoscale surface features on the metallic materials that have been indicated to greatly mimic the bone natural anisotropy and consequently improve the function of osteoblasts [18].

The results from different studies indicated that the behavior of the bone cells was strongly affected by the size of the surface features wherever nanoscale and sub-micron surface features could significantly improve the functions of osteoblast cells for a longer time. In fact, it is anticipated that within a short period of time, the commercialization process of the optimized nanostructure implants will be accomplished, and these materials will enter the orthopedic and/or dental implant markets. In this regard, some NMs were already approved by the FDA for implant applications in the human bodies [12].

A variety of studies have been conducted on a large number of different metals and their oxides to produce nanoparticles that can be used in the field of bone regeneration. Nanoparticles of gold, platinum, silver, palladium, tantalum, zinc, copper, iron oxide, Ti dioxide, magnesium oxide, nickel oxide, calcium oxide, cerium dioxide, silicon dioxide, strontium nanoparticles, and zirconia NPs are examples of these nanoscale materials.

Carbon-based NMs such as graphene and CNTs are also used in bone TE [2,19].

Carbon NMs also have exclusive biological and physical characteristics such as antibacterial properties and ability to express different genes that play essential roles in tissue regeneration [16,20]. In addition, NMs with a combination of silver, Ti, and hydroxy apatite, such as Ag:HA/Ti and Ag:HA/TiO₂ nanotubes can be used as antifungal scaffolds for regeneration of the damaged bone [16].

Gold nanoparticles (AuNPs) can drive Periodontal Ligament Stem Cells (PDLSC) sheets toward osteogenic differentiation by upregulating the expression of bone-related proteins and mineralization [21]. In 2019, Liang et al. conducted a study to investigate the modulating effects of a mesopore silica nanoparticle loaded with AuNP (Au-MSNs) on the macrophages and its subsequent impact on the responses of osteoblast cell lines. They reported the potential of Au-MSNs to generate an optimal immune microenvironment by triggering an anti-inflammatory response as well as stimulating the macrophages for secretion of cytokines with osteogenic properties [22]. A list of NMs used in the regeneration of bone tissue is summarized in Figure 2.

Since HA is an essential part of the native bone tissue, nanoparticles of HA are widely applied in the manufacture of nanocomposite hydrogels in order to improve the function of HA scaffolds in the regeneration of injured bone [23]. In addition, Nanoclays can be used in bone regeneration approaches. They are layered mineral materials formed naturally with at least one dimension in the range of 1-100 nm. They are engaging in terms of low cost and being environmentally friendly [23,24].

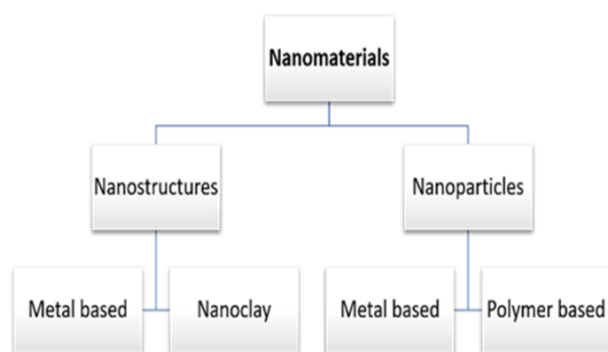


Figure 2. Candidate nanomaterials for repairing and regeneration of bone tissue

Computed tomography and *in vivo* histology analyses demonstrated that application of the Au-MSNs could enhance the constitution of new bone at the site of a cranial defect of critical size in rats. Outright, the new Au-MSNs can remarkably improve the osteogenic properties through the immune microenvironment

modulation, thus approving the therapeutic potential of these NMs for repairing and regenerating bone tissue [22]. Other studies conducted later in this field showed that in a preclinical model, AuNPs (especially 45 nm) have the ability to promote the osteogenic differentiation process of PDLSC sheets both *in vitro* and *in vivo* [25].

Despite the great deal of researches conducted on various NMs with the objective of functionalizing the polymer matrix to enhance the desirable properties, these scaffolds are still under *in vivo/in vitro* investigation; hence, further experiments should be done before clinical applications [2]. Regardless of the type of materials used in the bone tissue reconstruction, a comprehensive understanding of the dispersal of these materials in a solid phase and interfacial relationships of two phases is required to improve the force transmission and fabricate tissues with the high similarity to the bone tissue in terms of natural toughness and strength [26].

Although developing new construction methods can improve scaffold designing, control the properties of the scaffolds, and enhance their mechanical properties, but nanotechnology alone cannot ensure a promising method for regeneration of bone tissue. Studies have demonstrated the significance of growth factors such as BMP2 and VEGF, osteoinductive factors such as adenosine and ions, and development of antibacterial materials and scaffolds in improvement of osteoinduction and vascularisation to support regeneration of serious bone injuries [27].

4. SKIN RECONSTRUCTION

The objective skin TE pursues is to reduce the scar formation, improve the wound healing, and restore the functional and structural components of the skin. NMs such as nanocomposites, nanoparticles, brackets, and hydrogels are currently used for skin wounds healing purposes; for instance, engineered nanoscale materials are efficiently used for managing infections and therapy purposes, and nanofibrous matrices based on the biomimetic elastomeric peptide and nanotechnology for regeneration and repair of the skin wounds [28]. Nanoparticles composed of a single species of chemicals such as metals and metal oxides are not only excellent antibacterial agents but also can be effective in the healing of skin wounds and lesions. For example, nanoclusters of silver and gold with the size range of 1.1-1.6 nm proved to contribute to repairing the skin lesions of rat models *in vivo* [6]. On the contrary, according to the *in vitro* studies, Au nanoclusters are the best effective materials to be used in the wound healing processes due to their specific anti-inflammatory effects, better uptake by cells, and promoting proliferation and migration of cells. Generally, Au nanoparticles are biologically compatible that can decrease inflammation and improve the constitution of granulation tissue. Instead, AgNPs can

promote the proliferation of keratocytes and fibroblasts. In addition, they can repress the innate immune system which, in turn, accelerate the wound healing rate and decrease the scarring rate. The first commercially available AgNP-containing wound dressing is ACTICOAT. Other instances are copper nanoparticles and nanoceria [6].

Hollow colloidal nanoparticles have gained significance in recent years owing to their unique features including low density, significant loading capacity, great surface permeability, and excellent morphology. The inimitable characteristics of these NPs facilitate their widespread applications in biomedicine, chemical catalysis, electronics, optics, environment protection, storage, and conversion of energy, anti-oxidation, anti-tumor treatment, TE, and drug delivery. A favorite hollow colloid known as HPDAIR was synthesized in 2021 by loading Hollow Polydopamine (HPDA) nanoparticles with RL-QN15 (a peptide with amphibian origin) that enjoy distinct prohealing properties [28].

Skin replacement is one of the first prosperous applications of tissue regeneration that has made the regrowth of damaged tissue possible. Multiple products of TE succeeded in getting FDA approval for applications as the graft materials in the treatment of individuals with severe skin damages caused by burns or diabetic ulcers. Apligraf is a popular product available in the market that is constructed by culturing a layer of human keratinocytes on top of a matrix of human skin fibroblasts and bovine type I collagen. It is successfully used in the treatment of ulcers of the venous leg and diabetic foot. Unfortunately, all the skin products of TE incur high costs due to the expenses of the longtime cell culture that is required for full maturation of the graft in vitro before its clinical applications. However, applying the nanoscale scaffolds may help shorten the culture time and benefit the production of artificial grafts for the treatment of skin damage [29].

In this regard, Chang et al. investigated the application of nano-structured Chitosan Scaffold (CS) for the growth of human skin fibroblasts. Primarily, they cast a flat surface of Poly(ϵ -Caprolactone) (PCL) and produced a nanoscale PCL model. Then, they cast a crosslinked form of chitosan over this model, followed by introduction of an extra layer of PCL to the smooth side of the chitosan film. These CS/PCL nanostructures demonstrated remarkably improved proliferation rate and viability of fibroblasts, compared to the smooth CS/PCL surfaces or nano-rough PCL surfaces. Therefore, it can be concluded that nano-polymer-based techniques can provide a cost-effective approach to the production of nanoscale scaffolds as advanced synthetic skin grafts [30].

Skin wound healing currently utilizes a novel approach called Autologous Layered Dermal Reconstitution (ALDR). This procedure is based on new TE scaffolds composed of electrospun PCL and gelatin fiber scaffolds of 300-600 nm in diameter and 28 mm in thickness.

Human dermal fibroblasts are seeded onto the scaffolds that remain viable in the scaffold during all times tested (for up to two weeks), and the doubling time of the cells was about every 3 days [31].

Despite the insufficiency of the in vivo results, upon using electrospun TE scaffolds, ALDR proved to be superior to the conventional strategies. Briefly, ALDR ensures rapid reconstruction of the damaged tissue layer-by-layer, in deep wounds, with the overall distribution of skin fibroblasts. Followed by 48-72 hours of implantation, the wound dressing may be replaced with a new scaffold/construct, and this process will be repeated until the wound completely heals. Prior to the implantation, each scaffold was lonely seeded with skin fibroblasts that decreased the prolonged times of in vitro culture, compared to previously described single-layer scaffolds. Through this LbL method, a continuous layer of skin tissue with porous nano-scaffold is formed, allowing rapid cells proliferation and layers integration. Overall, numerous studies on the TE of skin wounds have been conducted, the results of which were in agreement with those obtained from using nanoscale scaffolds to achieve efficient wound healing properties [31]. In this regard, combination of the biomaterials with innovative scaffold fabrication techniques can improve the resultant scaffolds in an ECM-mimicking bioenvironment and even the scaffolds capable of enhancing the ECM of the injured skin to favor tissue regeneration. Development of some novel strategies such as responsive scaffolds can pave the way for the generation of 4D scaffolds capable of modulating tissue microenvironment by sensing biological and physicochemical parameters. Scaffolds should be constructed from materials that allow many signals and interactions to be activated. Similarly, stem cell-based therapies can be appropriate candidates for treating chronic wounds given their capability of both renewing lost tissue and promoting wound healing via paracrine pathways. It is still necessary to address several questions about the best source of stem cells, ideal approaches of cell delivery, and long-term harmful effects of these cells [32].

Along with all the advances that have been made in skin TE, application of materials with the utmost negligible toxicity can help enhance the efficacy of this treatment [6].

5. DENTAL REGENERATION

Nanodentistry, i.e., application of nanoparticles in dentistry, is affected by specific nanostructure topography of the tooth and promising advantages of NMs. This field benefits the application of NPs for anti-inflammatory and antibacterial activities, remineralization, local anesthesia, differentiation of stem cells, and bone conduction. In addition to the application of NPs in dental tissue regeneration, NMs can improve

the mechanical features of dental composites, enhance their anchorage and bonding, and decrease the possibility of friction [33].

The nanoscale size of NPs facilitates their increased penetration into the areas with more serious damages and enhances the mechanical strength of the dental composites through porosity reduction. Biological activity is also improved by the high surface-to-volume ratio, including bonding and integration, and antimicrobial activity will be enhanced as well. In addition, the controlled release of functional molecules (drugs, growth factors, etc.) from the NPs leads to site-specific precise delivery of these molecules to achieve localized therapy. These characteristics bring advances to multiple fields of dentistry, including endodontics and periodontology as well as the reengineering of dental braces and prosthetics. Nanoparticles of metals or metal oxides intrinsically show bactericidal activity. In addition, encapsulation of drugs within nano-polymers improves the solubility of drugs in the aqueous phase and transfer into bacteria besides the controlled release of the drugs. The higher surface-volume ratio also facilitates the simultaneous loading of multiple drugs resulting in a synergistic antibacterial effect, thus eliminating microbial resistance [33].

Nanoparticles such as CNTs are progressively applied in the resin matrices of orthodontic and prosthetic composites, improving the filler load by filling the gaps up, advancing the mechanical features, and decreasing polymerization shrinkage. There was also an improvement in the bond strength, pressure, flexibility, hardness, and toughness of fractures [33].

Studies have confirmed the improving effect of using biomimetic implants on the prosperity of dental implants for diabetic individuals. The antimicrobial features of these implants may contribute to the prohibition of peri-implantitis. Of note, application of nanostructures of carbon can effectively advance drug delivery and enable mimicking protein channels, thus improving wound healing and reducing the rate of dental implant failure. The adaptation of NPs to alter the biomimetic implants may enable them to solve problems such as infections, slow wound healing, and osseointegration, thus leading to the creation of long-lasting implants and advancement of personalized therapy for dental tissue of individuals with slow wound healing [34].

Periodontal reconstruction consists of a complicated set of tissues and constructions in and around the tooth. Therefore, a good biomaterial-based approach requires a functionalized scaffold where the chemical formula and three-dimensional architecture of each compartment are following the biochemical mixture, fine organization, and mechanical features of the target tissues. The application of multilayered nanoscale scaffolds in tissue regeneration is in its infancy, not limited to dental implants but also for all tissue types, hence the high possibility of promising results for the future of

regenerative medicine. The investigated LbL scaffolds for regenerating various tissues are usually manufactured by using NMs that can precisely mimic the fine properties of the tissue to reconstruct [35].

In spite of great advances in the field of nanobiomaterials, nano dentistry is still lagged, and a majority of research studies on dental NMs are *in vitro*. Given that the effect of the dental NMs was not examined or shown *in vivo*, more research in real clinical trials/on patients is required to promote the development of efficacious and affordable nanotheranostics [36,37].

6. REGENERATIVE MEDICINE FOR HEART DISEASES

Recently, great deal of efforts have been made to construct heart functional tissues; however, there are still some challenges such as the need for cardiac myocyte culture. In a preliminary study, submicron size scaffolds of electrospun Poly(Lactic-co-Glycolic) Acid (PLGA), and Poly(L-Lactide) (PLLA) fibers were produced. They yielded positive results in terms of cardiac tissue regeneration, indicating that cardiomyocytes could attach and grow on the scaffolds and crawling inside and align with the orientation of constructed fibers [12].

In addition to the regeneration of functional myocardium, a considerable number of research studies have been conducted on the development of tissue-engineered heart valves *in vitro* due to the increasing prevalence of heart valve replacement using artificial/animal-derived valves. There is an expectation that TE will resolve issues related to artificial valves (the need for chronic anticoagulant treatment) as well as animal-derived valves (calcification and hardening). Of note, it can grow to be further adapted with an enlarged heart by maturing pediatric patients [12].

Characterization of the porcine decellularized membrane of aortic valves through Scanning Electron Microscopy and Atomic Force Microscopy revealed a nanoscale fiber matrix of 30 nm with the pore diameter and depth of about 30 nm and 22 nm, respectively. Such nanoscale membranes are remarkably smaller than the endothelial membranes of the mammalian cornea and bladder tissues. Given the nanoscale size of this membrane, a proper TE scaffold for the regeneration of heart valves is required to have a similar surface scale to ensure successful interaction with endothelial cells [12].

Different kinds of NMs are examined as the contrast agents of ultrasound for diagnosis of cardiac diseases, including Nanobubbles (NBs), Microbubbles (MBs), Nanocapsules (NCs), and Nanodroplets (NDs) [38,39].

In order to achieve successful cardiac regeneration, numerous biological properties such as adhesion, proliferation, differentiation, mechanical and electrical properties, and vascularisation are required, all obtained

by combining various NMs (organic/inorganic) with different properties and features. The hybrid scaffolds can provide improved and tunable rheological and mechanical properties that result in their enhanced performance for soft tissue regeneration. In addition, from a biological viewpoint, understanding of the pathways involved in the interaction of the cells with the structural, mechanical, and electrical properties of NMs can be helpful in achieving prosperous myocardial regeneration [40].

7. VASCULAR TISSUE ENGINEERING

Development of surfaces that can enhance the attachment, proliferation, and qualified function of the smooth muscle cells of endothelium. Here the vessels are considered the quickly developing parts of TE. Recent studies have focused on two primary purposes namely the development of vascular grafts with small diameters and fabrication of the next generation materials as a vascular stent. In order to achieve appropriate vascular cell interactions, several investigations have focused on fine-tuning the surface structures at the submicron and nanoscale dimensions. Samaroo et al. reported nano surfaces based on PLGA as well as nitinol and Ti while developing vascular cell function [41]. They also reported the improved attachment and proliferation of the smooth muscle cells of endothelium and vessels on the nanoscale PLGA, compared to the smooth surfaces. Further, they synthesized a series of PLGA nanosurfaces with the same chemical composition and variable submicron scales. They revealed that surfaces with the lateral diameter of 200 nm and spherical surface properties could remarkably enhance the adhesion of the smooth muscle cells, compared to the smooth surfaces or spherical surfaces of 100 or 500 nm [42,43].

In another study, Carpenter et al. found that addition of collagen type IV and fibronectin could improve the adhesion of the endothelial cells to the PLGA surfaces, regardless of their exact size. In addition, they remarked that adsorption of collagen type IV and fibronectin, as well as the attachment of endothelial cells, was highly dependent on the vertical dimension of surfaces rather than the lateral dimension, and approximately 20 nanometers were reported as the ideal vertical dimension for surfaces [44]. Furthermore, a study on the Ti stent surfaces showed that the nanoscale surfaces of Ti showed improved levels of attachment and proliferation of the endothelial cells, compared to the surface features with a micron scale. Altogether, use of nanotechnology in the regenerative medicine of cardiovascular diseases provides promising results in adhesion enhancement and proliferation of endothelial cells [45]. It can be anticipated that nanotechnologists in cooperation with physicians, cellular/molecular biologists, and pharmaceutical companies can design and develop novel

nanomedical devices for cardiac regeneration with potential clinical applicability [46].

8. REGENERATIVE MEDICINE FOR NEUROLOGICAL DISORDERS

Nanotechnology has the potential to extend the application of regenerative medicine to the treatment of neurological disorders in the brain as well as eyes and peripheral nervous system (Figure 3). Today, with the emergence of topics such as the applicability of NMs as a tool for understanding the pathology of Central Nervous System (CNS) diseases, stroke treatment through targeting neuroplasticity of the brain using biomaterials, possibility of designing nanotheranostics to treat neurological disorders through personalized medicine, use of NMs as the gene carriers to reprogram the cells, and consideration of the potential of NMs while modulating the immune system for creating an environment suitable for regeneration of nerve cells. Hopefully, it is expected that NMs can be used in the treatment of neurological diseases or regeneration of nerve cells. In this regard, some studies have been conducted to identify nanotechnology-based methods that can promote endogenous regeneration processes in the brain as well as the production of various NMs and their therapeutic effects, especially in the spinal cord [47].

In this respect, several pre-clinical studies were conducted using advanced regenerative therapies, and promising results were obtained. However, the clinical application of these therapeutic approaches is still challenging. To be specific, despite the common characteristics of the CNS disorders, they also have differences, and one should consider these characteristics while designing regenerative nanoparticles. However, nanomaterial-based approaches are considered qualified alternatives for the repair and regeneration of the damaged nervous systems [47].

8.1 Nanomaterial-Mediated Neural Stem Cell Therapy for Neurological Diseases and Their Current Clinical Status

Neural Stem Cell (NSC) therapy with NMs mediation has been developed to treat neurological diseases.

Particular characteristics of NMs including unique nano-bio interface, minimal size, and high delivery/loading capacity can be considered in regulating the biochemical and mechanical microenvironment of transplanted cells that help advance our knowledge of cell behavior management. Altogether, the unique characteristics of these materials can result in the optimization of tissue regeneration approaches to neurological diseases [21]. For instance, some nanofibers/nanocomposites of Lignin, including Poly (vinyl alcohol)-poly (glycerol sebacate-lignin fibers), can

be beneficial to the regeneration engineering mainly because the lignin promotes the proliferation and differentiation of neural cells in a positive way [48].

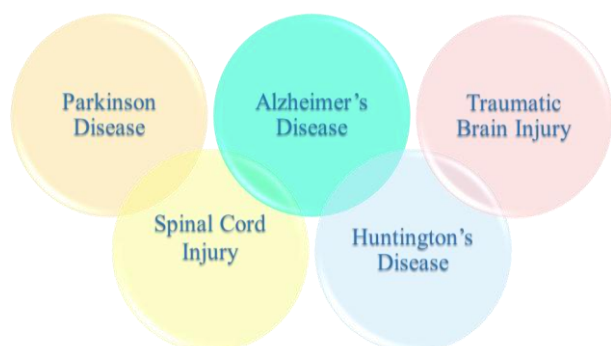


Figure 3. Neurological diseases that nanomaterials play a role in their treatment

8.2. Spinal Cord Injury

Spinal Cord Injury (SCI) is one of the most dangerous disorders of the nervous system, and no efficient treatment for this disease has been reported yet. Nanoparticles can be advantageous in stem cell-based therapy of SCI. For instance, they can be used for the targeted delivery of therapeutics to the site of injury and lessen the adverse effects [49-51]. In addition, NPs can improve the regeneration of axons in order to restart the transmission of neural messages in the damaged spinal cord by accelerating the regrowth of axons. Of note, NMs play a key role in the targeted delivery of neurotrophic factors to the site of damaged tissue, and better the microenvironment for nerve regeneration, stem cell adhesion, and migration [52,53]. Multiple attempts were made in order to find the appropriate NPs for neural regeneration. A study demonstrated that nanocomposites of chitosan-NT3 or PLGA nanoparticles loaded with flavopiridol (CDK inhibitor) could assist in the differentiation of endogenous neural stem cells and regrowth of axons in order to regenerate the damaged spinal cord. These nanocomposites are particularly noteworthy for treatment of spinal cord injuries because they are degradable, characterized by less cytotoxicity to the CNS and significant regeneration functions. Overall, the combination of nanotechnology with NSCs has opened a new chapter in treating neural system injuries [21,53,54].

8.3. Alzheimer's Disease

Alzheimer's Disease (AD) is a chronic disorder of neuro-degeneration that is primarily defined as the deposition of β -amyloid and hyperphosphorylation of tau with an unknown onset and slow development [55]. The cognitive defect as the main symptom of AD can be recovered through the regeneration of the neural network by NSCs transplantation. However, the efficiency of this

method is relatively low, and only a few portions of the transplanted stem cells can differentiate into neurons while a majority of them do not end up with the desired fate. Nanoparticles can be applied to improve the transfer of the genes/drugs/stem cells, stimulate the neural differentiation of cells, and ensure real-time monitoring of the nervous system. In one study, charge reversible NPs of Poly(Carboxy Betaine) (PCB) and traceable superparamagnetic iron oxide nanoparticles of ABC/SPIONs/siSOX9 were applied to the AD mice, and the obtained results indicated that the applied nanoparticles were capable of fine-tuning the NSCs to differentiate into neural cells and rescue their memory [21,56]. Fan et al. developed a new nanoparticle, i.e., poly(lactide-co-glycolide)-block-poly(ethylene glycol) (PLGA-PEG) conjugated with B6 peptide and loaded with Curcumin. They studied the effect of this nanoparticle in vitro by administrating it into HT22 cells and APP/PS1 Al transgenic mice and found that this nanoparticle could be effective in reducing the diameter of the cur, enhancing cellular uptake, improving the spatial learning and memory, and decreasing the β -amyloid formation and deposition in hippocamp and hyperphosphorylation [55].

However, it should be noted that use of NMs and NSCs in treating AD is a new and promising field with great deal of uncertainty [21].

8.4. Huntington's Disease

Huntington's Disease (HD) is a neurodegenerative condition with no efficient therapeutic for its recovery or even for its delayed progression [57]. There are some reports about the usefulness of SCs transplantation and tissue regeneration in the rescue of HD in some rodents as well as in humans. Nowadays, Pluripotent Stem Cells (PSCs) are considered novel therapeutic choices for HD treatment. Nevertheless, this approach faces some problems, including ethical limitations, low reprogramming efficiency, and genetic instability. Application of nanotechnology provides a good solution to these problems that in turn encourages conducting further studies on the NPs in the SC-based therapy of HD including lipid NCs, liposomes, dendrimers, poly(ethylene imine) NPs, and chitosan. In addition, there are several reports of the benefits of exosomes in HD treatment. In one study, exosomes from adipose stem cells remarkably reduced the aggregation of mHtt in neuronal cells of R6/2 mice. They raised the abnormal level of apoptotic protein within an HD model in vitro [58,59].

Even though there is limited data about the benefits of applying stem cells with nanocarriers in Huntington's disease treatment, it is still a promising method under investigation [21].

In addition, integration of knowledge about the biological processes that were found to be effective in the development of Huntington's disease with

nanotechnology led to the development of new methods to restore nerve function in this disease. For example, the decreased levels of cholesterol and its biosynthesis in mouse models of HD are indicative of the role of local synthesis of cholesterol in synapse integrity and regeneration. Then, Valenza et al. developed an NP that was modified with glycopeptide (g7) and loaded with cholesterol (g7-NPs-Chol). They found that intraperitoneal injection of this biocompatible and biodegradable NP to the HD mice resulted in the localization of this NP in glial and nerve cells in different parts of the brain [60].

Another study revealed that insufficient amounts of selenium (Se) in the brain of HD patients contribute to the neurological loss and dysfunction. Accordingly, Cong et al. used nanoparticles of Se (Nano-Se NPs) to treat the disease in transgenic HD models of *Caenorhabditis elegans* (*C. elegans*). They found that low doses of Nano-Se NPs could reduce the neuronal deaths, relieve the behavioral disorders, and protect the *C. elegans* against stress-related damages. According to their observations, Nano-Se can be a great potential treatment for Huntington's disease [61].

8.5. Traumatic Brain Injury

Traumatic Brain Injury (TBI) is a severe head injury caused by events such as car accidents. It is found that degradable NMs, particularly nanocomposites, can positively affect the self-renewal and differentiation of stem cells to neurons in TBI amelioration [21]. For example, Zinger et al. developed a novel leukocyte-based biomimetic nanoparticle system to directly access the inflamed areas in a mouse model of TBI through the peripheral organs 24 hours after injury [62].

Development of nanomaterial-based NSC therapy for neurological disorders benefits from the particular properties of NMs, including inimitable nano-bio interface, small size, and high delivery capacity that can regulate the mechanical and biochemical microenvironment of the transplanted stem cells in order to control the behavior of cells and optimize tissue regeneration process. Despite the advent of promising results obtained from nanotechnology-based NSC therapy, there are yet many challenges to overcome before this approach can go under clinical evaluations. These challenges include the safety of the applied NMs, metabolism of these scaffolds in the body, their toxicity to the target organ, genotoxicity, and neurotoxicity. In addition, NMs and neural stem cells of different origins should be optimized for TE purposes. Eventually, a problem may arise regarding the underlying mechanisms in the complicated systems of the nanomaterial-based NSC therapy. In this respect, alterations of the hub-gene and their related signaling pathways followed by addition of NMs was recommended, a fascinating field to explore [21].

Briefly, nanomaterial-based approaches can ensure a promising way to recreate an intimate environment for nerve regeneration. However, application of these materials requires consideration of their toxicity, biosafety, and metabolic effects on the living organism as well as investigation of the impacts of NMs in large animals or non-human mammals [63]. An additional demand still exists for further studies on the synthesis and design of the optimized multifunctional nano scaffolds with characteristics that can improve neuroregeneration in clinical models [64].

9. BLADDER TISSUE

Congenital abnormality or acquired disorders of the urinary system may damage the organs of this system, hence the demand for tissue regeneration. A standard approach to the reconstruction of the bladder is to use the parts of the gastrointestinal system. However, there are essential physiological differences between these tissues so that bladder cells inhibit the absorbance of some solutions while digestive tissue usually absorbs these solutes. These differences can result in complications such as metabolic disorders. In this regard, it is recommended that regenerative studies be carried out to achieve a proper alternative graft for the reconstruction of bladder tissue [65]. A favorite method for this purpose is the application of synthetic biomaterials since their material composition is defined, and they can be provided off-the-shelf with constant features for all the batches. Poly-dl-Lactide-co-Glycolide (PLGA) is a biodegradable material with FDA approval that can successfully promote the growth of smooth muscles of the bladder and urothelial cells in vitro [12,65,66]. However, not all biodegradable conventional synthetic polymers and natural polymer scaffolds succeeded in the reconstruction of bladder tissue mainly due to the weak strength and negative immune and tissue responses [67].

Therefore, development of new strategies for the reconstruction of the bladder using advanced newly designed biodegradable polymers rather than conventional polymers is required. Application of these advanced polymers results in the rapid and efficient replacement of the synthetic biodegradable material by healthy bladder tissues of the host. The response of bladder cells to some features such as nanosize, microsize, and flat surface is different probably because the surface of these nanoscale synthesized materials mimics the natural environment of these cells. In line with this observation, recent studies have found that the nanoscale polymers of PLGA and polyurethane (PU), compared to the conventional PU and PLGA, enhanced the growth of smooth muscle cells in the bladder [68]. Surprisingly, the reconstructed bladders also face a challenge related to the recurrent formation of calcium oxalate stones [69].

Chun et al. remarked that application of rough nanometer PU with submicron pores, compared to conventional materials, would lead to the adhesion and proliferation improvement of the urothelial cells as well as a decrease in the formation of calcium oxalate stones. It seems that the surface pores of the advanced nanoscale polymers can absorb calcium and oxalate separately, hence prevention of the required interactions for forming calcium oxalate [69].

Another study investigated the new 3D porous scaffolds of PLGA in comparison with the conventional microscale scaffolds, and the results highlighted the advancing effect of new polymers in promoting the adhesion, growth rate, and protein production of the smooth muscle cells of the bladder [70]. These synthesized nanoscale scaffolds can guarantee advancement of favorite in vivo alternatives for the bladder wall in the future [12].

In one study, a three-layer PLGA mesh was seeded by cells and fibrin that confirmed some useful pressure-withholding features. In addition, PLGA scaffolds seeded with human adipose stem cells produced smooth muscle cells as an engineered bladder. These cells are capable of regenerating the muscular layer of the bladder and supporting urothelial ingrowth that results in an entirely functional bladder. Further, inspection of the bladder structures regenerated after two weeks of implantation indicated that the PLGA scaffolds remained intact and visible with no collapse or shrinkage, and there were no apparent signs of inflammation, infection, or necrosis. These observations confirm that the PLGA scaffolds that are biocompatible with the host have the sufficient mechanical strength to provide pressure-withholding properties [65].

10. RISKS AND CHALLENGES OF APPLICATION OF NANOMATERIALS FOR TISSUE REGENERATION

Although NMs have unique characteristics owing to their nanoscale size that facilitates regeneration of damaged tissues, they may cause some potential risks to tissues and cells. According to an in vitro study, NMs exhibit higher toxicity than micromaterials even at limited concentrations and short term exposure [71]. A study by Napierska et al. highlighted an obvious relationship between the cytotoxicity and concentration of silica NMs. According to the findings of that study, localized concentration and nanotopography are main causes of nanotoxicity [72]. In another study, Yang et al. investigated the toxicity of various NMs including CNT, carbon black, ZnO, and SiO₂ nanoparticles at different concentrations. They found that NMs with the concentrations of > 50 µg/ml show higher cytotoxicity in vitro while under this threshold, no significant difference was observed [73].

Recent observations indicated that even lower concentrations of NMs (5 µg/cm²) may result in cellular malfunction by irreversibly binding to biomolecules and cellular organelles, interfering with the replication of DNA, inducing cell death by disrupting membrane integrity, and causing systemic inflammation through blocking microcirculation [74,75].

In addition, the morphology of a nanomaterial can also affect its cytotoxicity [76]. Biological molecules, lipids, enzymes, nucleic acids, and polysaccharides are structurally and dimensionally analogous to NMs and for this reason, they can easily interact with different kinds of biological receptors, easily cross the biological membranes, travel all over the body and then being accumulated in organs that results in potentially harmful reactions [77,78]. In many studies, nanotubes are more likely to damage DNA than other NMs with spherical shapes or crystal structures. It was concluded that the shape of NMs may contribute to the genotoxicity of NMs at lower exposure doses [73]. In addition, NMs smaller than 10 nm were proved to be toxic and reactive due to the increased density of their surfaces and increased number of electrons present on them [79]. According to Wang et al. and Lee et al., several types of NMs, such as nHA and TiO₂ nanoparticles, can accumulate in heart, kidney, liver, lungs, and spleens of animals via blood circulation [80,81] and could be toxic to humans when tested in vivo [82,83]. A toxic effect has also been demonstrated by overproducing Reactive Oxygen Species (ROS) and cytokines such as IL-4 and IL-13 in vitro [84]. Accordingly, the results of these studies suggest that the localized concentrations and topography of the NMs may contribute to their toxicity. The threshold concentration of NMs can induce inflammation, cause the formation of free radicals, accumulate the peroxide products, and reduce antioxidants, and trigger cellular apoptosis [74,85]. To investigate the potential risks of NMs in cells with specific organs and tissues, Wu et al. conducted RNA sequencing on the body-wide organ transcriptome data. His lab research developed Nano Genome Atlas (NGA) that analysed NMs. According to their findings, some of them not only triggered inflammation but also significantly affected ion transport activities, metabolism, and cell behavior [86]. It is inevitable for NMs to cause nanotoxic effects due to their nanoscale size and high surface activity. Thus, prior to their in vitro and in vivo applications, biocompatibility, biodistribution, bioelimination, and environmental impact, as well as their nanotoxicity should be assessed [87].

11. CONCLUSION

Biomedical engineering has been developed to facilitate restoration of normal biological function of the

damaged tissues or organs. Regenerative medicine as a branch of biomedical engineering has attracted considerable attention concerning replacement or reconstruction of the injured cells and tissues in order to improve the life quality of the affected individuals. Introduction of nanotechnology to the regenerative studies remarkably improved the relevant investigations and advanced the tissue regeneration approaches towards obtaining low-cost long-lasting nanoscale scaffolds to be further applied in clinical practices. In many cases, the nanomaterial-based tissue regeneration process exhibited higher efficacy than the conventional artificial or animal-derived grafts facing some issues related to high costs, infection probability, inflammatory responses, immune responses, and need for replacement after a time period. Overall, nanomaterial-based tissue regeneration have brought promising results in tissue regeneration and repair of the damaged tissues of the bone, skin, tooth, cardiovascular disorders, neurological diseases, and abnormality of bladder tissue. Of note, one should be cautious that the nanotechnology in regenerative medicine is still in its early stages, and further research studies are required to broaden its applications from laboratories to clinics and the market.

ACKNOWLEDGEMENTS

I would like to thank Azarbaijan Shahid Madani University for financial support of this work.

NOMENCLATURE

AD	Alzheimer's disease
ADV	Acoustic Droplet Vaporization
ALDR	Autologous Lamellar Dermal Regeneration
AMI	Acute Myocardial Infarction
AuNPs	Gold Nanoparticles
BP	Black Phosphorous
BPQDs	Black Phosphorous Quantum Dots
C. elegans	Caenorhabditis elegans
CDK	Cyclin Dependent Kinase
CNS	Central Nervous System
CNTs	Carbon Nanotubes
CS	Chitosan Scaffold
ECM	Extracellular Matrix
FDA	Food And Drug Administration
HA	Hydroxyapatite
HD	Huntington's Disease
HNSS	Hollow Nanometer Silica Structures
HPDA	Hollow Polydopamine
IL	Interleukin
LbL	Layer-by-Layer
MBs	Microbubbles
NBs	Nanobubbles
NCs	Nanocapsules
NDs	Nanodroplets
NGA	Nano Genome Atlas
NMs	Nanomaterials
NNI	National Nanotechnology Initiative
NPs	Nanoparticles

NSC	Neural Stem Cell
NSTC	National Science And Technology Council
PCB	Poly(carboxybetaine)
PCL	Poly(ϵ -caprolactone)
PDLSC	Periodontal Ligament Stem Cells
PDT	Photodynamic Therapy
PLGA	Poly (lactic-co-glycolic) acid
PLGA	Poly-dl-Lactide-co-Glycolide
PLGA-PEG	Poly(lactide-co-glycolide)-block-poly(ethylene glycol)
PLLA	Poly(L-lactide)
PSCs	Pluripotent Stem Cells
PTT	Photothermal Therapy
PU	Polyurethane
QDs	Quantum Dots
ROS	Reactive Oxygen Species
SCI	Spinal Cord Injury
TBI	Traumatic Brain Injury
TE	Tissue Engineering
Ti	Titanium
TiO ₂	Titanium Dioxide
TIDE	Titanium Inductively Coupled Plasma Etching
UTMD	Ultrasound-Centered Microbubble Destruction

REFERENCES

- Gong, T., Xie, J., Liao, J., Zhang, T., Lin, S., Lin, Y., "Nanomaterials and Bone Regeneration", *Bone Research*, Vol. 3., No. 1, (2015), 15029. <https://doi.org/10.1038/boneres.2015.29>
- Babuska, V., Kasi, P. B., Chocholata, P., Wiesnerova, L., Dvorakova, J., Vrzakova, R., Neklionova, A., Landsmann, L., Kulda, V., "Nanomaterials in Bone Regeneration", *Applied Sciences*, Vol. 12, No. 13, (2022), 6793. <https://doi.org/10.3390/app12136793>
- Verma, S., Domb, A. J., Kumar, N., "Nanomaterials for Regenerative Medicine", *Nanomedicine*, Vol. 6, No. 1, (2011), 157-181. <https://doi.org/10.2217/nmm.10.146>
- Mitchell, M. J., Billingsley, M. M., Haley, R. M., Wechsler, M. E., Peppas, N. A., Langer, R., "Engineering Precision Nanoparticles for Drug Delivery", *Nature Reviews Drug Discovery*, Vol. 20, No. 2, (2021), 101-124. <https://doi.org/10.1038/s41573-020-0090-8>
- Liu, X. L., Chen, S., Zhang, H., Zhou, J., Fan, H. M., Liang, X. J., "Magnetic Nanomaterials for Advanced Regenerative Medicine: the Promise and Challenges", *Advanced Materials*, Vol. 31, No. 45, (2019), 1804922. <https://doi.org/10.1002/adma.201804922>
- Bellu, E., Medici, S., Coradduzza, D., Cruciani, S., Amler, E., Maioli, M., "Nanomaterials in Skin Regeneration and Rejuvenation", *International Journal of Molecular Sciences*, Vol. 22, No. 13, (2021), 7095. <https://doi.org/10.3390/ijms22137095>
- Engel, E., Michiardi, A., Navarro, M., Lacroix, D., Planell, J. A., "Nanotechnology in Regenerative Medicine: the Materials Side", *Trends in Biotechnology*, Vol. 26, No. 1, (2008), 39-47. <https://doi.org/10.1016/j.tibtech.2007.10.005>
- Bozorgi, A., Khazaei, M., Soleimani, M., Jamalpoor, Z., "Application of Nanoparticles in Bone Tissue Engineering; A Review on the Molecular Mechanisms Driving Osteogenesis", *Biomaterials Science*, Vol. 9, No. 13, (2021), 4541-4567. <https://doi.org/10.1039/D1BM00504A>
- Li, Y., Liu, C., "Nanomaterial-Based Bone Regeneration", *Nanoscale*, Vol. 9, No. 15, (2017), 4862-4874. <https://doi.org/10.1039/C7NR00835J>
- Li, G., Zhou, T., Lin, S., Shi, S., Lin, Y., "Nanomaterials for Craniofacial and Dental Tissue Engineering", *Journal of Dental Research*, Vol. 96, No. 7, (2017), 725-732. <https://doi.org/10.1177/0022034517706678>
- Huang, J., Chen, Y., Tang, C., Fei, Y., Wu, H., Ruan, D., Paul, M. E., Chen, X., Yin, Z., Heng, B. C., "The Relationship between Substrate Topography and Stem Cell Differentiation in the

- Musculoskeletal System”, *Cellular and Molecular Life Sciences*, Vol. 76, No. 3, (2019), 505-521. <https://doi.org/10.1007/s00018-018-2945-2>
12. Khang, D., Carpenter, J., Chun, Y. W., Pareta, R., Webster, T. J., “Nanotechnology for Regenerative Medicine”, *Biomedical Microdevices*, Vol. 12, No. 4, (2010), 575-587. <https://doi.org/10.1007/s10544-008-9264-6>
 13. Yun'an Qing, R. L., Li, S., Li, Y., Wang, X., Qin, Y., “Advanced Black Phosphorus Nanomaterials for Bone Regeneration”, *International Journal of Nanomedicine*, Vol. 15, (2020), 2045. <https://doi.org/10.2147/IJN.S246336>
 14. Yao, C., Slamovich, E. B., Webster, T. J., “Enhanced Osteoblast Functions on Anodized Titanium with Nanotube-Like Structures”, *Journal of Biomedical Materials Research Part A: An Official Journal of the Society for Biomaterials, the Japanese Society for Biomaterials, and the Australian Society for Biomaterials and the Korean Society for Biomaterials*, Vol. 85, No. 1, (2008), 157-166. <https://doi.org/10.1002/jbm.a.31551>
 15. Agour, M., Abdal-Hay, A., Hassan, M. K., Bartnikowski, M., Ivanovski, S., “Alkali-Treated Titanium Coated with a Polyurethane, Magnesium and Hydroxyapatite Composite for Bone Tissue Engineering”, *Nanomaterials*, Vol. 11, No. 5, (2021), 1129. <https://doi.org/10.3390/nano11051129>
 16. Serrano-Aroca, A., Cano-Vicent, A., I Serra, R. S., El-Tanani, M., Aljabali, A., Tambuwala, M. M., Mishra, Y. K., “Scaffolds in the Microbial Resistant Era: Fabrication, Materials, Properties and Tissue Engineering Applications”, *Materials Today Bio*, (2022), 100412. <https://doi.org/10.1016/j.mtbio.2022.100412>
 17. Webster, T. J., Ejiolor, J. U., “Increased Osteoblast Adhesion on Nanophase Metals: Ti, Ti₆Al₄V, and CoCrMo”, *Biomaterials*, Vol. 25, No. 19, (2004), 4731-4739. <https://doi.org/10.1016/j.biomaterials.2003.12.002>
 18. Khang, D., Lu, J., Yao, C., Haberstroh, K.M., Webster, T.J., “The Role of Nanometer and Sub-Micron Surface Features on Vascular and Bone Cell Adhesion on Titanium”, *Biomaterials*, Vol. 29, No. 8, (2008), 970-983. <https://doi.org/10.1016/j.biomaterials.2007.11.009>
 19. Rathee, G., Bartwal, G., Rathee, J., Mishra, Y. K., Kaushik, A., Solanki, P. R., “Emerging Multimodal Zirconia Nanosystems for High-Performance Biomedical Applications”, *Advanced NanoBiomed Research*, Vol. 1, No. 9, (2021), 2100039. <https://doi.org/10.1002/anbr.202100039>
 20. Sarkar, P., Ghosal, K., Chakraborty, D., Sarkar, K., “Chapter 20 - Biocompatibility and Biomedical Applications of Various Carbon-Based Materials”, In Thomas, S., Sarathchandran, C., Ilangoan, S. A., Moreno-Piraján, J. C. (Eds.), *Handbook of Carbon-Based Nanomaterials*, Elsevier, Amsterdam, The Netherlands, (2021), 829-875. <https://doi.org/10.1016/B978-0-12-821996-6.00015-4>
 21. Zhang, B., Yan, W., Zhu, Y., Yang, W., Le, W., Chen, B., Zhu, R., Cheng, L., “Nanomaterials in Neural-Stem-Cell-Mediated Regenerative Medicine: Imaging and Treatment of Neurological Diseases”, *Advanced Materials*, Vol. 30, No. 17, (2018), 1705694. <https://doi.org/10.1002/adma.201705694>
 22. Liang, H., Jin, C., Ma, L., Feng, X., Deng, X., Wu, S., Liu, X., Yang, C., “Accelerated Bone Regeneration by Gold-Nanoparticle-Loaded Mesoporous Silica Through Stimulating Immunomodulation”, *ACS Applied Materials & Interfaces*, Vol. 11, No. 44, (2019), 41758-41769. <https://doi.org/10.1021/acsami.9b16848>
 23. Erezuma, I., Eufrazio-Da-Silva, T., Golafshan, N., Deo, K., Mishra, Y. K., Castilho, M., Gaharwar, A. K., Leeuwenburgh, S., Dolatshahi-Pirouz, A., Orive, G., “Nanoclay Reinforced Biomaterials for Mending Musculoskeletal Tissue Disorders”, *Advanced Healthcare Materials*, Vol. 10, No. 16, (2021), 2100217. <https://doi.org/10.1002/adhm.202100217>
 24. Pena-Paras, L., Maldonado-Cortes, D., Taha-Tijjerina, J., Irigoyen, M., Guerra, J., “Experimental Evaluation of the Tribological Behaviour of CeO₂ Nanolubricants Under Extreme Pressures”, In *IOP conference series: Materials Science and Engineering*, August 2018, IOP Publishing, Vol. 400, No. 7, (2018), 072003. <https://doi.org/10.1088/1757-899X/400/7/072003>
 25. Zhang, Y., Wang, P., Wang, Y., Li, J., Qiao, D., Chen, R., Yang, W., Yan, F., “Gold Nanoparticles Promote the Bone Regeneration of Periodontal Ligament Stem Cell Sheets Through Activation of Autophagy”, *International Journal of Nanomedicine*, Vol. 16, (2021), 61-73. <https://doi.org/10.2147/IJN.S282246>
 26. J Hill, M., Qi, B., Bayaniahangar, R., Araban, V., Bakhtiari, Z., Doschak, M. R., Goh, B. C., Shokouhimehr, M., Vali, H., Presley, J. F., Zadpoor, A. A., “Nanomaterials for Bone Tissue Regeneration: Updates and Future Perspectives”, *Nanomedicine*, Vol. 14, No. 22, (2019), 2987-3006. <https://doi.org/10.2217/nmm-2018-0445>
 27. Hajiali, H., Ouyang, L., Llopis-Hernandez, V., Dobre, O., Rose, F. R., “Review of Emerging Nanotechnology in Bone Regeneration: Progress, Challenges, and Perspectives”, *Nanoscale*, Vol. 13, No. 23, (2021), 10266-10280. <https://doi.org/10.1039/D1NR01371H>
 28. Sun, H., Wang, Y., He, T., He, D., Hu, Y., Fu, Z., Wang, Y., Sun, D., Wang, J., Liu, Y., “Hollow Polydopamine Nanoparticles Loading with Peptide RI-Qn15: A New Pro-Regenerative Therapeutic Agent for Skin Wounds”, *Journal of Nanobiotechnology*, Vol. 19, No. 1, (2021), 1-20. <https://doi.org/10.1186/s12951-021-01049-2>
 29. Trent, J., Kirsner, R. S., “Tissue Engineered Skin: Apligraf, A Bi-Layered Living Skin Equivalent”, *International Journal of Clinical Practice*, Vol. 52, No. 6, (1998), 408-413. <https://pubmed.ncbi.nlm.nih.gov/9894378/>
 30. Gholipour-Kanani, A., Mohsenzadegan, M., Fayyazi, M., Bahrami, H., Samadikuchaksaraei, A., “Poly (ε-Caprolactone)-Chitosan-Poly (Vinyl Alcohol) Nanofibrous Scaffolds for Skin Excisional and Burn Wounds in a Canine Model”, *IET Nanobiotechnology*, Vol. 12, No. 5, (2018), 619-625. <https://doi.org/10.1049/iet-nbt.2017.0115>
 31. Chong, E. J., Phan, T. T., Lim, I. J., Zhang, Y. Z., Bay, B. H., Ramakrishna, S., Lim, C. T., “Evaluation of Electrospun Pcl/Gelatin Nanofibrous Scaffold for Wound Healing and Layered Dermal Reconstitution”, *Acta Biomaterialia*, Vol. 3, No. 3, (2007), 321-330. <https://doi.org/10.1016/j.actbio.2007.01.002>
 32. Goonoo, N., Bhaw-Luximon, A., “7 - Nanomaterials Combination for Wound Healing And Skin Regeneration”, In Du Toit, L. C., Kumar, P., Choonara, Y. E., Pillay, V. (Eds.), *Advanced 3D-Printed Systems and Nanosystems for Drug Delivery and tissue Engineering*, Elsevier, (2020), 159-217. <https://doi.org/10.1016/B978-0-12-818471-4.00007-8>
 33. Mok, Z. H., Proctor, G., Thanou, M., “Emerging Nanomaterials for Dental Treatments”, *Emerging Topics in Life Sciences*, Vol. 4, No. 6, (2020), 613-625. <https://doi.org/10.1042/ETLS20200195>
 34. Vijay, R., Mendhi, J., Prasad, K., Xiao, Y., Macleod, J., Ostrikov, K. K., Zhou, Y., “Carbon Nanomaterials Modified Biomimetic Dental Implants for Diabetic Patients”, *Nanomaterials*, Vol. 11, No. 11, (2021), 2977. <https://doi.org/10.3390/nano11112977>
 35. Iviglia, G., Kargozar, S., Baino, F., “Biomaterials, Current Strategies, and Novel Nano-Technological Approaches for Periodontal Regeneration”, *Journal of Functional Biomaterials*, Vol. 10, No. 1, (2019), 3. <https://doi.org/10.3390/jfb10010003>
 36. Sreenivasalu, P. K. P., Dora, C. P., Swami, R., Jasthi, V. C., Shiroorkar, P. N., Nagaraja, S., Asdaq, S. M. B., Anwer, M. K., “Nanomaterials in Dentistry: Current Applications and Future Scope”, *Nanomaterials*, Vol. 12, No. 10, (2022), 1676. <https://doi.org/10.3390/nano12101676>
 37. Jandt, K. D., Watts, D. C., “Nanotechnology in Dentistry: Present and Future Perspectives on Dental Nanomaterials”, *Dental Materials*, Vol. 36, No. 11, (2020), 1365-1378. <https://doi.org/10.1016/j.dental.2020.08.006>
 38. Alphandéry, E., “Nanomaterials As Ultrasound Theragnostic Tools for Heart Disease Treatment/Diagnosis”, *International Journal of Molecular Sciences*, Vol. 23, No. 3, (2022), 1683. <https://doi.org/10.3390/ijms23031683>
 39. Guo, J., Yang, Z., Wang, X., Xu, Y., Lu, Y., Qin, Z., Zhang, L.,

- Xu, J., Wang, W., Zhang, J., Tang, J., "Advances in Nanomaterials for Injured Heart Repair", *Frontiers in Bioengineering and Biotechnology*, Vol. 9, (2021). <https://doi.org/10.3389/fbioe.2021.686684>
40. Cristallini, C., Vitale, E., Giachino, C., Rastaldo, R., "Nanoengineering in Cardiac Regeneration: Looking Back and Going Forward", *Nanomaterials*, Vol. 10, No. 8, (2020), 1587. <https://doi.org/10.3390/nano10081587>
 41. Samaroo, H. D., Lu, J., Webster, T. J., "Enhanced Endothelial Cell Density on Nitinol Surfaces with Sub-Micron to Nanometer Roughness", *International Journal of Nanomedicine*, Vol. 3, No. 1, (2008), 75-82. <https://doi.org/10.2147/ijn.s2384>
 42. Miller, D. C., Thapa, A., Haberstroh, K. M., Webster, T. J., "Endothelial and Vascular Smooth Muscle Cell Function on Poly (Lactic-Co-Glycolic Acid) with Nano-Structured Surface Features", *Biomaterials*, Vol. 25, No. 1, (2004), 53-61. [https://doi.org/10.1016/S0142-9612\(03\)00471-X](https://doi.org/10.1016/S0142-9612(03)00471-X)
 43. Miller, D. C., Haberstroh, K. M., Webster, T. J., "PLGA Nanometer Surface Features Manipulate Fibronectin Interactions for Improved Vascular Cell Adhesion", *Journal of Biomedical Materials Research Part A*, Vol. 81, No. 3, (2007), 678-684. <https://doi.org/10.1002/jbm.a.31093>
 44. Carpenter, J., Khang, D., Webster, T. J., "Nanometer Polymer Surface Features: the Influence on Surface Energy, Protein Adsorption and Endothelial Cell Adhesion", *Nanotechnology*, Vol. 19, No. 50, (2008), 505103. <https://doi.org/10.1088/0957-4484/19/50/505103>
 45. Lu, J., Rao, M. P., Macdonald, N. C., Khang, D., Webster, T. J., "Improved Endothelial Cell Adhesion and Proliferation on Patterned Titanium Surfaces with Rationally Designed, Micrometer to Nanometer Features", *Acta Biomaterialia*, Vol. 4, No. 1, (2008), 192-201. <https://doi.org/10.1016/j.actbio.2007.07.008>
 46. Cassani, M., Fernandes, S., Vrbosky, J., Ergir, E., Cavalieri, F., Forte, G., "Combining Nanomaterials and Developmental Pathways to Design New Treatments for Cardiac Regeneration: The Pulsing Heart of Advanced Therapies", *Frontiers in Bioengineering and Biotechnology*, Vol. 8, (2020), 323. <https://doi.org/10.3389/fbioe.2020.00323>
 47. Lowe, T. L., Agrahari, V., Kannan, R. M., Kannan, S., "Nanotechnology Enabled Regenerative Medicine for Neurological Disorders", *Advanced Drug Delivery Reviews*, Vol. 148, (2019), 1-2. <https://doi.org/10.1016/j.addr.2019.11.006>
 48. Kumar, R., Butreddy, A., Kommineni, N., Reddy, P. G., Bunekar, N., Sarkar, C., Dutt, S., Mishra, V. K., Aadil, K. R., Mishra, Y. K., "Lignin: Drug/Gene Delivery and Tissue Engineering Applications", *International Journal of Nanomedicine*, Vol. 16, (2021), 2419-2441. <https://doi.org/10.2147/IJN.S303462>
 49. Pourhassan-Moghaddam, M., Zarghami, N., Mohsenifar, A., Rahmati-Yamchi, M., Gholizadeh, D., Akbarzadeh, A., De La Guardia, M., Nejati-Koshki, K., "Watercross-Based Gold Nanoparticles: Biosynthesis, Mechanism of Formation and Study of their Biocompatibility in Vitro", *Micro & Nano Letters*, Vol. 9, No. 5, (2014), 345-350. <https://doi.org/10.1049/mnl.2014.0063>
 50. Stenudd, M., Sabelström, H., Frisén, J., "Role of Endogenous Neural Stem Cells in Spinal Cord Injury and Repair", *JAMA Neurology*, Vol. 72, No. 2, (2015), 235-237. <https://doi.org/10.1001/jamaneurol.2014.2927>
 51. Cardenas, D. D., Dalal, K., "Spinal Cord Injury Rehabilitation", *Physical Medicine and Rehabilitation Clinics of North America*, Elsevier Health Sciences, Vol. 25, No. 3, (2014), xv-xvi. <https://doi.org/10.1016/j.pmr.2014.06.001>
 52. Yasuda, A., Tsuji, O., Shibata, S., Nori, S., Takano, M., Kobayashi, Y., Takahashi, Y., Fujiyoshi, K., Hara, C. M., Miyawaki, A., Okano, H. J., Toyama, Y., Nakamura, M., Okano, H., "Significance of Remyelination By Neural Stem/Progenitor Cells Transplanted into the Injured Spinal Cord", *Stem Cells*, Vol. 29, No. 12, (2011), 1983-1994. <https://doi.org/10.1002/stem.767>
 53. Duan, H., Ge, W., Zhang, A., Xi, Y., Chen, Z., Luo, D., Cheng, Y., Fan, K. S., Horvath, S., Sofroniew, M. V., Cheng, L., Yang, Z., Sun, Y. E., Li, X., "Transcriptome Analyses Reveal Molecular Mechanisms Underlying Functional Recovery after Spinal Cord Injury", *Proceedings of the National Academy of Sciences*, Vol. 112, No. 43, (2015), 13360-13365. <https://doi.org/10.1073/pnas.1510176112>
 54. Ren, H., Han, M., Zhou, J., Zheng, Z. F., Lu, P., Wang, J. J., Wang, J. Q., Mao, Q. J., Gao, J. Q., Ouyang, H. W., "Repair of Spinal Cord Injury by Inhibition of Astrocyte Growth and Inflammatory Factor Synthesis Through Local Delivery of Flavopiridol in PIGA Nanoparticles", *Biomaterials*, Vol. 35, No. 24, (2014), 6585-6594. <https://doi.org/10.1016/j.biomaterials.2014.04.042>
 55. Fan, S., Zheng, Y., Liu, X., Fang, W., Chen, X., Liao, W., Jing, X., Lei, M., Tao, E., Ma, Q., Zhang, X., Guo, R., Liu, J., "Curcumin-Loaded PLGA-PEG Nanoparticles Conjugated with B6 Peptide for Potential Use in Alzheimer's Disease", *Drug Delivery*, Vol. 25, No. 1, (2018), 1091-1102. <https://doi.org/10.1080/10717544.2018.1461955>
 56. Zhang, R., Li, Y., Hu, B., Lu, Z., Zhang, J., Zhang, X., "Traceable Nanoparticle Delivery of Small Interfering Rna and Retinoic Acid with Temporally Release Ability to Control Neural Stem Cell Differentiation for Alzheimer's Disease Therapy", *Advanced Materials*, Vol. 28, No. 30, (2016), 6345-6352. <https://doi.org/10.1002/adma.201600554>
 57. Cong, W., Bai, R., Li, Y. F., Wang, L., Chen, C., "Selenium Nanoparticles as an Efficient Nanomedicine for the Therapy of Huntington's Disease", *ACS Applied Materials & Interfaces*, Vol. 11, No. 38, (2019), 34725-34735. <https://doi.org/10.1021/acsami.9b12319>
 58. Singh, V. K., Kalsan, M., Kumar, N., Saini, A., Chandra, R., "Induced Pluripotent Stem Cells: Applications in Regenerative Medicine, Disease Modeling, and Drug Discovery", *Frontiers in Cell and Developmental Biology*, Vol. 3, (2015), 2. <https://doi.org/10.3389/fcell.2015.00002>
 59. Lee, M., Liu, T., Im, W., Kim, M., "Exosomes from Adipose-Derived Stem Cells Ameliorate Phenotype of Huntington's Disease in Vitro Model", *European Journal of Neuroscience*, Vol. 44, No. 4, (2016), 2114-2119. <https://doi.org/10.1111/ejn.13275>
 60. Valenza, M., Chen, J. Y., Di Paolo, E., Ruozi, B., Belletti, D., Ferrari Bardile, C., Leoni, V., Caccia, C., Brillì, E., Di Donato, S., Boido, M. M., Vercelli, A., Vandelli, M. A., Forni, F., Cepeda, C., Levine, M. S., Tosi, G., Cattaneo, E., "Cholesterol-Loaded Nanoparticles Ameliorate Synaptic and Cognitive Function in Huntington's Disease Mice", *EMBO Molecular Medicine*, Vol. 7, No. 12, (2015), 1547-1564. <https://doi.org/10.15252/emmm.201505413>
 61. Sanai, N., Nguyen, T., Ihrie, R. A., Mirzadeh, Z., Tsai, H. H., Wong, M., Gupta, N., Berger, M. S., Huang, E., Garcia-Verdugo, J. M., Rowitch, D. H., Alvarez-Buylla, A., "Corridors of Migrating Neurons in the Human Brain and their Decline During Infancy", *Nature*, Vol. 478, No. 7369, (2011), 382-386. <https://doi.org/10.1038/nature10487>
 62. Zinger, A., Soriano, S., Baudo, G., De Rosa, E., Taraballi, F., Villapol, S., "Biomimetic Nanoparticles as a Theranostic Tool for Traumatic Brain Injury", *Advanced Functional Materials*, Vol. 31, No. 30, (2021), 2100722. <https://doi.org/10.1002/adfm.202100722>
 63. Qian, Y., Lin, H., Yan, Z., Shi, J., Fan, C., "Functional Nanomaterials in Peripheral Nerve Regeneration: Scaffold Design, Chemical Principles and Microenvironmental Remodeling", *Materials Today*, Vol. 51, (2021), 165-187. <https://doi.org/10.1016/j.mattod.2021.09.014>
 64. Javed, R., Ao, Q., "Nanoparticles in Peripheral Nerve Regeneration: A Mini Review", *Journal of Neurorestoratology*, Vol. 10, No. 1, (2022), 1-12. <https://doi.org/10.26599/JNR.2022.9040001>
 65. Salem, S. A., Rashidbenam, Z., Jasman, M. H., Ho, C. C. K., Sagap, I., Singh, R., Yusof, M. R., Haji Idrus, R. B., Ng, M. H., "Incorporation of Smooth Muscle Cells Derived from Human Adipose Stem Cells on Poly (Lactic-Co-Glycolic Acid) Scaffold for the Reconstruction of Subtotally Resected Urinary Bladder in

- Athymic Rats”, *Tissue Engineering and Regenerative Medicine*, Vol. 17, No. 4, (2020), 553-563. <https://doi.org/10.1007/s13770-020-00271-7>
66. Atala, A., “Tissue Engineering of Artificial Organs”, *Journal of Endourology*, Vol. 14, No. 1, (2000), 49-57. <https://doi.org/10.1089/end.2000.14.49>
67. Ayad, S., Boot-Handford, R., Humphries, M. J., Kadler, K. E., Shuttleworth, A., *The Extracellular Matrix Factsbook*, 2nd ed., Elsevier, (1998). <https://www.sciencedirect.com/book/9780120689118/the-extracellular-matrix-factsbook#book-description>
68. Kay, S., Thapa, A., Haberstroh, K. M., Webster, T. J., “Nanostructured Polymer/Nanophase Ceramic Composites Enhance Osteoblast and Chondrocyte Adhesion”, *Tissue Engineering*, Vol. 8, No. 5, (2002), 753-761. <https://doi.org/10.1089/10763270260424114>
69. Chun, Y. W., Khang, D., Haberstroh, K. M., Webster, T. J., “The Role of Polymer Nanosurface Roughness and Submicron Pores in Improving Bladder Urothelial Cell Density and Inhibiting Calcium Oxalate Stone Formation”, *Nanotechnology*, Vol. 20, No. 8, (2009), 085104. <https://doi.org/10.1088/0957-4484/20/8/085104>
70. Pattison, M. A., Wurster, S., Webster, T. J., Haberstroh, K. M., “Three-Dimensional, Nano-Structured PPGA Scaffolds for Bladder Tissue Replacement Applications”, *Biomaterials*, Vol. 26, No. 15, (2005), 2491-2500. <https://doi.org/10.1016/j.biomaterials.2004.07.011>
71. Armstead, A. L., Arena, C. B., Li, B., “Exploring the Potential Role of Tungsten Carbide Cobalt (WC-Co) Nanoparticle Internalization in Observed Toxicity Toward Lung Epithelial Cells in Vitro”, *Toxicology and Applied Pharmacology*, Vol. 278, No. 1, (2014), 1-8. <https://doi.org/10.1016/j.taap.2014.04.008>
72. Napierska, D., Thomassen, L. C., Rabolli, V., Lison, D., Gonzalez, L., Kirsch-Volders, M., Martens, J. A., Hoet, P. H., “Size-Dependent Cytotoxicity of Monodisperse Silica Nanoparticles in Human Endothelial Cells”, *Small*, Vol. 5, No. 7, (2009), 846-853. <https://doi.org/10.1002/sml.200800461>
73. Yang, H., Liu, C., Yang, D., Zhang, H., Xi, Z., “Comparative Study of Cytotoxicity, Oxidative Stress and Genotoxicity Induced by Four Typical Nanomaterials: The Role of Particle Size, Shape and Composition”, *Journal of Applied Toxicology*, Vol. 29, No. 1, (2009), 69-78. <https://doi.org/10.1002/jat.1385>
74. Cheng, H., Chawla, A., Yang, Y., Li, Y., Zhang, J., Jang, H. L., Khademhosseini, A., “Development of Nanomaterials for Bone-Targeted Drug Delivery”, *Drug Discovery Today*, Vol. 22, No. 9, (2017), 1336-1350. <https://doi.org/10.1016/j.drudis.2017.04.021>
75. Liu, L. Z., Ding, M., Zheng, J. Z., Zhu, Y., Fenderson, B. A., Li, B., Yu, J. J., Jiang, B. H., “Tungsten Carbide-Cobalt Nanoparticles Induce Reactive Oxygen Species, AKT, ERK, AP-1, NF- κ B, VEGF, and Angiogenesis”, *Biological Trace Element Research*, Vol. 166, No. 1, (2015), 57-65. <https://doi.org/10.1007/s12011-015-0331-6>
76. Albanese, A., Tang, P. S., Chan, W. C., “The Effect of Nanoparticle Size, Shape, and Surface Chemistry on Biological Systems”, *Annual Review of Biomedical Engineering*, Vol. 14, No. 1, (2012), 1-16. <https://doi.org/10.1146/annurev-bioeng-071811-150124>
77. Katz, E., Willner, I., “Integrated Nanoparticle-Biomolecule Hybrid Systems: Synthesis, Properties, and Applications”, *Angewandte Chemie International Edition*, Vol. 43, No. 45, (2004), 6042-6108. <https://doi.org/10.1002/anie.200400651>
78. Feng, X., Chen, A., Zhang, Y., Wang, J., Shao, L., Wei, L., “Application of Dental Nanomaterials: Potential Toxicity to the Central Nervous System”, *International Journal of Nanomedicine*, Vol. 10, No. 1, (2015), 3547-3565. <https://doi.org/10.2147/IJN.S79892>
79. Yi, H., Ur Rehman, F., Zhao, C., Liu, B., He, N., “Recent Advances in Nano Scaffolds for Bone Repair”, *Bone Research*, Vol. 4, No. 1, (2016), 16050. <https://doi.org/10.1038/boneres.2016.50>
80. Lee, C. M., Jeong, H. J., Yun, K. N., Kim, D. W., Sohn, M. H., Lee, J. K., Jeong, J., Lim, S. T., “Optical Imaging to Trace Near Infrared Fluorescent Zinc Oxide Nanoparticles Following Oral Exposure”, *International Journal of Nanomedicine*, Vol. 7, (2012), 3203-3209. <https://doi.org/10.2147/IJN.S32828>
81. Sun, J., Xie, G., “Tissue Distribution of Intravenously Administered Hydroxyapatite Nanoparticles Labeled With ¹²⁵I”, *Journal of Nanoscience and Nanotechnology*, Vol. 11, No. 12, (2011), 10996-11000. <https://doi.org/10.1166/jnn.2011.3956>
82. Wang, Y., Chen, Z., Ba, T., Pu, J., Chen, T., Song, Y., Gu, Y., Qian, Q., Xu, Y., Xiang, K., “Susceptibility of Young and Adult Rats to the Oral Toxicity of Titanium Dioxide Nanoparticles”, *Small*, Vol. 9, No. 9-10, (2013), 1742-1752. <https://doi.org/10.1002/sml.201201185>
83. Murphy, C. J., Gole, A. M., Stone, J. W., Sisco, P. N., Alkhalil, A. M., Goldsmith, E. C., Baxter, S. C., “Gold Nanoparticles in Biology: Beyond Toxicity to Cellular Imaging”, *Accounts of Chemical Research*, Vol. 41, No. 12, (2008), 1721-1730. <https://doi.org/10.1021/ar800035u>
84. Chen, L., Liu, J., Zhang, Y., Zhang, G., Kang, Y., Chen, A., Feng, X., Shao, L., “The Toxicity of Silica Nanoparticles to the Immune System”, *Nanomedicine*, Vol. 13, No. 15, (2018), 1939-1962. <https://doi.org/10.2217/nmm-2018-0076>
85. Oberdörster, G., Oberdörster, E., Oberdörster, J., “Nanotoxicology: an Emerging Discipline Evolving from Studies of Ultrafine Particles”, *Environmental Health Perspectives*, Vol. 113, No. 7, (2005), 823-839. <https://doi.org/10.1289/ehp.7339>
86. Wu, B., Li, Y., Nie, N., Xu, J., An, C., Liu, Y., Wang, Y., Chen, Y., Gong, L., Li, Q., Giusto, E., Bunpetch, V., Zhang, D., Ouyang, H. W., Zou, X. H., “Nano Genome Altas (NGA) of Body Wide Organ Responses”, *Biomaterials*, Vol. 205, (2019), 38-49. <https://doi.org/10.1016/j.biomaterials.2019.03.019>
87. Ye, G., Bao, F., Zhang, X., Song, Z., Liao, Y., Fei, Y., Bunpetch, V., Heng, B. C., Shen, W., Liu, H., Zhou, J., Ouyang, H., “Nanomaterial-Based Scaffolds for Bone Tissue Engineering and Regeneration”, *Nanomedicine*, Vol. 15, No. 20, (2020), 1995-2017. <https://doi.org/10.2217/nmm-2020-0112>



Materials and Energy Research Center

MERC

Contents lists available at [ACERP](#)

Advanced Ceramics Progress

Journal Homepage: www.acerp.ir

Advanced Ceramics Progress

Original Research Article

Green Synthesis of Silica Extracted from Rice Husk Ash

Nazli Aharipour^a, Ali Nemati^b, Adrine Malek Khachatourian^c, *^a MSc, Department of Materials Science and Engineering, Sharif University of Technology, Tehran, Tehran, Iran^b Professor, Department of Materials Science and Engineering, Sharif University of Technology, Tehran, Tehran, Iran^c Assistant Professor, Department of Materials Science and Engineering, Sharif University of Technology, Tehran, Tehran, Iran* Corresponding Author Email: khachatourian@sharif.edu (A. Malek Khachatourian)URL: https://www.acerp.ir/article_159416.html

ARTICLE INFO

ABSTRACT

Article History:

Received 22 september 2022

Received in revised form 5 October 2022

Accepted 24 October 2022

Keywords:

Rice Husk
Amorphous Silica
Agricultural Waste
Green Synthesis

There has been a significant rise in the scientific, technological, ecological, economic, and social popularity of applications of by-products or waste materials in various industries including the agricultural sector. A by-product of rice4 milling is Rice Husk (RH), which, when burned, produces Rice Husk Ash (RHA). RHA is considered an economically viable raw material used for developing silica-based products since it contains a significant amount of amorphous silica (between 85 and 95 percent). The current research aims to create a green process for producing silica powders from RHA, an inexpensive source rich in biocompatible silica. High-purity silica was successfully generated from RHA through alkaline extraction using the reflux technique and subsequent acidification. For this purpose, RH was burned in an electric furnace for five hours to create RHA at 700 °C. The obtained ash was washed with hydrochloric acid to eliminate the metallic impurities. The sodium silicate solution was then obtained by refluxing the acid-washed RHA in a NaOH solution. The final step was to precipitate silica from sodium silicate solution by adding hydrochloric acid to decrease the pH by 4. Characterizations made in general are Thermo-Gravimetric Analysis (TGA), X-Ray Fluorescence (XRF) for identifying the mineral contents of RHA, Fourier-Transform Infrared Spectroscopy (FTIR), X-Ray Diffraction (XRD), and Scanning Electron Microscopy (SEM). Simple, efficient, environmentally-friendly, and ideal for mass production are all attributes of the synthetic process.

<https://doi.org/10.30501/acp.2022.363265.1103>

1. INTRODUCTION

Silica (SiO₂), as an essential inorganic substance [1], has been used as a major precursor for many materials in applications such as industrial manufacturing, drug delivery, electronics, composites, packaging, ceramic materials, adsorption, biosensing, and catalytic applications [2,3]. Among the remarkable properties of pure SiO₂ are low toxicity, high chemical and physical

stability, and great surface chemistry properties that allow SiO₂ to be combined or functionalized with various functional species or molecules. While sodium silicate is the main source of SiO₂ production, it is the production mechanism that determines the energy waste, environmental effects, and purity of the final SiO₂ [4,5]. Both organic and inorganic materials can be used in SiO₂ production. Rice wheat and coffee husks, barley grass, corn cob, sugar can bagasse, and palm oil are the

Please cite this article as: Aharipour, N., Nemati, A., Malek Khachatourian, A., "Green Synthesis of Silica Extracted from Rice Husk Ash", *Advanced Ceramics Progress*, Vol. 8, No. 4, (2022), 15-20. <https://doi.org/10.30501/acp.2022.363265.1103>

2423-7485/© 2022 The Author(s). Published by MERC.

This is an open access article under the CC BY license (<https://creativecommons.org/licenses/by/4.0/>).

potential bio-sources from which sodium silicate can be extracted [6]. Plants acquire and collect SiO₂ in addition to lignin and cellulose, which is then utilized to cover the hard-material components of the plant such as the husk [7]. Ash left from rice husk (RH) burning may be one of the most important sources of making sodium silicate [8] because it is a prominent agriculture industry waste product [9,10]. RH is the hard outer cover of the rice kernel which is removed during the rice milling process [11]. On average, about 20 % of the produced paddy turns to husk on a weight basis [12-14]. The husk itself is mainly composed of lignin, silicon, other inorganic components, and a small quantity of protein. Upon burning RH, organic materials are broken down into carbon dioxide and water vapor, and the remaining ash is mostly of SiO₂ composition [15].

A large amount of RH, about 150 million metric tons per year, as a by-product is being produced worldwide [16]. Depending on the weather, types of rice, and location of the farmland, each ton of RH can yield 0.18 to 0.20 tons of ash [17]. Therefore, a proper waste utilization or disposal method should be adopted for this agricultural waste [10]. Depending on the components of RH, its decomposition time varies that eventually results in a huge amount of waste over time [8]. Moreover, its utilization as fodder should be avoided due to its high SiO₂ content [18]. In this regard, it could be a great alternative source for common methods for sodium silicate production [19] to be used to solve the problem of burying rice in fields [20].

It is possible to obtain sodium silicate solution from rice husk ash (RHA) through a low-temperature chemical process called alkaline extraction which is cost-effective and environmentally-friendly with low energy consumption, compared to other commercial SiO₂ manufacturing methods with multiple steps at high temperatures and pressure [7,10,21,22].

SiO₂ gel is generally produced from acidification of sodium silicate [4]. Amorphous SiO₂ has very low solubility at pH less than 10 [23]. At pH above 10, the solubility increases sharply. Such distinctive behavior allows us to extract pure SiO₂ through the alkaline extraction method and subsequent precipitation by decreasing the pH [6,17]. It turns out that alkali extraction is a practical method that provides a high SiO₂ yield [24,25] depending on the concentration of NaOH used for extraction as well as the type of acid used for pre-washing RHA before extraction. NaOH provides a slightly high SiO₂ yield that can be utilized even at low concentrations. In this study, 1 M NaOH solution used for extraction provided a SiO₂ yield of more than 85 % [23,26]. In addition, according to the literature, use of HCl to acidify sodium silicate solution and create SiO₂ gel results in final SiO₂ with high purity both in acid leaching and precipitation step. The chemical reaction of precipitation confirms the production of NaCl with high solubility in water which can be easily washed with

DI water [23,26,27]. A comparison of the acid-washed RHA with the unwashed one revealed that the percentage yield of the extracted SiO₂ was higher in the washed sample than that in the unwashed one [27]. A number of acids such as HCl, HNO₃, H₂SO₄, etc. can act as the leaching agents. According to several studies, hydrochloric acid is more effective as an RH leaching agent than its other types. Previous studies also confirmed its superiority as a leaching agent in generating high-purity amorphous SiO₂ with enhanced pozzolanic characteristics. Additionally, leaching of RH with hydrochloric acid can essentially eliminate the additional contaminants such as Al₂O₃, Fe₂O₃, CaO, and MgO from RH [17,23]. In this respect, leaching requires an acid concentration of at least 1 M. 1 M HCl which is reported as a suitable leaching agent for this purpose [28,29].

According to the literature, NaOH and HCl with the concentration of 1 M provide a high yield of SiO₂ from RHA, high metal impurity elimination (among inorganic acids), and with soluble and washable products (NaCl) in addition to the SiO₂ during the precipitation. These parameters are separately assessed in the previous studies [23,28,29]. In this paper, both NaOH and HCl solutions with the effective concentrations mentioned in different papers were used.

This study aims to efficiently extract pure SiO₂ with amorphous nature and uniform morphology from RHA waste as a raw material. This eco-friendly synthesis procedure has a high yield. The SiO₂ extraction has been through alkaline extraction (1 M NaOH), followed by selective precipitation and self-assembly of components by acid titration (1 M HCl) to achieve SiO₂ with high purity. The synthesis procedure as well as the physical and structural properties of the produced amorphous SiO₂ are thoroughly investigated in the following sections.

2. MATERIALS AND METHODS

2.1. Materials

The raw RH used in this study was obtained from an Iranian rice processing facility located in Mazandaran, Iran. The used chemicals were concentrated hydrochloric acid (HCl 37 %, Sigma-Aldrich), sodium hydroxide (NaOH, Merck), and deionized (DI) water.

2.2. Methods

In order to dispose of dust, RH was thoroughly washed with DI water and dried for 10 hours at 90 °C. According to the TGA results presented in the following section, the suitable temperature for burning RH is 700 °C. This temperature is also suitable to prevent crystalline SiO₂ formation [30]. Therefore, RH is combusted at 700 °C for five hours to produce RHA. The fundamental steps of the SiO₂ production are the SiO₂ extraction as sodium silicate solution and SiO₂ generation from the solution.

2.2.1. Acid Washing RHA

Five grams of RHA was mixed with 45 ml DI water and 1 M HCl solution dropwise until the pH reached 1. The suspension was stirred for 12 hours. Followed by filtering and washing with DI water, the metallic ions of the suspension were completely removed to maintain the neutral pH. The solid residue, acid-washed RHA, was dried in an oven at 90 °C for 12 hours. Then, ash was used as the primary component in the SiO₂ extraction process.

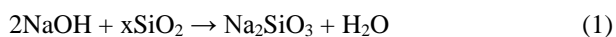
2.2.2 Silica Extraction as Sodium Silicate Solution

Four grams of RHA was added to 90 ml of 1 M sodium hydroxide (NaOH) solution. The sample was boiled in a covered Erlenmeyer flask for six hours with constant stirring to give enough time for soaking.

The solution was then filtered with filter paper. A tiny amount of boiling water was used to rinse the residue. The filtrate was then allowed to age for 19 hours while being cooled at room temperature.

2.2.3 Silica Precipitation

The obtained yellowish clear and transparent sodium silicate (Na₂SiO₃) solution was transformed into silicic acid (H₃SiO₄) by titration with 1 M hydrochloric acid under constant stirring to reach pH 4. Adding HCl to the obtained Na₂SiO₃ solution caused the formation and condensation of the Silanol group (R₃Si-OH). To remove the NaCl residue, the final product was rinsed with hot DI water. In case pH was < 10, SiO₂ gel started to precipitate. The slurry gained by introducing DI water to the gel was centrifuged three times for 10 minutes at 4000 rpm. The clear supernatants were discarded. The gel was dried at 70 °C for 14 h to get SiO₂ powder. The obtained powder was then washed and dried at the same temperature for five hours to wash the possible residual sodium [21]. The procedure is illustrated through the chemical reactions (1) and (2) [24]:



2.2.4 Materials Characterization Techniques

The following techniques were further used for characterization of the synthesized powder: Thermo-Gravimetric Analysis (TGA, Mettler Toledo), X-Ray Fluorescence (XRF, XEPOS), Fourier-Transform Infrared Spectroscopy (FT-IR, Perkin Elmer-Spectrum 65), X-Ray Diffractometer (XRD, PANalytical X'Pert Pro MPD), Field Emission Scanning Electron Microscope (FESEM, TESCAN company, MIRA3).

3. RESULTS AND DISCUSSION

3.1. TGA

TGA was accomplished with the air on the RH at the temperatures ranging from 25 to 800 °C. Figure 1 shows a graph of the weight changes of RH with regard to temperature. Three main steps are depicted in this graph. The first step is done in the temperature range of 145.58-26.48 °C with the weight loss of 5.22 %, the second step in the temperature range of 375.91-145.58 °C with the weight loss of 44.09 %, and the third step in the temperature range of 637.33-373.91 °C with the weight loss of 31.46 %. Therefore, it can be concluded that a total weight loss of 80.77 % leaves 19.19 % residual substance that represents the ash content.

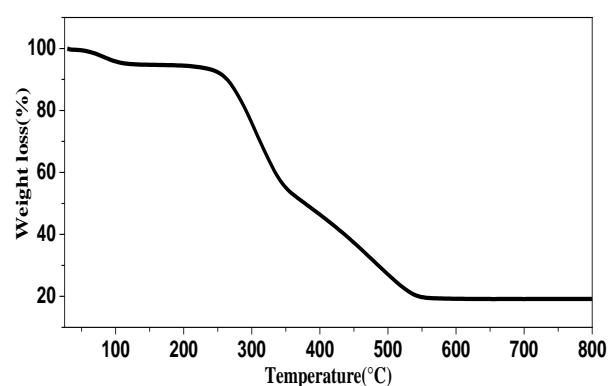


Figure 1. TGA graph of RH

Based on the temperature ranges of these steps, it can be concluded that the weight loss in the first step in the TG curve, which exhibits a weak endothermic response, can be attributed to RH's dehydration. The second weight loss is due to the release of organic and flammable materials. The third and final stage is related to carbonate and carbon decomposition associated with CO₂ emissions. However, at temperatures higher than 637.33 °C, no weight loss can be observed in the sample, indicating that the RH combustion is completed. Consequently, if we heat the husks at this temperature or higher temperatures, we can obtain RHA with relatively highly pure SiO₂ [31,32].

3.2. XRF

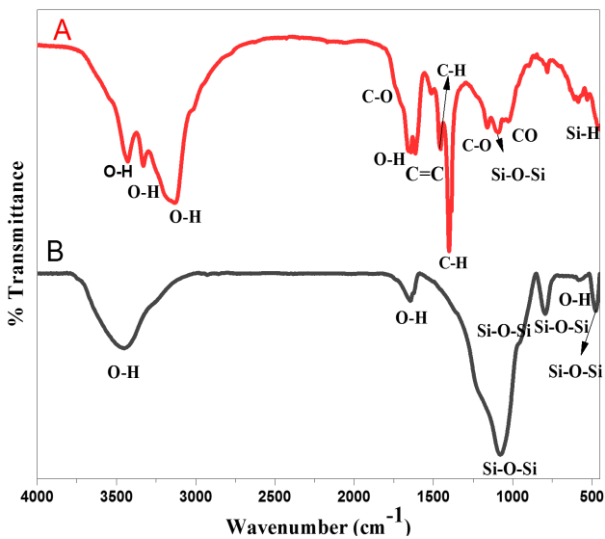
XRF test was carried out on RHA prepared at 850 °C. The percentages of oxide compositions of the available elements are tabulated in Table 1, where RHA has a high percentage of SiO₂, i.e., 89.40 wt. %.

3.3. FTIR

The samples as-received RH and extracted SiO₂ were investigated through FTIR. Figure 2 illustrates the FTIR spectra of RH and extracted SiO₂.

TABLE 1. Elements in RHA, in wt. %

Element	wt. %	Element	wt. %	Element	wt. %
SiO ₂	89.4	CoO	< 0.01	I	< 0.01
K ₂ O	1.94	NiO	< 0.01	La	< 0.01
CaO	0.87	CuO	< 0.01	Cs	< 0.01
P ₂ O ₅	0.64	Ga	< 0.01	Ba	< 0.01
SO ₃	0.5	Ge	< 0.01	Ce	< 0.01
MgO	0.45	As ₂ O ₃	< 0.01	Pr	< 0.01
Al ₂ O ₃	0.22	Se	< 0.01	Nd	< 0.01
Fe ₂ O ₃	0.13	Br	< 0.01	Hf	< 0.01
MnO	0.08	Rb ₂ O	< 0.01	Ta ₂ O ₅	< 0.01
Cl	0.04	Y	< 0.01	WO ₃	< 0.01
PbO	0.027	ZrO ₂	< 0.01	Hg	< 0.01
TiO ₂	0.02	Nb ₂ O ₅	< 0.01	Tl	< 0.01
Cr ₂ O ₃	0.01	Mo	< 0.01	Bi	< 0.01
SrO	0.01	Ag	< 0.01	Th	< 0.01
ZnO	0.01	Cd	< 0.01	U	< 0.01
Na ₂ O	< 0.01	SnO ₂	< 0.01		
V ₂ O ₅	< 0.01	Te	< 0.01		

**Figure 2.** FTIR spectra of (A) RH, (B) silica extracted from RHA

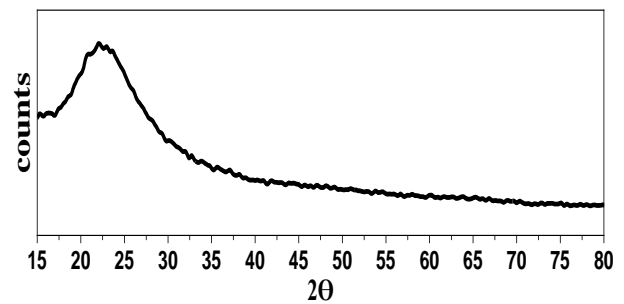
The FTIR spectra of the raw RH shows the peaks at around 3130-3517 cm⁻¹ (O-H group), 3015-2770 cm⁻¹ (C-H group), 1744 cm⁻¹ (C=O group), 1613 cm⁻¹ (C=C group), 1455-1401 cm⁻¹ (CH₂ and CH₃ groups), 1158 cm⁻¹ (CO group), and 953 cm⁻¹ reflected the Si-O-Si stretch vibration modes of the SiO₂, and 862.1-476.4 cm⁻¹ (Si-H group) [33,34]. In the FTIR spectra of the RH extracted SiO₂, the peaks related to the organic components disappeared as a result of RH combustion.

In addition, removal of inorganic elements from the

surface of the RH through base treatment and combustion resulted in the formation of SiO₂ functional group (Si-O-Si) of the RHA-extracted SiO₂ sample appearing more intense than that of the raw RH [35]. The wide peak in the range of 3000-3600 cm⁻¹ is attributed to the vibration of O-H functional groups of the water molecules adsorbed on the SiO₂ as moisture.

3.4. XRD

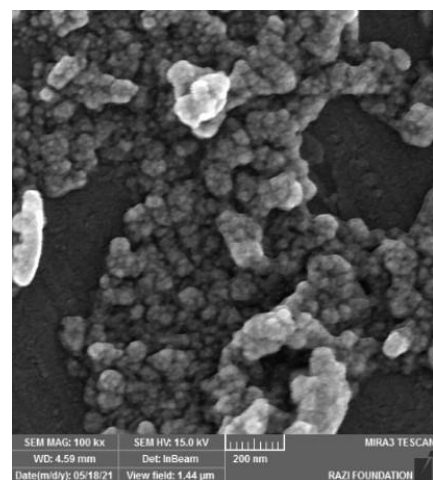
The crystalline structure of the extracted SiO₂ was analyzed using XRD. Figure 3 demonstrates the XRD pattern of RHA-extracted SiO₂.

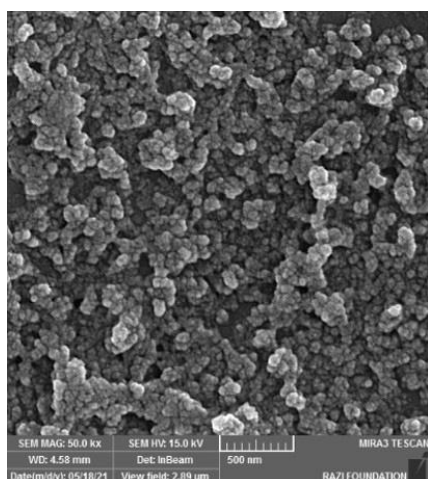
**Figure 3.** XRD pattern of RHA-extracted silica

In this figure, the obtained diffraction has no diffraction peak but a wide peak at $2\theta = 23^\circ$, which is considered a characteristic of amorphous SiO₂ [36], thus confirming the extraction and synthesis of amorphous SiO₂.

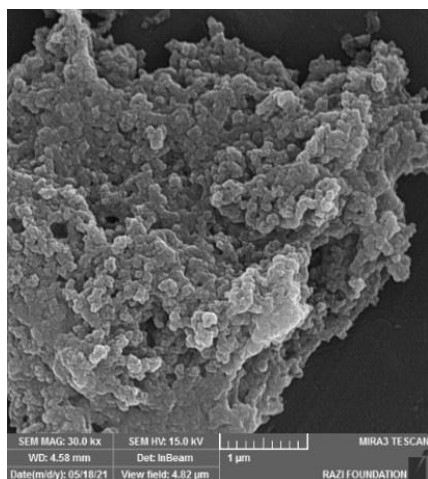
3.5. SEM

Based on FESEM, the morphology of the produced product was evaluated. Figure 4 depicts the FESEM images of SiO₂ extracted from RHA with different magnifications that show the agglomerated SiO₂ particles of spherical shape with the average particle size of 40 nm.

**(a)**



(b)



(c)

Figure 4. SEM images of alkaline-extracted silica with magnifications of (a) 100 kx, (b) 50 kx, and (c) 30 kx

4. CONCLUSION

In this study, a simple, low-cost, environmentally-friendly, and low-energy method was employed to produce SiO_2 from the abundantly-in-reach RHA called the alkaline extraction of SiO_2 from RHA and its precipitation through sodium silicate solution acidification. The obtained results revealed that RH was composed of a significant amount of SiO_2 . The best combustion temperature and duration to achieve carbon-free RHA were 700°C and five hours, respectively. The produced SiO_2 was amorphous with no unconventional functional group attached. In addition, the resulting SiO_2 particles were spherical in shape with the average size of 40 nm. Synthesized RHA extracted SiO_2 could be utilized as catalysts in chemical applications as

adsorbents as well as in other industries such as chromatograph packing columns, cosmetics, pharmaceuticals, paint and coating, etc.

ACKNOWLEDGEMENTS

The authors would like to acknowledge Sharif University of Technology for supporting this research.

REFERENCES

- Lu, P., Hsieh, Y. L., "Highly pure amorphous silica nano-disks from rice straw", *Powder Technology*, Vol. 225, (2012), 149-155. <https://doi.org/10.1016/j.powtec.2012.04.002>
- Liou, T. H., "Preparation and characterization of nano-structured silica from rice husk", *Materials Science and Engineering: A*, Vol. 364, No. 1-2, (2004), 313-323. <https://doi.org/10.1016/j.msea.2003.08.045>
- Moniri Javadhesari, S., Jabraili, M., Koochi, M., "A Review on the Application of Nanoparticles for Targeted Gene Delivery", *Advanced Ceramics Progress*, Vol. 8, No. 1, (2022), 44-55. <https://doi.org/10.30501/ACP.2022.345741.1091>
- Affandi, S., Setyawan, H., Winardi, S., Purwanto, A., Balgis, R., "A facile method for production of high-purity silica xerogels from bagasse ash", *Advanced Powder Technology*, Vol. 20, No. 5, (2009), 468-472. <https://doi.org/10.1016/j.appt.2009.03.008>
- Shojaeepour, F., Kazemzad Asiabi, M., Rahimpour, M. R., Khanlarkhani, A., "Pseudomorphic Reaction: A New Approach to Produce Bulk Mesoporous Silica as Catalyst Support in Methane Reforming", *Advanced Ceramics Progress*, Vol. 3, No. 4, (2017), 13-20. <https://doi.org/10.30501/acp.2017.90760>
- Porrang, S., Davaran, S., Rahemi, N., Allahyari, S., Mostafavi, E., "How Advancing are Mesoporous Silica Nanoparticles? A Comprehensive Review of the Literature", *International Journal of Nanomedicine*, Vol. 17, (2022), 1803-1827. <https://doi.org/10.2147/IJN.S353349>
- Molo, A. D. R. P., Susanti, E., Wonorahardjo, S., "Application of Silica Rice Husk Ash for Cellulase Immobilized By Sol-Gel Entrapment", *Scientific Study & Research Chemistry & Chemical Engineering, Biotechnology, Food Industry*, Vol. 22, No. 1, (2021), 47-55. <https://pubs.ub.ro/dwnl.php?id=CSCC6202101V01S01A0005>
- Costa, J. A. S., Paranhos, C. M., "Systematic evaluation of amorphous silica production from rice husk ashes", *Journal of Cleaner Production*, Vol. 192, (2018), 688-697. <https://doi.org/10.1016/j.jclepro.2018.05.028>
- Ajeel, S. A., Sukkar, K. A., Zedin, N. K., "Extraction of high purity amorphous silica from rice husk by chemical process", In *IOP Conference Series: Materials Science and Engineering*, IOP Publishing, Vol. 881, No. 1, (2020), 012096. <https://doi.org/10.1088/1757-899X/881/1/012096>
- Yue, D., Larock, R. C., "Synthesis of 2, 3-Disubstituted Benzo[b]thiophenes via Palladium-Catalyzed Coupling and Electrophilic Cyclization of Terminal Acetylenes", *The Journal of Organic Chemistry*, Vol. 67, No. 6, (2002) 1905-1909. <https://doi.org/10.1021/jo011016q>
- FAO, *FAO Rice Market Monitor (RMM)*, Vol. XXI, No. 1, (2018), 1-38. <https://www.fao.org/3/19243EN/i9243en.pdf> (Accessed: April 2018)
- Kamath, S. R., Proctor, A., "Silica gel from rice hull ash: Preparation and characterization", *Cereal Chemistry*, Vol. 75, No. 4, (1998), 484-487. <https://doi.org/10.1094/CCHEM.1998.75.4.484>
- Chakraverty, A., Kaleemullah, S., "Production of amorphous silica and combustible gas from rice straw", *Journal of Materials*

- Science*, Vol. 26, No. 17, (1991) 4554–4560. <https://doi.org/10.1007/BF00612389>
14. An, D., Guo, Y., Zhu, Y., Wang, Z., “A green route to preparation of silica powders with rice husk ash and waste gas”, *Chemical Engineering Journal*, Vol. 162, No. 2, (2010) 509–514. <https://doi.org/10.1016/j.cej.2010.05.052>
 15. Purwaningsih, H., Raharjo, S., Pratiwi, V. M., Susanti, D., Purniawan, A., “Porous silica nanomaterial derived from organic waste rice husk as highly potential drug delivery material”, In *Materials Science Forum*, Trans Tech Publications Ltd., Vol. 964, (2019), 88–96. <https://doi.org/10.4028/www.scientific.net/MSF.964.88>
 16. Kalapathy, U., Proctor, A., Shultz, J., “A simple method for production of pure silica from rice hull ash”, *Bioresource Technology*, Vol. 73, No. 3, (2000), 257–262. [https://doi.org/10.1016/S0960-8524\(99\)00127-3](https://doi.org/10.1016/S0960-8524(99)00127-3)
 17. Kwan, W. H., Wong, Y. S., “Acid leached rice husk ash (ARHA) in concrete: A review”, *Materials Science for Energy Technologies*, Vol. 3, (2020), 501–507. <https://doi.org/10.1016/j.mset.2020.05.001>
 18. Nayak, P. P., Nandi, S., Datta, A. K., “Comparative assessment of chemical treatments on extraction potential of commercial grade silica from rice husk”, *Engineering Reports*, Vol. 1, No. 2, (2019), e12035. <https://doi.org/10.1002/eng2.12035>
 19. Liu, Y., Guo, Y., Zhu, Y., An, D., Gao, W., Wang, Z., Ma, Y., Wang, Z., “A sustainable route for the preparation of activated carbon and silica from rice husk ash”, *Journal of Hazardous Materials*, Vol. 186, No. 2-3, (2011), 1314–1319. <https://doi.org/10.1016/j.jhazmat.2010.12.007>
 20. Conradt, R., Pimkhaokham, P., Leela-Adisorn, U., “Nano-structured silica from rice husk”, *Journal of Non-Crystalline Solids*, Vol. 145, (1992), 75–79. [https://doi.org/10.1016/S0022-3093\(05\)80433-8](https://doi.org/10.1016/S0022-3093(05)80433-8)
 21. Kalapathy, U., Proctor, A., Shultz, J., “A simple method for production of pure silica from rice hull ash”, *Bioresource Technology*, Vol. 73, No. 3, (2000), 257–262. [https://doi.org/10.1016/S0960-8524\(99\)00127-3](https://doi.org/10.1016/S0960-8524(99)00127-3)
 22. Fernandes, I. J., Calheiro, D., Sánchez, F. A., Camacho, A. L. D., Rocha, T. L. A. D. C., Moraes, C. A. M., Sousa, V. C. D., “Characterization of silica produced from rice husk ash: Comparison of purification and processing methods”, *Materials Research*, Vol. 20, (2017), 512–518. <https://doi.org/10.1590/1980-5373-MR-2016-1043>
 23. Dhaneswara, D., Fatriansyah, D., Situmorang, F. W., Haqoh, A. N., “Synthesis of Amorphous Silica from Rice Husk Ash: Comparing HCl and CH₃COOH Acidification Methods and Various Alkaline Concentrations”, *International Journal of Technology*, Vol. 11, No. 1, (2020), 200–208. <https://doi.org/10.14716/ijtech.v11i1.3335>
 24. Iler, R. K., *The Chemistry of Silica: Solubility, Polymerization, Colloid and Surface Properties and Biochemistry*, Wiley, New York, (1979). <https://doi.org/10.1002/ange.19800920433>
 25. Park, J. Y., Mun, W., Chun, J., Sang, B. I., Mitchell, R. J., Lee, J. H., “Alkali Extraction to Detoxify Rice Husk-Derived Silica and Increase Its Biocompatibility”, *ACS Sustainable Chemistry & Engineering*, Vol. 10, No. 24, (2022), 7811–7817. <https://doi.org/10.1021/acssuschemeng.2c01307>
 26. Haq, I. U., Akhtar, K., Malik, A., “Effect of experimental variables on the extraction of silica from the rice husk ash”, *Journal of the Chemical Society of Pakistan*, Vol. 36, No. 3, (2014), 382–387. https://www.researchgate.net/profile/Khalida-Akhtar/publication/286071234_Effect_of_Experimental_Variables_on_the_Extraction_of_Silica_from_the_Rice_Husk_Ash/link/s/569dd2a208aed27a702fe065/Effect-of-Experimental-Variables-on-the-Extraction-of-Silica-from-the-Rice-Husk-Ash.pdf
 27. Park, J. Y., Gu, Y. M., Park, S. Y., Hwang, E. T., Sang, B. I., Chun, J., Lee, J. H., “Two-stage continuous process for the extraction of silica from rice husk using attrition ball milling and alkaline leaching methods”, *Sustainability*, Vol. 13, No. 13, (2021), 7350. <https://doi.org/10.3390/su13137350>
 28. Azhakesan, A., Yadav, S., Rajesh, V. M., “Extraction of silica nanoparticles from Rice Husk Ash and its characterization”, *Journal of Scientific and Industrial Research*, Vol. 79, No. 7, (2020), 656–660. <https://inis.iaea.org/search/searchsinglerecord.aspx?recordsFor=SingleRecord&RN=51098508>
 29. Twej W. A., Shihab, B. F., “Enhancement in extraction silica percentage from Iraqi Jasmine Rice Husk through controlling leaching process”, *International Journal of Advanced Research in Science, Engineering and Technology*, Vol. 5, No. 7, (2018), 6406–6410. <https://www.ijarset.com/upload/2018/july/16-IJARSET-Wesam-1.pdf>
 30. Siddique, R., Kunal, Mehta, A., “11 - Utilization of industrial by-products and natural ashes in mortar and concrete development of sustainable construction materials”, In *Nonconventional and Vernacular Construction Materials Characterisation, Properties and Applications*, 2nd Ed., Edited by Harries, K. A., Sharma, B., Woodhead Publishing Series in Civil and Structural Engineering, Cambridge, UK, (2020), 247–303. <https://doi.org/10.1016/B978-0-08-102704-2.00011-1>
 31. Ahiduzzaman, M., Sadrul Islam, A. K. M., “Thermo-gravimetric and Kinetic Analysis of Different Varieties of Rice Husk”, *Procedia Engineering*, Vol. 105, (2015), 646–651. <https://doi.org/10.1016/j.proeng.2015.05.043>
 32. Alias, N., Ibrahim, N., Hamid, M. K. A., Hasbullah, H., Ali, R. R., Sadikin, A. N., Asli, U. A., “Thermogravimetric analysis of rice husk and coconut pulp for potential biofuel production by flash pyrolysis”, *The Malaysian Journal of Analytical Sciences*, Vol. 18, No. 3, (2014), 705–710. http://www.ukm.my/mjas/v18_n3/Noorhaza_18_3_27.pdf
 33. Kaur, P., Kaur, P., Kaur, K., “Adsorptive removal of imazethapyr and imazamox from aqueous solution using modified rice husk”, *Journal of Cleaner Production*, Vol. 244, (2020), 118699. <https://doi.org/10.1016/j.jclepro.2019.118699>
 34. Srivastava, V. C., Mall, I. D., Mishra, I. M., “Characterization of mesoporous rice husk ash (RHA) and adsorption kinetics of metal ions from aqueous solution onto RHA”, *Journal of Hazardous Materials*, Vol. 134, No. 1-3, (2006), 257–267. <https://doi.org/10.1016/j.jhazmat.2005.11.052>
 35. Asadi, F., Shariatmadari, H., Mirghaffari, N., “Modification of rice hull and sawdust sorptive characteristics for remove heavy metals from synthetic solutions and wastewater”, *Journal of Hazardous Materials*, Vol. 154, No. 1-3, (2008), 451–458. <https://doi.org/10.1016/j.jhazmat.2007.10.046>
 36. Nangir, M., Massoudi, A., Yazdani Rad, R., Tayebifard, S. A., “Optimization of the Nano-Porous Silicon Structures by Magnesiothermic Reduction of the As-Synthesized Silica”, *Advanced Ceramics Progress*, Vol. 2, No. 1, (2016), 32–37. <https://doi.org/10.30501/ACP.2016.70016>



Materials and Energy Research Center

MERC

Contents lists available at [ACERP](#)

Advanced Ceramics Progress

Journal Homepage: www.acerp.ir

Advanced Ceramics Progress

Original Research Article

Tailoring Bioactivity and Corrosion Properties of Plasma Electrolytic Oxidized Titanium Using GO-Silane Particles

Behnaz Hamrahi ^a, Benyamin Yarmand ^{b,*}, Abouzar Massoudi ^c^a PhD, Department of Nanotechnology and Advanced Materials, Materials and Energy Research Center, Karaj, Iran^b Associate Professor, Department of Nanotechnology and Advanced Materials, Materials and Energy Research Center, Karaj, Iran^c Assistant Professor, Department of Semiconductors, Materials and Energy Research Center, Karaj, Iran* Corresponding Author Email: byarmand@merc.ac.ir (B. Yarmand)URL: https://www.acerp.ir/article_161858.html

ARTICLE INFO

ABSTRACT

Article History:

Received 8 October 2022
 Received in revised form 15 November 2022
 Accepted 29 November 2022

Keywords:

GO-Silane
 Plasma Electrolytic Oxidation
 Titanium
 Bioactivity
 Corrosion

In this study, the effects of GO-silane particles embedded into the oxide coating during Plasma Electrolytic Oxidation (PEO) of titanium on the growth mechanism, bioactivity, and corrosion properties were investigated. The results revealed that participation of GO-silane particles in titanium oxidation reactions led to the preparation of the oxide coating at higher responding voltages as well as the predominance of rutile over anatase. Introduction of the maximum amount of 5 g.L⁻¹ of GO-silane particles decreased the oxide coating thickness by about 51 % and increased its surface roughness up to around 48 %. The bioactivity of the oxide coating was improved by embedding GO-silane particles and consequently, the amount of induced calcium phosphate compounds increased. Compared to titanium in normal and inflammatory simulated body fluid, pure PEO-treated titanium promoted the polarization resistance and expanded the passivation region. Followed by incorporation of the GO-silane particles into the oxide coating, the protective function was weakened, hence the possibility of tailoring the corrosion properties according to the clinical applications.


<https://doi.org/10.30501/acp.2022.364326.1106>

1. INTRODUCTION

Titanium alloys are widely used to produce dental and orthopedic implants. Their biological superiority originates from the formation of a natural bioinert layer in the human body. Therefore, unlike bioactive materials such as bioglass and calcium phosphate ceramics, titanium alloys cannot form bone at the interface with the surrounding tissues [1,2]. To date, several techniques have been used for the surficial biological activation of

titanium alloys, one of the newest of which is Plasma Electrolytic Oxidation (PEO) method. The PEO is a surface modification technique used for preparing oxide coatings which not only improves hardness, wear resistance, and chemical stability but provides a porous substrate for bone cell growth and proper implant adhesion. In this method, bioactive elements such as calcium, silicon, and strontium can be added to the structure of the oxide coating to promote its bioactivity [3-6].

Please cite this article as: Hamrahi, B., Yarmand, B., Massoudi, A., "Tailoring Bioactivity and Corrosion Properties of Plasma Electrolytic Oxidized Titanium Using GO-Silane Particles", *Advanced Ceramics Progress*, Vol. 8, No. 4, (2022), 21-31. <https://doi.org/10.30501/acp.2022.364326.1106>

2423-7485/© 2022 The Author(s). Published by MERC.

This is an open access article under the CC BY license (<https://creativecommons.org/licenses/by/4.0/>).

Silicon is the main element used for the proliferation and growth of connective tissues and bones and for this reason, the presence of silicon improves the bioactivity of implants as well as the proliferation of osteoblasts [7-9]. In the context of adding silicon to the PEO coatings, Zhao et al. [10] created the Si-doped TiO₂ coating. They reported that this coating promoted osteoblast adhesion, cell proliferation, and differentiation. In addition, they reported that the porous coating improved the initial stage of osseointegration and osteogenic ability of titanium implants in clinical performances. Yu et al. [11] studied the morphological changes of the PEO coatings prepared on Ti-6Al-4V in solutions containing calcium, phosphorus, strontium, and silicon ions. They found that addition of strontium and silicon increased the cell proliferation and bone-like apatite formation. In another study, Mumjitha et al. [12] prepared a TiO₂ coating that contained SiO₂ using sodium silicofluoride electrolyte. The immersion experiment in Simulated Body Fluid (SBF) clarified that compared to the pure TiO₂ coating, placement of SiO₂ could significantly promote bioactivity.

Carbon-based nanomaterials such as Graphene Oxide (GO) are a group of additives to PEO coatings capable of improving their properties greatly. Fattah-Alhosseini et al. reviewed the beneficial effects of graphene and GO additives on the corrosion properties and wear performance of the PEO coatings formed on titanium and magnesium [13,14]. Moreover, Chen et al. [15,16] reported that using graphene nanosheets in the silicate electrolyte promoted the corrosion behavior of magnesium and aluminum alloys. Zhao et al. [17] found that adding GO up to the optimum amount promoted the corrosion features of the PEO coating formed on magnesium. However, addition of excess amounts was found to weaken the corrosion resistance. Gao et al. [18] reported that upon adding GO to the PEO coating prepared on titanium, the corrosion features of the coating increased due to the blockage of the penetration path of corrosive ions. In another study, Bordbar-Khiabani et al. [19] found that followed by adding GO nanosheets to the coating prepared on titanium, the corrosion behavior would be significantly improved. Wen et al. [20] created an oxide coating containing HA/GO particles on magnesium using the PEO method. They reported enhancement in the corrosion properties of the oxide coating with particle placement and an increase in the polarization resistance. They also found that GO functional groups stimulated the biomineralization and bone regeneration.

This study aimed to investigate the effects of GO-silane particles on the growth of oxide coating on titanium using the PEO method for the first time. Moreover, the bioactivity and corrosion behavior of the prepared oxide coatings were evaluated in normal and inflammatory SBF.

2. MATERIALS AND METHODS

2.1. Synthesis of GO-Silane Particles

To synthesize GO-silane particles, GO nanosheets were produced through the modified Hummers method proposed in the previous work [19]. Silane particles were precipitated on the GO nanosheets through hydrolysis of tetraethyl orthosilicate. For this purpose, 30 mL of aqueous GO solution with the concentration of 0.4 g.mL⁻¹ was ultrasonically diluted with 300 mL of ethanol for 30 min. As a result, the pH of the solution increased up to 9 followed by adding ammonia. Next, 2 mL of tetraethyl orthosilicate was added to the previous solution and reacted ultrasonically for 1 h. The resulting precipitations were dried at 90 °C for 24 h.

2.2. Preparation of PEO Coatings

Commercially pure titanium was chosen as the substrate. The plate was cut in dimensions of 3 × 1 × 0.2 cm³ and polished with silicon carbide papers. The coupons were rinsed with ethanol and exposed to hot air. The PEO was run using an alternating current power supply. Here, titanium was considered the anode, and the stainless-steel tube the cathode. Oxidation was achieved for 10 min at the constant current of 200 mA.cm⁻² in an electrolyte of 10 g.L⁻¹ Na₃PO₄ and 2 g.L⁻¹ KOH. The electrolyte was kept uniform during oxidation using stirring. To create coatings containing GO-silane particles, specific amounts of additives were first added to the based electrolyte and then mixed. The samples containing 0, 1, 3, and 5 g.L⁻¹ GO-silane particles were coded S0, S1, S3, and S5, respectively. The sample conditions are presented in Table 1.

TABLE 1. The specifications of the samples and electrolytes

Sample	Na ₃ PO ₄ (g.L ⁻¹)	KOH (g.L ⁻¹)	GO-Silane (g.L ⁻¹)	Conductivity (mS.cm ⁻¹)	pH
S0	10	2	0	15.2	11.8
S1	10	2	1	14.6	12.1
S3	10	2	3	12.5	12.5
S5	10	2	5	11.4	12.6

2.3. Characterization Methods

The microstructure of the samples was studied using a Field Emission Scanning Electron Microscope (FESEM, TESCAN). The results from elemental analysis were then evaluated using Energy-Dispersive X-Ray Spectroscopy (EDS, OXFORD) at the accelerating voltage of 15 kV. The coating thickness was determined by measuring ten points via a Phynix thickness gauge. The coating roughness was measuring by determining six points at the center of the sample and three times in each of the horizontal and vertical axes using a Phynix contact roughness meter. Crystalline structure was characterized using Cu K α X-ray. Chemical bonds were detected

through Fourier Transform Infrared Spectroscopy (FTIR, Perkin Elmer).

2.4. In-vitro Bioactivity Experiment

The bioactivity test was done by immersing the specimens in the SBF. In this regard, the specimens were soaked vertically in a container containing 30 mL of SBF at 37 °C for 14 days based on Kokubo's method [21]. Thereafter, the specimens were rinsed, dried, and stored in a vacuum chamber.

2.5. Electrochemical Corrosion Test

Corrosion tests were conducted by a potentiostat galvanostat (EG & G) at 37 °C in both normal and inflammatory SBF. A standard cell with three electrodes was used for all corrosion tests. The Ag/AgCl electrode, the platinum plate, and samples were connected to the reference, auxiliary, and working electrodes, respectively. Then, 1 cm² of each specimen was exposed to the electrolyte. The potentiodynamic polarization experiment was performed in the limit potential of -1000 to 3000 mV compared to the open circuit potential with a sweep rate of 1 mV.s⁻¹, and the results were analyzed using CorrView software. The polarization resistance (R_p) was estimated based on Stern-Geary Equation (1), where β_c and β_a represent the cathodic and anodic slopes, respectively. These parameters were calculated by

extrapolating the potentiodynamic polarization graphs in the Tafel region. Inflammatory SBF was produced by adding 150 mM H₂O₂ and adjusting the pH at 5.2 using HCl solution.

$$R_p = \frac{\beta_a \times \beta_c}{2.3 \times i_{\text{corr}} \times (\beta_a + \beta_c)} \quad (1)$$

3. RESULTS AND DISCUSSION

3.1. Characterization of GO-Silane Particles

The microstructure of the synthesized GO and GO-silane particles is illustrated in Figures 1a and 1b. As observed in these figures, the GO particles have a layered microstructure. In the GO-silane, silane particles are almost densely and uniformly deposit on the carbon layers so that they cover the entire surface. Formation of the silane particles triggers use of hydrolysis and then condensation of the tetraethyl orthosilicate precursor and bonding with the oxygen groups of GO layers, thus leading to the nucleation and growth of particles. The EDS analysis presented in Figure 1c shows the presence of Si, O, and C, which confirms the synthesis and formation of the silane particles on the GO layers.

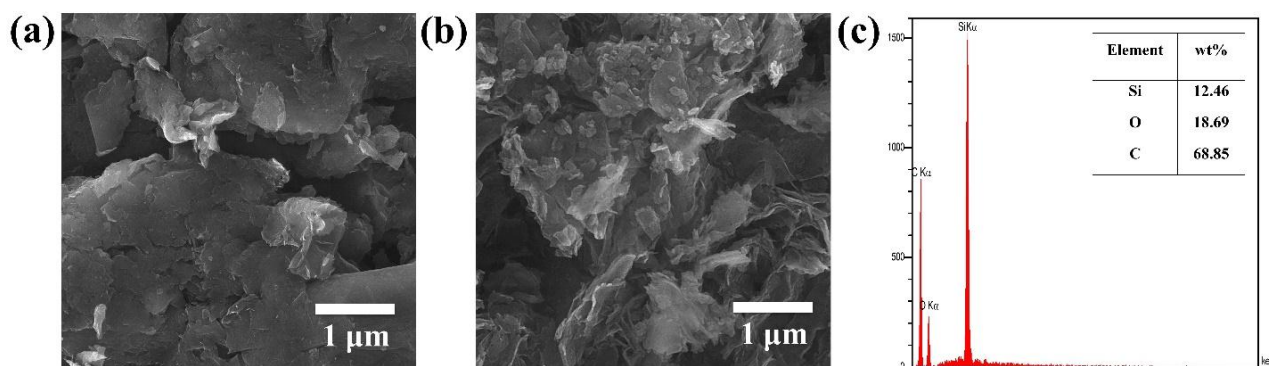


Figure 1. FESEM images of (a) GO and (b) GO-silane particles, and (c) EDS spectrum of GO-silane particles

The XRD patterns of the GO and GO-silane particles are illustrated in Figure 2a. In the XRD pattern of GO, only one sharp peak appears at 10.03° that corresponds to the (001) plane. This peak is very weak in the GO-silane pattern, which may be due to the destruction of the layered microstructure of GO during the synthesis of silane or the higher mass ratio of silane particles compared to GO. In the XRD pattern of GO-silane, a broad peak with low intensity appears at 24.3° that confirms the formation of silane with an amorphous structure [19,22]. The chemical bonds of GO and GO-silane particles detected by FTIR spectroscopy are displayed in Figure 2b where the C–O–C bands of the

epoxy group appear at 1067 cm⁻¹ and 1247 cm⁻¹ in the GO spectrum. In addition, the C=C and C=O bands of carboxylic groups are observed at 1635 and 1744 cm⁻¹, respectively, which are all characteristics of GO.

In addition, the broad O–H band concentrates at 3424 cm⁻¹, which can be due to the adsorbed moisture.

In the spectrum of the GO-silane, new peaks appear at 470, 824, and 1100 cm⁻¹, which belong to the Si–O–Si band that result from the self-condensation of the silane bonds. Moreover, Si–OH and Si–O–C bands are located at 973 and 1249 cm⁻¹, respectively. The appearance of these bands simultaneous with the removal of epoxy and carboxyl bands is indicative of the reaction of silane

bonds with the functional groups of GO. More detailed identification of GO and GO-silane chemical bonds is completed by Raman spectroscopy (Figure 2c). In both spectra, the D and G bands are located at 1355 and 1582 cm^{-1} , respectively. Furthermore, the 2D and D+G bands concentrate at 2700 and 2960 cm^{-1} , respectively.

The fitted intensity ratio (I_D/I_G) with the Lorentzian function increases from 0.90 in GO to 0.96 in GO-silane, indicating the formation of covalent bonding of silane particles with GO layers along with the slight destruction of the carbon network [19,23,24].

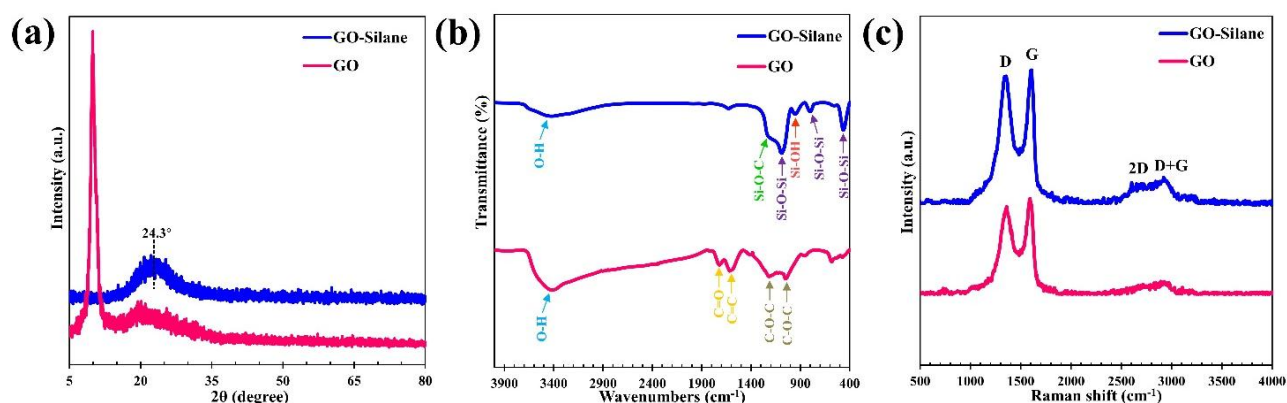


Figure 2. (a) XRD patterns, (b) FTIR, and (c) Raman spectra of GO and GO-silane particles

3.2. Responding Voltage During Oxidation

The responding voltage variations were studied to evaluate the effect of GO-silane particles on the formation mechanism of the oxide coating. Figure 3 shows the voltage changes as a function of process time for electrolytes containing different concentrations of GO-silane particles.

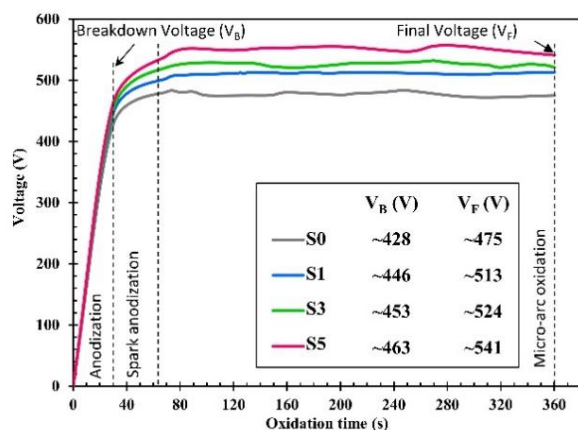


Figure 3. Voltage changes versus oxidation time

It is evident that the PEO process has three steps including the conventional anodization, spark anodization, and micro-arc oxidation [25]. In the first step, anodization occurs, which leads to a rapid linear increase in the voltage and involves the growth of a thin passive layer on titanium. The formation of the oxide layer occurs through the following reactions [26]:



It is found that the growth of the primary oxide layer on the anode involves the penetration of O^{2-} from the oxide network to the oxide/metal interface as well as the reduction of oxygen at the electrolyte/oxide interface [25,27]. Given that all the curves have the same growth rate in this step, it can be concluded that addition of GO-silane particles does not have a considerable effect on the preparation of the oxide layer in the anodization step. Upon further increasing the responding voltage, gaseous products are formed, and the titanium surface is covered with a layer of insulating gas. The gas layer is ionized due to the electric field that eventually leads to the plasma formation at the electrolyte/oxide interface. At the same time, the porous oxide layer grows until the power of the electric field reaches a critical value and dielectric breakdown occurs. The second step (spark anodization) begins with the appearance of micro-sparks as well as increase in the voltage drop. Dielectric breakdown first begins in local defects in the oxide layer and finally spreads over the entire surface. According to the experimental model of Ikonopisov [28], the breakdown voltage (V_B) when the first sparks appear depends on the conductivity of the electrolyte (σ), as observed in Equation (6) where a_B and b_B are the constants associated with the material.

$$V_B = a_B + b_B \log(1/\sigma) \quad (6)$$

The comparison of the curves in the second step reveals that the V_B enhances from 428 V in S0 to 446, 453, and 463 V in S1, S3, and S5, respectively. In addition, as shown in Table 1, with addition of the GO-silane particles, the electrolyte conductivity would decrease.

Followed by passing the V_B , the voltage rate slows down due to the occurrence of micro-sparks in a larger area of the oxide coating. In the third step (micro-arc oxidation), the responding voltage changes become more stable, and the oxide layer develops with repeated melting and freezing of the material. In fact, when the electric current passes through the discharge channel, some of the adjacent materials are melted and pushed out by the emitted gases. These substances will immediately freeze in contact with the electrolyte and accumulate in the opening of the channel and form the oxide layer. The micro-arc oxidation step has a similar process in all samples, and the responding voltage enhances with an increase in the number of GO-silane particles. The final voltage also changes according to the forming voltage [25,27].

3.3. Morphology and Chemical Analysis

The microstructure of the coatings is demonstrated in Figure 4. According to which, a rough oxide coating with many pores is created on the surface of all the specimens. The pores are originally formed due to the gas released by melting the compounds during the coating growth process. The frequent occurrence of micro-arcs and high energy discharges causes the local melting of the materials in the discharge channel, their eruption outside, and finally their rapid freezing by the cold electrolyte [27]. Introduction of GO-silane particles to the electrolyte changes the characteristics of pores as a result

of which, more pores with smaller sizes are formed in S5 compared to S0. The formation of different microstructural features originates from the variations in the electrochemical reactions during the coating growth process, hence occurrence of further relative changes.

The coating composition was evaluated using EDS, the results of which are illustrated in Figure 4. The results confirm that Ti, O, and P are present in all coatings. Ti and O are the results of the participation of the substrate in the electrochemical interactions with the electrolyte, which leads to the titanium oxidation. According to the Albella model, the presence of P in all the coatings results from the entry of anionic electrolyte species in the electrochemical processes due to their electric charge [26]. Si and C are present in S1, and their values increase in S3 and S5. These results confirmed the formation of titanium oxide in all the coatings as well as the proper placement of GO-silane particles. The elemental distribution of the coatings was checked using the EDS map of S5, the results of which are presented in Figure 5.

The analysis of the images revealed that all of the elements were uniformly distributed on the coating surface, and Si showed somewhat higher accumulation in the openings of the pores mainly due to the greater adsorption of GO-silane particles by electrostatic forces or their trapping in the eruptions of molten materials [4,27].

Figure 6 shows the FESEM cross-sectional microstructure of the specimens. As observed, all the coatings grew on the substrate surface without defects and gaps, hence well connected. The coating substrate interface in all samples is wavy that can be smoothed by increasing the concentration of GO-silane particles. This phenomenon occurs due to the non-uniform dissolution of titanium during electrochemical processes. A two-part microstructure, including the inner and outer sections, is

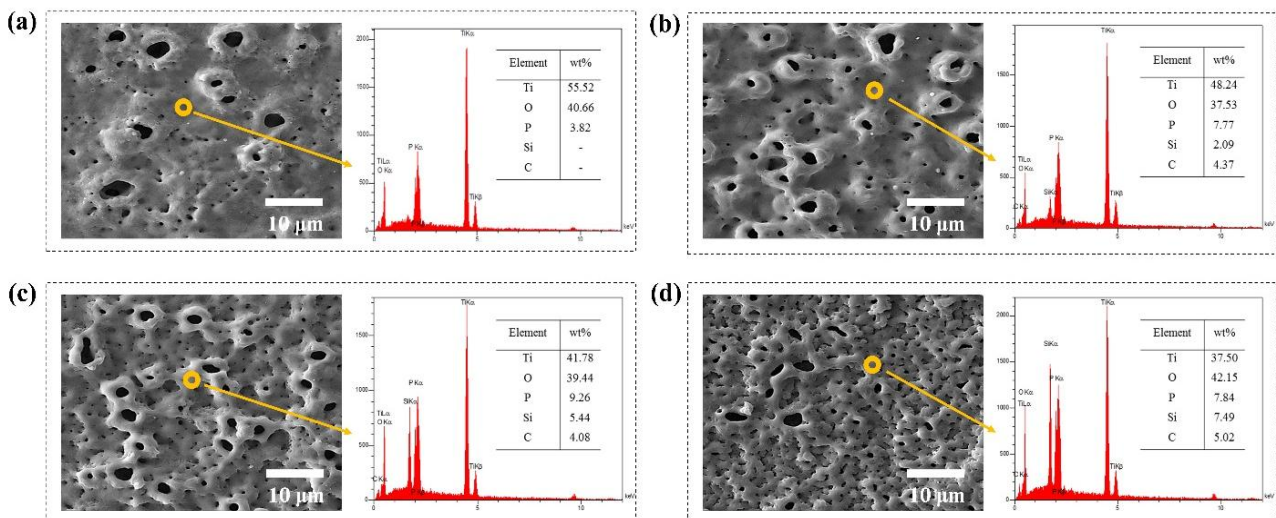


Figure 4. FESEM surface morphologies and corresponding EDS spectra of (a) S0, (b) S1, (c) S3, and (d) S5

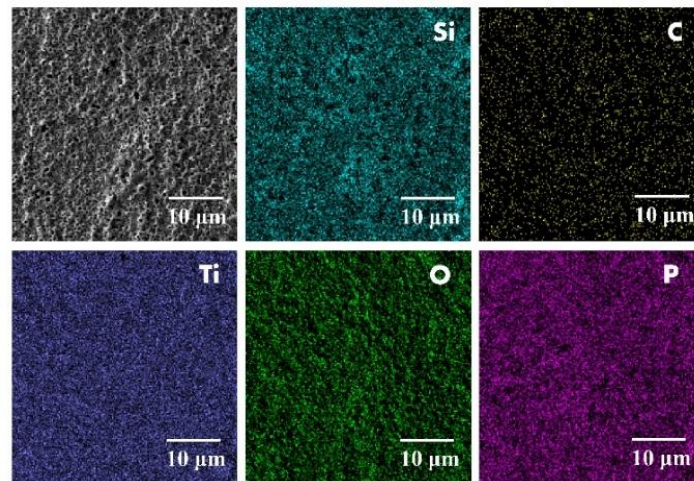


Figure 5. EDS elemental maps of S5

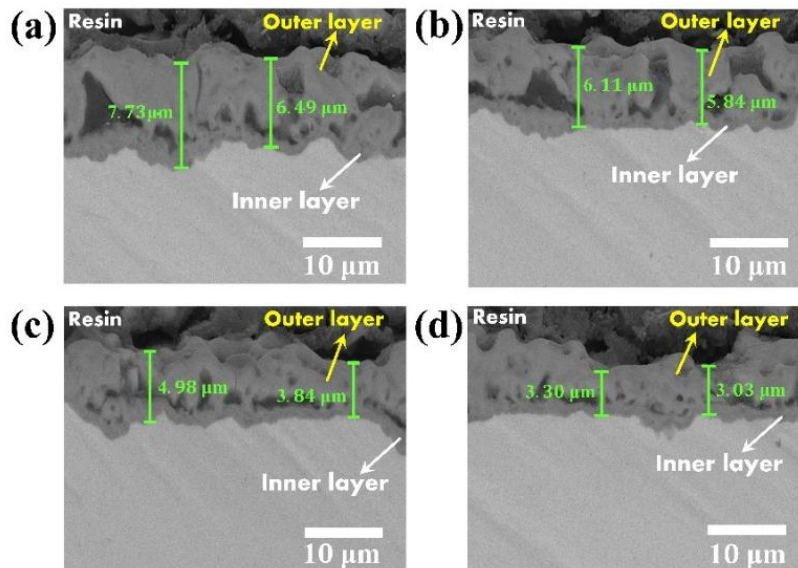


Figure 6. FESEM cross-sectional images of (a) S0, (b) S1, (c) S3, and (d) S5

observed in all of the coatings. The inner part that is less thick is in contact with titanium. The outer part is thicker than the inner part and therefore, it has more defects due to the occurrence of numerous micro-arcs. Upon increasing the concentration of GO-silane particles, the thickness of the coatings would decrease due to the change in the nature of the coating growth processes [27].

3.4. Thickness and Roughness

The thickness and roughness changes are displayed in Figure 7. According to the observations, upon increasing the concentration of the GO-silane particles, the thickness decreased from $7.18 \pm 0.87 \mu\text{m}$ in S0 to $3.55 \pm 0.38 \mu\text{m}$ in S5.

The surface roughness followed an upward trend, reaching the value from $0.56 \pm 0.06 \mu\text{m}$ in S0 to 0.83 ± 0.08

μm in S5. These results confirmed the FESEM observations.

In the PEO method, the oxide coating is repeatedly developed through the processes of local material melting, oxidation, and solidification due to micro-arcs occurring on the coating surface. In the case of the intensity enhancement of the micro-arcs, the resulting energy may destroy a large part of the previously formed oxide coating so that the amount of the new oxide layer cannot compensate for it. In this case, the growth rate of the layer was reduced, and smaller thickness values were obtained, similar to what happened in S1, S3, and S5. The increasing trend of roughness also confirmed the intensification of the oxide coating destruction processes, which is also in accordance with the responding voltage changes [25].

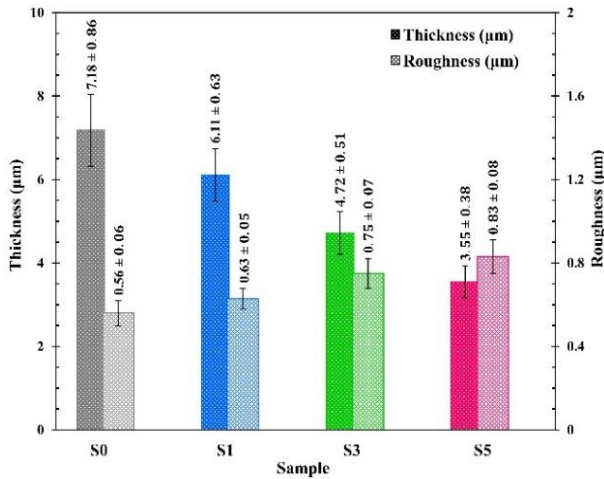


Figure 7. Thickness and surface roughness of the specimens

3.5. Crystal Structure

The XRD patterns of both S0 and S5 are demonstrated in Figure 8. The diffracted peaks were identified using the reference cards, clearly implying that the peaks attributed to anatase, rutile, and titanium appeared in both samples. According to JCPDS card no. 001-0562, the peaks located at 29.6°, 56.8°, 63.7°, and 65.1° correspond to (101), (200), (105), and (105) planes of anatase, respectively. According to JCPDS card no. 004-0551, the peak that appeared at 32.1° belongs to the (110) plane of rutile. In addition, the peaks centered at 41.1°, 44.9°, 47.2°, 62.5°, 74.6°, and 84.4° are attributed to (100), (002), (101), (102), (110), and (103) planes of titanium, respectively, according to JCPDS card no. 044-1294. In both patterns, the peaks related to the compounds containing Si and Ti are not detected, indicating that the GO-silane particles are placed in the TiO₂ structure without reacting.

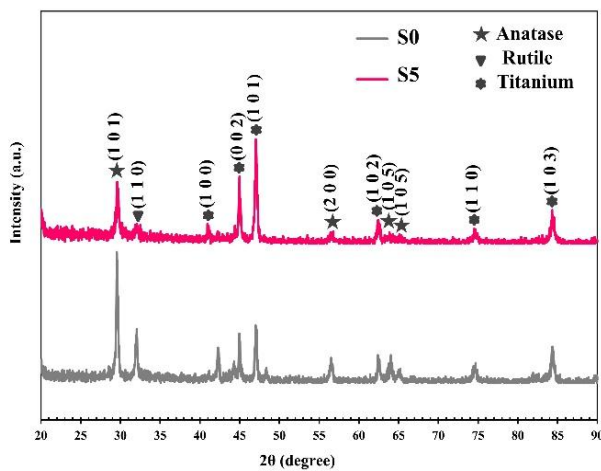


Figure 8. XRD patterns of S0 and S5

The intensity of the diffracted peaks in S5 decreased significantly, compared to those in S0, probably due to the crystal weakening of the oxide phases and reduction of the coating thickness. The volume ratio of anatase (X_A) and rutile (X_R) is estimated through the following relationships [29]:

$$X_A = \frac{1}{1 + 1.265(I_R/I_A)} \quad (7)$$

$$X_R = 1 - X_A \quad (8)$$

where I_R and I_A are the intensities of the characteristic (110) and (101) planes of rutile and anatase, respectively.

It was found that the ratio of anatase to rutile decreased from 0.79 in S0 to 0.51 in S5. The phase transformation of anatase to rutile can be affected by the change in the characteristics of micro-arcs and heat produced during the growth of the oxide coating. The local temperature increase inside the discharge channels may provide the thermodynamic conditions required for the phase transformation [25,27].

3.6. In-Vitro Bioactivity

The surface morphology of the coatings after 14 days of immersion in normal SBF is displayed in Figure 9. As observed, nanometer precipitations were formed in a tiny amount on S0. The number of precipitations rised with the enhancement in the concentration of GO-silane particles; therefore the largest number of precipitations is deposited in S5 in the form of relatively spherical agglomerated particles.

The EDS results presented in Figure 9 confirm that calcium phosphate compounds are formed on all of the coatings. The amount of calcium and phosphorus as well as their ratio (Ca/P) increased with an increase in the GO-silane concentration, hence improvement of the bioactivity of the coatings along with the better stability of calcium phosphate precipitations. An increase in the amount of calcium phosphate compounds resulted from embedding Si in the oxide coating, the triggering factor for precipitation. Indeed, Ti-OH and Si-OH functional groups with a negative charge are created on the surface of the coatings due to their placement in the SBF. These groups positively adsorb the charged calcium ions in the SBF and facilitate the formation of calcium compounds. Next, these calcium compounds bind with the negative phosphate ions and form calcium phosphate. When the nuclei of hydroxyapatite are created, they became a uniform and dense layer by adsorbing calcium and phosphorus ions of the SBF. Moreover, the rougher surface of the oxide coating can play an influential role in providing nucleation sites for precipitations. Therefore, it can be concluded that addition of the GO-silane particles to the PEO-treated titanium coating improves its bioactive feature, which will also lead to faster proliferation and growth of the bone cells [30-33].

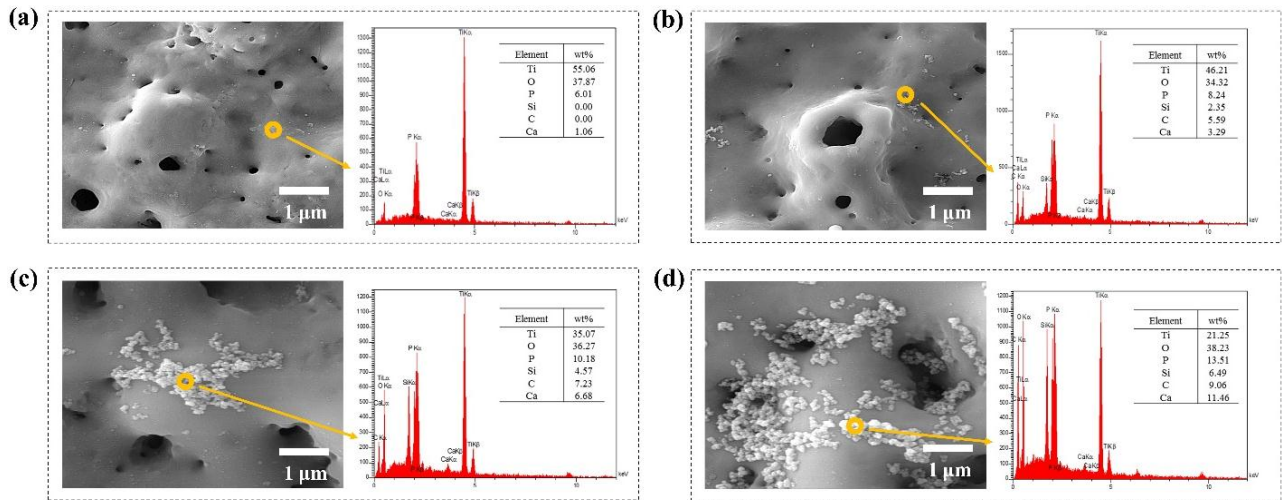


Figure 9. FESEM images and EDS spectra of (a) S0, (b) S1, (c) S3, and (d) S5 after immersion in normal SBF

3.7. Corrosion Properties

The corrosion properties of the specimens were investigated through the potentiodynamic polarization experiments at 37 °C in normal and inflammatory SBF. Figure 10 illustrates the potentiodynamic polarization graphs of the coatings as well as titanium. Corrosion characteristics estimated from the curves are presented in Table 2. A passive region is observed in all of the curves in the normal and inflammatory SBF.

The passive region for titanium in normal SBF ranges approximately from 239 to 1800 mV, which becomes wider with the preparation of PEO coating, S0 from -54 to 2102 mV, S1 from -105 to 2021 mV, S3 from -195 to 1950 mV, and S5 from -201 to 1770 mV. Since no coating failure is observed in any of the specimens, it can

be found that the coatings exhibit proper pitting corrosion resistance in normal SBF. The passive current density in S0 decreases by one order of magnitude compared to titanium; however, it increased slightly compared to S0 (Table 2) followed by adding the GO-silane particles. The lower values of the passive current density of the coatings are indicative of the improvement in their corrosion resistance, compared to titanium [34,35].

In addition, the comparison of the data in Table 2 showed that S0 was characterized by better corrosion features than those of titanium and consequently, the R_p increased from 23.47 up to 61.92 $k\Omega \cdot cm^2$ due to the protective power of the PEO coating, which prevents dissolution by blocking the path of corrosive ions toward the substrate.

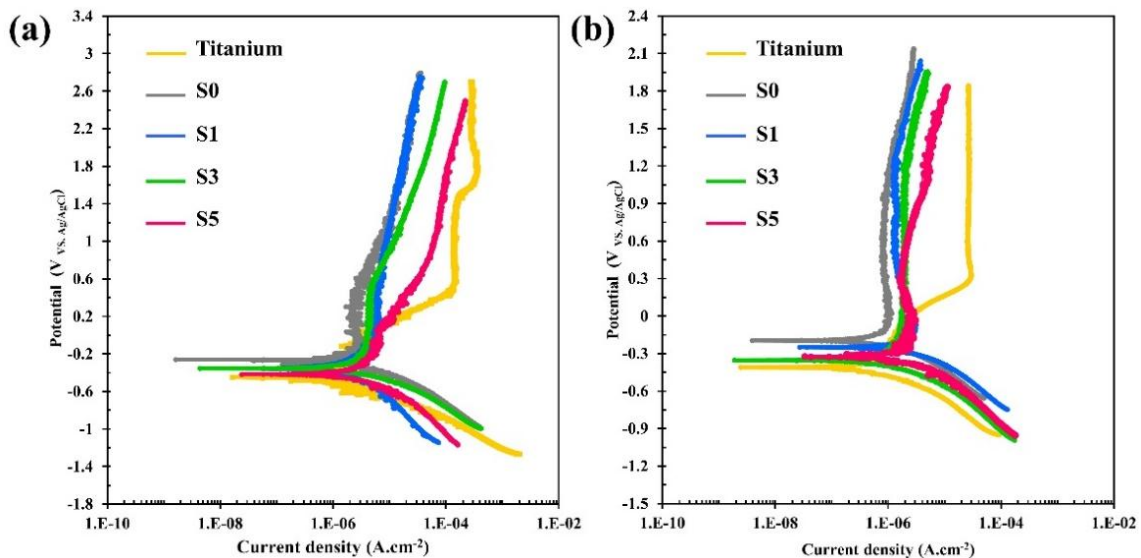


Figure 10. Potentiodynamic polarization graphs of the specimens in (a) normal and (b) inflammatory SBF

TABLE 2. Corrosion characteristics derived from potentiodynamic polarization graphs

Medium	Sample	E_{corr} (mV)	i_{corr} (A.cm ⁻²)	β_c (mV.dec ⁻¹)	β_a (mV.dec ⁻¹)	R_p (Ω .cm ²)	$I_{passive}$ (A.cm ⁻²)
Normal SBF	Ti	-408.85	2.21E-6	295.15	203.01	23470	2.57E-5
	S0	-194.84	1.24E-6	289.22	455.21	61920	7.28E-7
	S1	-249.28	3.27E-6	310.31	432.85	23990	1.33E-6
	S3	-353.26	4.11E-6	341.41	426.55	20030	1.84E-6
	S5	-350.11	4.74E-6	315.74	421.41	16530	1.34E-6
Inflammatory SBF	Ti	-474.28	4.89E-6	272.38	232.28	11130	1.32E-4
	S0	-258.58	3.56E-6	197.35	625.34	18290	2.40E-6
	S1	-360.11	5.21E-6	264.54	511.14	14520	4.12E-6
	S3	-351.26	6.10E-6	186.41	513.11	9730	3.97E-6
	S5	-416.21	6.85E-6	241.98	364.59	9210	4.71E-6

Followed by placing the GO-silane particles in the PEO coating, the corrosion characteristics will be degraded, indicating the deterioration of the stability of the coatings. This phenomenon can be directly caused by the reduction of the coating thickness, leading to less obstruction of the path of aggressive species. Moreover, an increase in the roughness is another influential factor because it increases the physical adsorption of corrosive ions [34,36,37].

In the polarization curve of titanium in inflammatory SBF, a narrower passive region appears from 442 to 1413 mV compared to normal SBF. In this region, an oxidation reaction starts at 1641 mV, and re-passivation occurs at 1955 mV. Such observations were already reported in the studies of Sowa et al. and Metikoš-Huković et al. during titanium polarization in Ringer's and Hanks' solutions, respectively [35,38]. In addition, the effect of inflammatory conditions on titanium includes shifting the corrosion potential to more negative values (from -408.85 to -474.28 mV) and increasing the corrosion current density (from 2.21E-6 to 4.89E-6 A.cm⁻²) along with the instability of the passive region.

Once the PEO coating is prepared, the R_p of titanium improved from 11130 to 18290 Ω .cm² in the inflammatory SBF, which is lower than the normal SBF.

The harsher conditions of the inflammatory medium made the passive region of the coatings become more unstable so that the coatings became passive at first and then, the passive layer failed. According to the reports of Yerokhin et al., this phenomenon resulted from the formation of metastable compounds due to the rapid melting and solidification of oxides during the PEO process.

These substances were subjected to oxidation or even degradation in the corrosive solution during the potentiodynamic polarization scan as a result of which, the thinning of the coating, which was intensified in the inflammatory SBF, occurred [27,39]. Reduction of the

corrosion rate by placing GO-silane particles in the coatings was also observed in the inflammatory SBF.

4. CONCLUSIONS

1. The intervention of the GO-silane particles in the processes of coating formation led to the intensification of micro-arcs as well as an increase in the responding voltage.
2. As a result of the rise in the energy from micro-arcs, the anatase-rutile transformation progressed.
3. Upon adding GO-silane particles, the coating thickness followed a decreasing trend while the coating surface roughness followed an increasing trend.
4. Placement of GO-silane particles induced the calcium phosphate precipitations on the oxide coating and improved its bioactivity.
5. Creation of the oxide coating on titanium led to different values of corrosion resistance in the normal and inflammatory SBF, thus making it possible to achieve features suitable for biological usages.

ACKNOWLEDGEMENTS

This research has been supported via grant No.: 247383 by Materials and Energy Research Center, Karaj, Iran.

REFERENCES

1. Matykina, E., Arrabal, R., Mingo, B., Mohedano, M., Pardo, A., Merino, M. C., "In vitro corrosion performance of PEO coated Ti and Ti6Al4V used for dental and orthopaedic implants", *Surface and Coatings Technology*, Vol. 307, (2016), 1255-1264. <https://doi.org/10.1016/j.surfcoat.2016.08.018>
2. Berbel, L. O., Banczek, E. D. P., Karoussis, I. K., Kotsakis, G. A., Costa, I., "Determinants of corrosion resistance of Ti-6Al-4V alloy dental implants in an In Vitro model of peri-implant

- inflammation”, *PLOS ONE*, Vol. 14, No. 1, (2019), e0210530. <https://doi.org/10.1371/journal.pone.0210530>
3. Hussein, R. O., Nie, X., Northwood, D. O., “The application of plasma electrolytic oxidation (PEO) to the production of corrosion resistant coatings on magnesium alloys: a review”, *Corrosion and Materials*, Vol. 38, No. 1, (2013), 55-65. <https://doi.org/10.1007/s11661-018-4824-8>
 4. Fattah-Alhosseini, A., Keshavarz, M. K., Molaei, M., Gashti, S. O., “Plasma electrolytic oxidation (PEO) process on commercially pure Ti surface: effects of electrolyte on the microstructure and corrosion behavior of coatings”, *Metallurgical and Materials Transactions A*, Vol. 49, No. 10, (2018), 4966-4979. <https://doi.org/10.1007/s11661-018-4824-8>
 5. Fattah-alhosseini, A., Molaei, M., Babaei, K., “The effects of nano-and micro-particles on properties of plasma electrolytic oxidation (PEO) coatings applied on titanium substrates: A review”, *Surfaces and Interfaces*, Vol. 21, (2020), 100659. <https://doi.org/10.1016/j.surfin.2020.100659>
 6. Aliofkhaezai, M., Macdonald, D. D., Matytkina, E., Parfenov, E. V., Egorin, V. S., Curran, J. A., Troughton, S. C., Sinebryukhov, S. L., Gnedenkov, S. V., Lampke, T., Simchen, F., “Review of plasma electrolytic oxidation of titanium substrates: Mechanism, properties, applications and limitations”, *Applied Surface Science Advances*, Vol. 5, (2021), 100121. <https://doi.org/10.1016/j.apsadv.2021.100121>
 7. Pietak, A. M., Reid, J. W., Stott, M. J., Sayer, M., “Silicon substitution in the calcium phosphate bioceramics”, *Biomaterials*, Vol. 28, No. 28, (2007), 4023-4032. <https://doi.org/10.1016/j.biomaterials.2007.05.003>
 8. Wang, B., Sun, J., Qian, S., Liu, X., Zhang, S., Liu, F., Dong, S., Zha, G., “Proliferation and differentiation of osteoblastic cells on silicon-doped TiO₂ film deposited by cathodic arc”, *Biomedicine & Pharmacotherapy*, Vol. 66, No. 8, (2012), 633-641. <https://doi.org/10.1016/j.biopha.2012.08.008>
 9. Toorani, M., Aliofkhaezai, M., Mahdavian, M., Naderi, R., “Effective PEO/Silane pretreatment of epoxy coating applied on AZ31B Mg alloy for corrosion protection”, *Corrosion Science*, Vol. 169, (2020), 108608. <https://doi.org/10.1016/j.corsci.2020.108608>
 10. Zhao, Q. M., Li, X. K., Guo, S., Wang, N., Liu, W.W., Shi, L., Guo, Z., “Osteogenic activity of a titanium surface modified with silicon-doped titanium dioxide”, *Materials Science and Engineering*, Vol. 110, (2020), 110682. <https://doi.org/10.1016/j.msec.2020.110682>
 11. Yu, J. M., Choe, H. C., “Morphology changes and bone formation on PEO-treated Ti-6Al-4V alloy in electrolyte containing Ca, P, Sr, and Si ions”, *Applied Surface Science*, Vol. 477, (2019), 121-130. <https://doi.org/10.1016/j.apsusc.2017.11.223>
 12. Mumjitha, M., Raj, V., “Fabrication of TiO₂-SiO₂ bioceramic coatings on Ti alloy and its synergetic effect on biocompatibility and corrosion resistance”, *Journal of the Mechanical Behavior of Biomedical Materials*, Vol. 46, (2015), 205-221. <https://doi.org/10.1016/j.jmbbm.2015.02.006>
 13. Fattah-alhosseini, A., Chaharmahali, R., “Enhancing corrosion and wear performance of PEO coatings on Mg alloys using graphene and graphene oxide additions: A review”, *FlatChem*, Vol. 27, (2021), 100241. <https://doi.org/10.1016/j.flatc.2021.100241>
 14. Fattah-alhosseini, A., Molaei, M., Nouri, M., Babaei, K., “Review of the role of graphene and its derivatives in enhancing the performance of plasma electrolytic oxidation coatings on titanium and its alloys”, *Applied Surface Science Advances*, Vol. 6, (2021), 100140. <https://doi.org/10.1016/j.apsadv.2021.100140>
 15. Chen, F., Zhang, Y., Zhang, Y., “Effect of graphene on microstructure and properties of MAO coating prepared on Mg-Li alloy”, *International Journal of Electrochemical Science*, Vol. 12, No. 7, (2017), 6081-6091. <https://doi.org/10.20964/2017.07.59>
 16. Chen, Q., Jiang, Z., Tang, S., Dong, W., Tong, Q., Li, W., “Influence of graphene particles on the micro-arc oxidation behaviors of 6063 aluminum alloy and the coating properties”, *Applied Surface Science*, Vol. 423, (2017), 939-950. <https://doi.org/10.1016/j.apsusc.2017.06.202>
 17. Zhao, J., Xie, X., Zhang, C., “Effect of the graphene oxide additive on the corrosion resistance of the plasma electrolytic oxidation coating of the AZ31 magnesium alloy”, *Corrosion Science*, Vol. 114, (2017), 146-155. <https://doi.org/10.1016/j.corsci.2016.11.007>
 18. Gao, Y., Yang, W., Xu, D., Chen, J., Jiang, B., “Microstructure and properties of graphene oxide-doped TiO₂ coating on titanium by micro arc oxidation”, *Journal of Wuhan University of Technology-Mater. Sci. Ed.*, Vol. 33, No. 6, (2018), 1524-1529. <https://doi.org/10.1007/s11595-018-2001-y>
 19. Bordbar-Khiabani, A., Ebrahimi, S., Yarmand, B., “Highly corrosion protection properties of plasma electrolytic oxidized titanium using rGO nanosheets”, *Applied Surface Science*, Vol. 486, (2019), 153-165. <https://doi.org/10.1016/j.apsusc.2019.05.026>
 20. Wen, C., Zhan, X., Huang, X., Xu, F., Luo, L., Xia, C., “Characterization and corrosion properties of hydroxyapatite/graphene oxide bio-composite coating on magnesium alloy by one-step micro-arc oxidation method”, *Surface and Coatings Technology*, Vol. 317, (2017), 125-133. <https://doi.org/10.1016/j.surfcoat.2017.03.034>
 21. Kokubo, T., Takadama, H., “How useful is SBF in predicting in vivo bone bioactivity?”, *Biomaterials*, Vol. 27, No. 15, (2006), 2907-2915. <https://doi.org/10.1016/j.biomaterials.2006.01.017>
 22. Kou, L., Gao, C., “Making silica nanoparticle-covered graphene oxide nanohybrids as general building blocks for large-area superhydrophilic coatings”, *Nanoscale*, Vol. 3, No. 2, (2011), 519-528. <https://doi.org/10.1039/C0NR00609B>
 23. Wu, H., Tang, B., Wu, P., “Development of novel SiO₂-GO nanohybrid/polysulfone membrane with enhanced performance”, *Journal of Membrane Science*, Vol. 451, (2014), 94-102. <https://doi.org/10.1016/j.memsci.2013.09.018>
 24. Zhang, W. L., Choi, H. J., “Silica-graphene oxide hybrid composite particles and their electroresponsive characteristics”, *Langmuir*, Vol. 28, No. 17, (2012), 7055-7062. <https://doi.org/10.1021/la3009283>
 25. Yerokhin, A. L., Nie, X., Leyland, A., Matthews, A., Dowey, S. J., “Plasma electrolysis for surface engineering”, *Surface and Coatings Technology*, Vol. 122, No. 2-3, (1999), 73-93. [https://doi.org/10.1016/S0257-8972\(99\)00441-7](https://doi.org/10.1016/S0257-8972(99)00441-7)
 26. Venkateswarlu, K., Rameshbabu, N., Sreekanth, D., Sandhyarani, M., Bose, A. C., Muthupandi, V., Subramanian, S., “Role of electrolyte chemistry on electronic and in vitro electrochemical properties of micro-arc oxidized titania films on Cp Ti”, *Electrochimica Acta*, Vol. 105, (2013), 468-480. <https://doi.org/10.1016/j.electacta.2013.05.032>
 27. Yerokhin, A. L., Nie, X., Leyland, A., Matthews, A., “Characterisation of oxide films produced by plasma electrolytic oxidation of a Ti-6Al-4V alloy”, *Surface and Coatings Technology*, Vol. 130, No. 2-3, (2000), 195-206. [https://doi.org/10.1016/S0257-8972\(00\)00719-2](https://doi.org/10.1016/S0257-8972(00)00719-2)
 28. Ikonopisov, S., “Theory of electrical breakdown during formation of barrier anodic films”, *Electrochimica Acta*, Vol. 22, No. 10, (1977), 1077-1082. [https://doi.org/10.1016/0013-4686\(77\)80042-X](https://doi.org/10.1016/0013-4686(77)80042-X)
 29. Venkateswarlu, K., Rameshbabu, N., Sreekanth, D., Bose, A. C., Muthupandi, V., Babu, N. K., Subramanian, S., “Role of electrolyte additives on in-vitro electrochemical behavior of micro arc oxidized titania films on Cp Ti”, *Applied Surface Science*, Vol. 258, No. 18, (2012), 6853-6863. <https://doi.org/10.1016/j.apsusc.2012.03.118>
 30. Shin, K. R., Ko, Y. G., Shin, D. H., “Influence of zirconia on biomimetic apatite formation in pure titanium coated via plasma electrolytic oxidation”, *Materials Letters*, Vol. 64, No. 24, (2010), 2714-2717. <https://doi.org/10.1016/j.matlet.2010.08.069>
 31. Ahmadi, A., Ramezanzadeh, B., Mahdavian, M., “Hybrid silane coating reinforced with silanized graphene oxide nanosheets with improved corrosion protective performance”, *RSC Advances*,

- Vol. 6, No. 59, (2016), 54102-54112. <https://doi.org/10.1039/C6RA04843A>
32. Molaei, M., Fattah-alhosseini, A., Nouri, M., Mahmoodi, P., Nourian, A., "Incorporating TiO₂ nanoparticles to enhance corrosion resistance, cytocompatibility, and antibacterial properties of PEO ceramic coatings on titanium", *Ceramics International*, Vol. 48, No. 14, (2022), 21005-21024. <https://doi.org/10.1016/j.ceramint.2022.04.096>
 33. Nikoomanzari, E., Fattah-alhosseini, A., Karbasi, M., Nourian, A., "A versatile TiO₂/ZrO₂ nanocomposite coating produced on Ti-6Al-4V via plasma electrolytic oxidation process", *Surfaces and Interfaces*, Vol. 32, (2022), 102128. <https://doi.org/10.1016/j.surfin.2022.102128>
 34. Marques, I. D. S. V., Barão, V. A. R., da Cruz, N. C., Yuan, J. C. C., Mesquita, M. F., Ricomini-Filho, A. P., Sukotjo, C., Mathew, M. T., "Electrochemical behavior of bioactive coatings on cp-Ti surface for dental application", *Corrosion Science*, Vol. 100, (2015), 133-146. <https://doi.org/10.1016/j.corsci.2015.07.019>
 35. Sowa, M., Simka, W., "Electrochemical behavior of plasma electrolytically oxidized niobium in simulated physiological environment", *Surface and Coatings Technology*, Vol. 344, (2018), 121-131. <https://doi.org/10.1016/j.surfcoat.2018.03.013>
 36. Hwang, I. J., Choe, H. C., "Effects of Zn and Si ions on the corrosion behaviors of PEO-treated Ti-6Al-4V alloy", *Applied Surface Science*, Vol. 477, (2019), 79-90. <https://doi.org/10.1016/j.apsusc.2017.12.015>
 37. Nikoomanzari, E., Fattah-alhosseini, A., Alamoti, M. R. P., Keshavarz, M. K., "Effect of ZrO₂ nanoparticles addition to PEO coatings on Ti-6Al-4V substrate: Microstructural analysis, corrosion behavior and antibacterial effect of coatings in Hank's physiological solution", *Ceramics International*, Vol. 46, No. 9, (2020), 13114-13124. <https://doi.org/10.1016/j.ceramint.2020.02.084>
 38. Metikos-Huković, M., Kwokal, A., Piljac, J., "The influence of niobium and vanadium on passivity of titanium-based implants in physiological solution", *Biomaterials*, Vol. 24, No. 21, (2003), 3765-3775. [https://doi.org/10.1016/S0142-9612\(03\)00252-7](https://doi.org/10.1016/S0142-9612(03)00252-7)
 39. Molaei, M., Fattah-alhosseini, A., Nouri, M., Mahmoodi, P., Navard, S. H., Nourian, A., "Enhancing cytocompatibility, antibacterial activity and corrosion resistance of PEO coatings on titanium using incorporated ZrO₂ nanoparticles", *Surfaces and Interfaces*, Vol. 30, (2022), 101967. <https://doi.org/10.1016/j.surfin.2022.101967>



Materials and Energy Research Center

MERC

Contents lists available at [ACERP](#)

Advanced Ceramics Progress

Journal Homepage: www.acerp.ir

Advanced Ceramics Progress

Review Article

Investigation of the Coating Methods and Types of Coatings Containing Hydroxyapatite for Applications in Tissue Engineering

Behnam Doudkanlouy Milan ^a, Hurieh Mohammadzadeh ^b*, Robabeh Jafari ^b, Mohammad Soltani ^c^a MS Student, Department of Materials Engineering, Faculty of Engineering, Urmia University, Urmia, West Azerbaijan, Iran^b Assistant Professor, Department of Materials Engineering, Faculty of Engineering, Urmia University, Urmia, West Azerbaijan, Iran^c PhD Candidate, Department of Materials Engineering, Faculty of Engineering, Tarbiat Modares University, Tehran, Tehran, Iran* Corresponding Author Email: h.mohamadzadeh@urmia.ac.ir (H. Mohammadzadeh)URL: https://www.acerp.ir/article_161855.html

ARTICLE INFO

ABSTRACT

Article History:

Received 11 October 2022
Received in revised form 8 November 2022
Accepted 29 November 2022

Keywords:

Hydroxyapatite
Coating
Metal Substrates
Osteoinduction
Tissue Engineering

In recent years, application of Hydroxyapatite (HA) as the coating on metal substrates for biological stabilization of implants, stimulation of bone growth around the implant, and optimization of recovery time has attracted the attention of many researchers around the world. In this regard, the current study presented a review of HA and its composite coatings for tissue engineering applications. HA is one of the bioceramics that has been an interesting subject of research in recent years owing to its in-vitro bioactivity, osteoinduction, and osteoconduction properties. According to the previous reports, coated implants were performed successfully to achieve high corrosion resistance, bone growth and regeneration, and reduction of corrosion current density. The current research presented a review of the previous research works on the coating mechanism, physico-mechanical, in-vitro bioactivity, and biocompatibility properties of HA and its composite coatings on substrates. The obtained results revealed that HA and its composites had a synergistic effect on the metal substrates in terms of improving corrosion resistance, providing biocompatibility, direct bonding to tissue, accelerating treatment, and reducing costs imposed on the health care sector.

<https://doi.org/10.30501/acp.2022.365116.1108>

1. INTRODUCTION

Stainless steel, Mg, Mg alloys, titanium, and titanium alloy are some of the metals used in the production of bone implants [1-5]. Due to the supply of suitable mechanical properties, implants have been used for several years to stabilize bones, teeth, and joints. Metals corrode in the body fluid that results in the release of metal ions around the tissue, hence the appearance of side effects. For this reason, surface treatment is required to improve the biocompatibility as well as bioactivity,

reinforce the connection to bone tissue, and promote bone formation by proliferation of osteoblast cells. In this regard, in order to improve the surface properties of the metal implants, biocompatible and bioactive materials should be coated [6-8].

Hydroxyapatite (HA) is a bioactive calcium phosphate ceramic with the chemical formula of $[Ca_{10}(PO_4)_6(OH)_2]$ [9-12]. Owing to its chemical and crystallographic characteristics similarity to the human bone, HA is currently utilized in the field of bone tissue repair and reconstruction and as bioactive coating on different metal

Please cite this article as: Doudkanlouy Milan, B., Mohammadzadeh, H., Jafari, R., Soltani, M., "Investigation of the Coating Methods and Types of Coatings Containing Hydroxyapatite for Applications in Tissue Engineering", *Advanced Ceramics Progress*, Vol. 8, No. 4, (2022), 32-41. <https://doi.org/10.30501/acp.2022.365116.1108>

2423-7485/© 2022 The Author(s). Published by MERC.

This is an open access article under the CC BY license (<https://creativecommons.org/licenses/by/4.0/>).

substrates for orthopedic applications [6,9,13-15]. Given that HA is mainly composed of calcium and phosphate and that its chemical composition and crystal structure are similar to the mineral content of the human bone, the biocompatible and bioactive and other related products are generally not dangerous for cell viability [16]. In addition, in clinical applications, HA ensures new bone formation due to its controlled biodegradability [17].

Hence, HA is used in various medical applications such as bioactive coatings on the bone metal implants, ear implants, dental materials, and tissue engineering applications [18-20]. However, HA has some drawbacks such as its low mechanical properties and low fracture toughness [21]. Therefore, it does not conform to the mechanical properties of the human bone, which is considered an obstacle to its in-vivo applications [22]. Therefore, reinforcements such as Al_2O_3 , TiO_2 , Y_2O_3 , Ni_3Al , and carbon nanotubes (CNTs) are composited with HA to enhance its mechanical characteristics [23-27]. However, the presence of these enhancers can sometimes cause damages to the surrounding tissues. For instance, HA decomposition occurs during the procedure manufacturing through ZrO_2 , which leads to a significant degrade in the biological behavior of HA [26].

Therefore, according to the factors mentioned above, HA has a high potential for bone tissue engineering applications, drug release, and bioactive coatings. In this review study, we attempted to cover the methods for HA coating and investigate the HA reinforcing materials on the metal substrates as much as possible. Hence, it is expected that this review study will be utilized as a practical reference for researches.

2. COATING TECHNIQUES

2.1. Sol-Gel

In sol-gel method, inorganic polymers/ceramics are obtained through converting solutes-soluble precursors into sol and then into a lattice structure called a gel [28]. This method enjoys several advantages namely its choice of coating composition, coating of complicated structures, homogeneity of the coating, and simplicity of the procedure [28]. On the contrary, the limitations of this method are the slow speed of the process and presence of inherent cracks [29]. $\text{Ca}(\text{NO}_3)_2 \cdot 4\text{H}_2\text{O}$ and P_2O_5 are usually used as precursors to prepare the HA sol. In addition, the most common solvent for dissolving the existing precursors is pure ethanol, to which a small amount of water is added to increase the hydrolysis of the prepared sol [29]. Then, the resultant solution is exposed to different temperatures at different time intervals to achieve the desired viscosity, evaporate the existing solvent, and obtain a sol-gel state [29]. Finally, the prepared sol-gel is subjected to aging, drying, and calcination processes to make it ready for use. It should be noted that to date, the sol-gel method has been

extensively utilized to coat the HA and HA composites on metal substrates [30-33]. Figure 1a presents a schematic of the overall sol-gel immersion coating procedure.

2.2. Electrophoretic Deposition (EPD)

Electrophoretic Deposition (EPD) is a colloidal process in which the charged particles in suspension are coated by applying an electric field to a conductive electrode (Figure 1b) [34]. However, in the EPD technique, application of water as a solvent is limited owing to electrolysis and production of small bubbles near the electrode. High adaptability and inclusion of a wide range of materials are among the effective factors that have drawn considerable attention to this method. It is worth noting that creating a stable suspension where the particles are well distributed inside the solvent is one of the important stages of EPD that should be further explored by researchers [35]. However, the disadvantages of this method can be remedied by reducing the ionic conductivity of water [35]. Moreover, the applied EPD method was utilized to coat different composites of HA on the metal substrates [36-39].

2.3. Thermal Spraying (TS)

Thermal Spraying (TS) method is among the physical deposition techniques for creating HA coatings. This technique is based on processes in which coating materials are heated and sprayed on the substrate. The reasons for using thermal spray coating are to protect the surface against physical corrosion, abrasion and scratches, chemical corrosion, electrical corrosion and oxidation [6]. It should be noted that through the TS method, Ti/HA composite coating can be applied on a stainless steel substrate that yields interesting physico-chemical results [40].

2.4. Physical Vapor Deposition (PVD)

Coating from vapor phase involves a wide range of vacuum coating processes in which materials are physically separated from a source through evaporation and transferred as a film on the surface of the substrate through a partial vacuum (Figure 1c) [41]. Deposition of the thin layers of the vapor phase is accomplished using a variety of techniques used in the optical, tribology, energy storage, and medical industries [41,42]. Moreover, this technique was employed to coat HA on the Ti-35Nb-xZ substrate [43].

2.5. Biomimetic Deposition (BD)

When the coating is formed under physiological conditions, it is called biomimetic (Figure 1d). This method was developed by researchers through forming a layer consisting of calcium and phosphate on a titanium substrate in a simulated body fluid [44]. The figure below exhibits a bioactive apatite coating formed by a biomimetic method on a substrate. Of note, formation of

the calcium phosphate layer is also indicative of the substrate bioactivity [45]. To date, the biomimetic deposition (BD) method has been used to coat HA on deferent metal substrates such as stainless steel, Ti, and TiO₂ [46-48].

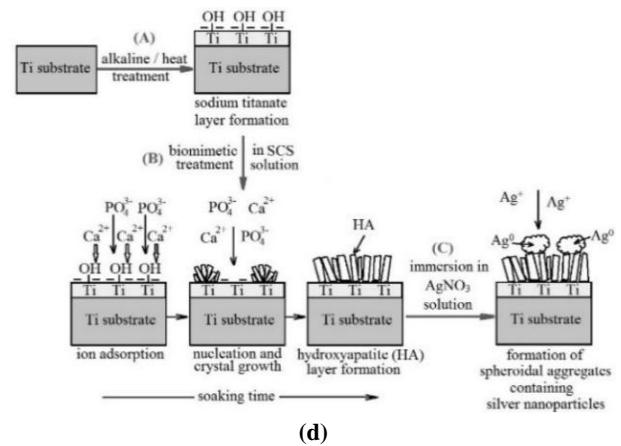
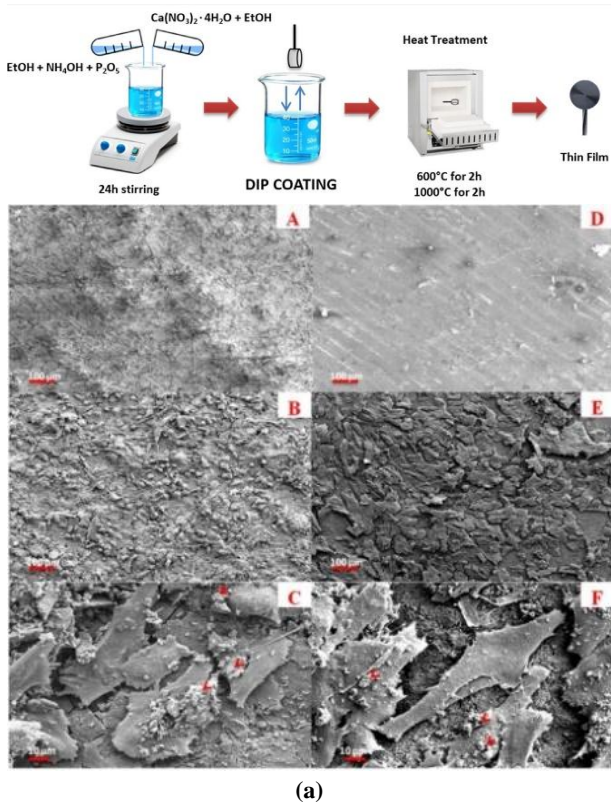


Figure 1. Schematics of HA coating through Sol-Gel, EPD, PVD, and BD, respectively (a-d) [34,41,49,50]

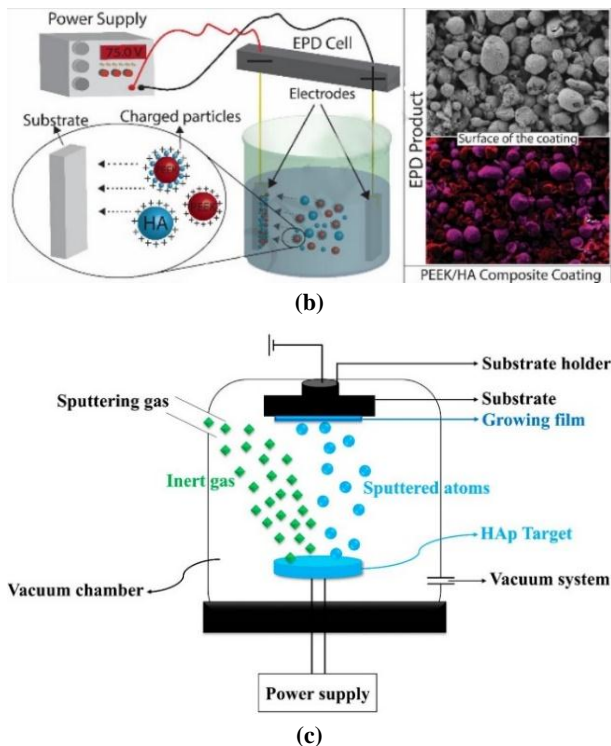
3. HA COMPOSITE COATING ON METAL SUBSTRATES

3.1. HA/Graphen Oxide

Owing to its high specific surface area, controlled drug release, good biocompatibility, and high stability Graphene oxide (GO) is widely used in various biological applications including biosensors, bio-imaging, and tissue engineering scaffolds [51,52]. In addition, GO is characterized by other acceptable mechanical properties. Among the effective factors involved in the stability of GO in solution are the oxygen groups that are placed on the edges and plates that facilitate applications of GO as an enhancer in biocomposites [53]. It should be noted that based on the previous report, upon adding 1 % by weight of GO to the composite composition, a significant increase in the biological and mechanical characteristics of the final sample was achieved. In addition, according to the literature data, in the presence of GO and HA nanoparticles, a significant increase in the bioactivity of gelatin and Polycaprolactone (PCL) was observed [54]. In a study by Sebastin et al., HA/GO composite coating was applied on the 316L stainless steel substrate. According to the results of this study, cell viability was reported to be above 95 % for HA composite coating containing 2 % by weight of GO (Figure 2a). In addition, the corrosion resistance of the HA/GO composite coating was significantly improved, compared to HA alone (Figure 2b and Figure 2c) [55].

3.2. HA/TiO₂

In recent years, TiO₂ has been highly acknowledged by researchers as a bioactive coating [56-58]. TiO₂ is characterized by good biocompatibility and good chemical stability in physiological environments [37]. Additionally, TiO₂ is currently used in biological applications such as drug delivery systems, bio-imaging, and cancer treatment [59-61]. Studies highlighted that



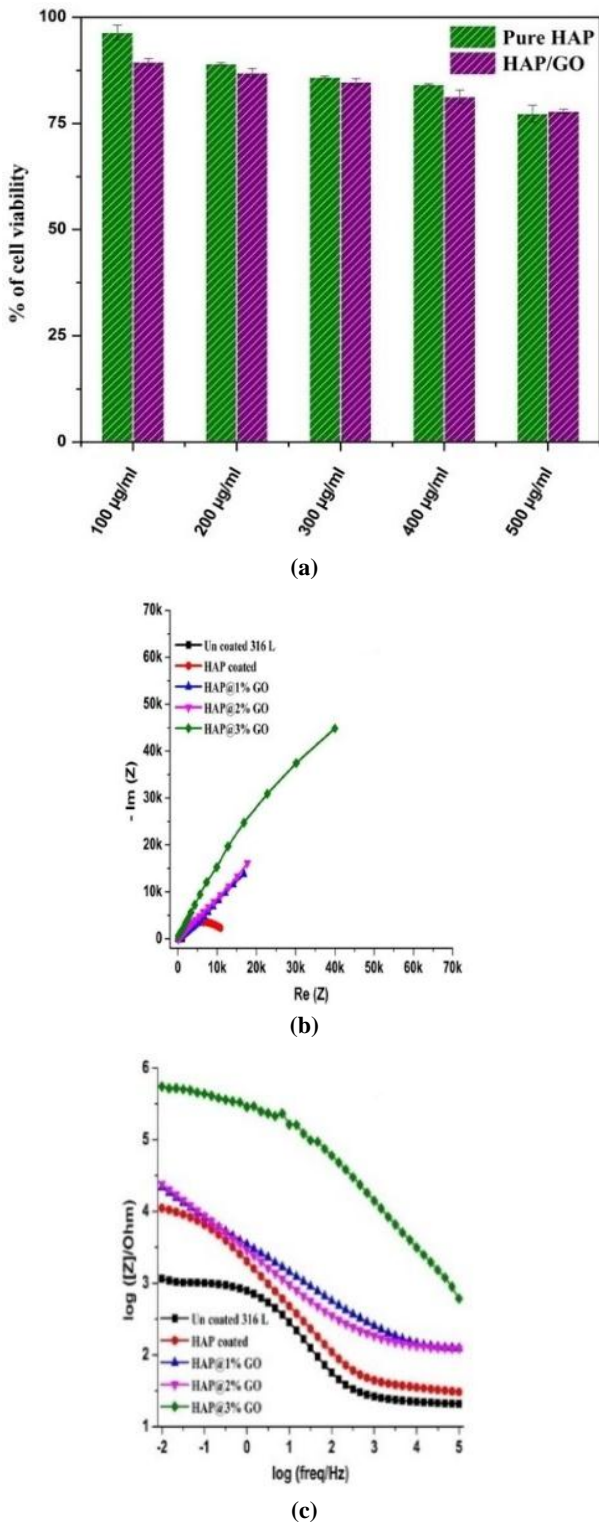


Figure 2. Viability of MG-63 cell lines (a), Nyquist (b), and Bode (c) plots [55]

HA and TiO₂ coatings could provide higher mechanical characteristics than neat HA coatings when TiO₂ was in the range of 20 to 25 by weight [62,63]. These results

were further employed to design more complicated structures with the ability to improve the biological and mechanical properties of the HA-based bioactive coatings [63]. According to the morphological investigations, the prepared HA coating is characterized by a porous morphology. In this case, an increase in the amount of TiO₂ leads to the higher density of the composite coatings, which increases the adhesion strength of the coating and enhances the bond between coating and substrate (Figure 3) [37].

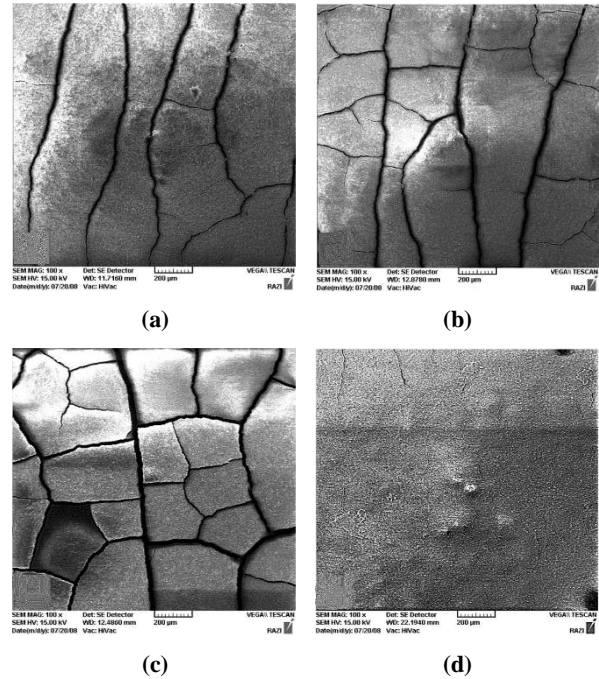


Figure 3. SEM images of HA / TiO₂ coatings deposited on 316L stainless steel [37]

3.3. HA/Chitosan

Biodegradable polymers are widely utilized in composite preparation [12,64,65]. Chitosan (CS) proved to be an excellent matrix for HA and HA composites. It is also a biocompatible, biodegradable, and available biopolymer [12,66]. Although CS has unique properties such as biocompatibility, non-toxicity, and antibacterial effect, it fails in binding to the bone [67]. According to the previous research work [68], CS coatings applied as a composite with HA on 316 L substrate revealed high in vitro bioactivity, biocompatibility, and corrosion resistance properties (Figure 4). In this study, the value range of 3.66-18.98 was the reported in GPa for Young's modulus [68].

The research studies conducted in recent years on the HA composites as a coating on mainly metallic substrates are presented in Table 1. In addition, a summary of the results already obtained regarding the addition of a new material to HA in the coating is reported.

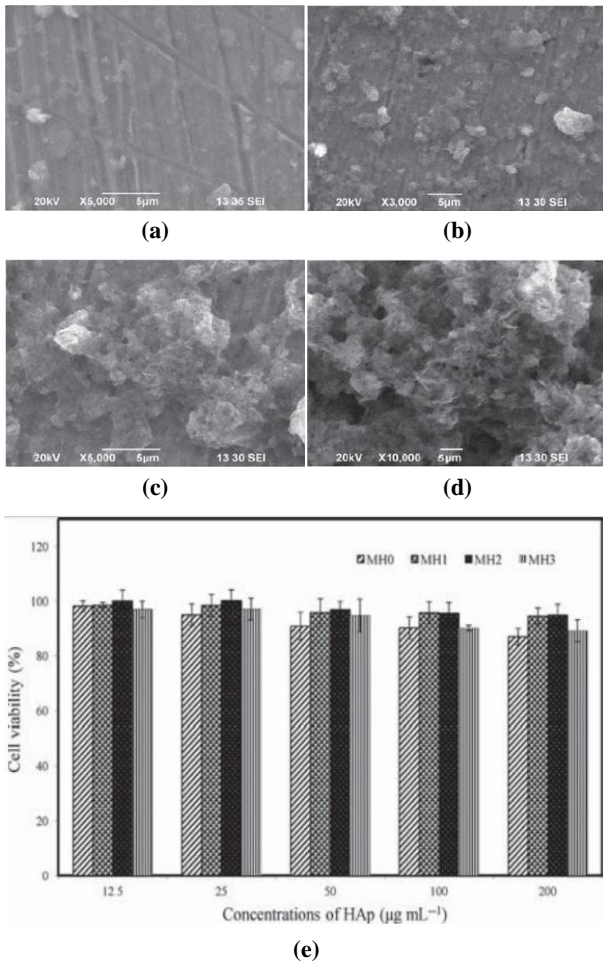


Figure 4. SEM images of the different concentrations of Mg doped HAP/CTS coatings on the 316L (a-d) and NIH 3T3 fibroblast cell viability results (e) [66]

TABLE 1. Hydroxyapatite composite coatings that have attracted the attention of researchers in recent years

HA Composite Coatings	Results	References
Zn	Good biomineralization capacity, conversion of HA tissue to bone-like tissue, biocompatibility, bioactive, antibacterial	[69-74]
Graphene Oxide	Compact structure, increasing corrosion resistance, antibacterial, improving hardness and elastic modulus, biocompatibility	[55,75-79]
Carbon Nanotube	Increasing the shear strength between the surface of the implant and the coating, improving hardness and elastic modulus	[80-83]
Chitosan (CS)	Bioactive, biocompatibility, increasing corrosion resistance, antibacterial	[39,66,84-87]

Gelatin	Biocompatibility, bioactive osteogenesis, improving mechanical properties	[88-90]
Collagen	Conversion of coating tissue to bone-like tissue, improving coating bonding strength, osteogenesis	[91-94]
MgO	Increasing corrosion resistance, control of corrosion of Mg substrate	[95,96]
TiO ₂	Improving coating bonding strength, bioactive, biocompatibility, decreasing porosity, increasing corrosion resistance, Improving scratch resistance	[37,63,97,98]
ZnO	Increasing corrosion resistance, antibacterial, load bearing, osteogenesis, improving coating bonding strength	[99-102]

3.4. HA/CNT

In a study conducted by Nabipour et al., HA/CNT composite coating was applied on the stainless steel substrate through EPD technique and then investigated. In this type of coating, the presence of CNT filled the gaps between the HA nanoparticles and prevented the formation of microcracks. As a result, the weight of HA-5 wt. % CNT coating became less than that of HA coating due to the lower density of CNT than that of HA particles. According to our observations, addition of CNT improved the uniformity of the coating; therefore, almost no difference was observed in the thickness of the coating [103].

According to the previous reports, one of the main applications of HA is a biocompatible and bioactive coating in all kinds of metal implants. Of note, the bioceramics based on the HA greatly reinforced the connection of bone cells to the implanted biological material and thus increased the integration of the cell with the biological material. As a result, the proliferation of the bone cells also increased. In other words, the HA coating stimulates the bone growth and consequently restores the lost bone [38,104]. In case the HA is placed in the human body, it facilitates the recovery and regeneration of the lost or damaged bone tissue mainly due to the type of protein called osteocalcin, which is a non-collagenous bone protein. Previous Studies revealed that osteocalcin protein could form the bonds with the calcium ions in HA [105,106]. It should be noted that HA, as a widely used biological material, does not cause toxicity in the body [107].

However, while using HA, researchers face a series of challenges namely the poor mechanical properties such as brittleness and low fracture toughness as well as low hardness, low load bearing capacity, and migration from the implant site and spread in the tissue that cause some problems such as deposition in the lymph nodes, cartilage, and bone marrow.

The solution proposed in the research literature for the first limitation is the coating of HA on the metal implants, use of reinforcing materials, and formation of composites. Examples of these methods were reported in detail in Table 1. Additionally, the proposed solution for the second challenge suggests adding the organic and polymer materials along with HA. These materials improved the adhesion of HA to the implant and prevented its dispersion in the body. Hence, new HA composites can compensate for its drawbacks [108-110]. Moreover, one of the main challenges in using HA composites is that the adhesion strength of these composites in processing methods such as EPD is not enough, and other coating methods such as PVD are not cost-effective despite providing adequate adhesion. On the contrary, use of some polymeric materials is also bound to some limitations such as toxicity and uncontrollable biodegradability [111-113]. Given what was already mentioned, more and more detailed research is still needed in this field.

In addition, in recent years, with the scientific advancements and emergence of nanotechnology, these coatings have become nanoscale. In addition to the greater adhesion to the substrate in this scale, porosity and microcracks are eliminated, hence improvements in mechanical properties and corrosion resistance. It was proved that nanomaterials interacted with cells better than their counterparts due to their dimensions and consequently yielded better results [38,104].

Among the challenges ahead in the field of coating HA composites on the metal substrates are:

1. Introducing the appropriate coating method in such a way that by changing the coating parameters, we can obtain a coating with appropriate adhesion and mechanical properties.
2. Using suitable polymers in such a way that they are biocompatible and at the same time, they ensure improvement of the HA adhesion to the substrate.
3. Using suitable ceramic materials of micron or nano in size to have a positive effect on the mechanical properties and biological properties of HA.
4. Using suitable metal nanoparticles to improve the biological properties of the HA coatings and bring the coating tissue closer to the bone tissue.

4. CONCLUSIONS

In the present review study, the authors attempted to investigate the physico-mechanical and biological characteristics of HA. In addition, a brief summary of the coating methods and HA composite coatings were presented. The main findings of the present research are briefly stated below:

1. The mechanical properties of HA and bioactivity of metal substrates, especially 316 L stainless steel, were enhanced by HA/metal substrate composites.

2. Sol-gel, EPD, TS, PVD, and BD were among the effective techniques for coating HA on the metal substrates.
3. GO/HA composite was the main cause of more than 95 % cell viability.
4. The combination of HA and TiO₂ as a composite played an effective role in reducing the porosity of the coatings.
5. HA/CS composite coatings applied on 316L stainless steel revealed proper corrosion resistance and biological properties.

5. ACKNOWLEDGMENT

Special thanks to the referee committee of the 3th International Conference on Ceramics.

REFERENCES

1. Ballarre, J., Manjubala, I., Schreiner, W. H., Orellano, J. C., Fratzl, P., Ceré, S., "Improving the osteointegration and bone-implant interface by incorporation of bioactive particles in sol-gel coatings of stainless steel implants", *Acta Biomaterialia*, Vol. 6, No. 4, (2010), 1601-1609. <https://doi.org/10.1016/j.actbio.2009.10.015>
2. Hao, L., Dadbakhsh, S., Seaman, O., Felstead, M., "Selective laser melting of a stainless steel and hydroxyapatite composite for load-bearing implant development", *Journal of Materials Processing Technology*, Vol. 209, No. 17, (2009), 5793-5801. <https://doi.org/10.1016/j.jmatprotec.2009.06.012>
3. Oliveira, N., Alaejos-Algarra, F., Mareque-Bueno, J., Ferrés-Padró, E., Hernández-Alfaro, F., "Thermal changes and drill wear in bovine bone during implant site preparation. A comparative in vitro study: twisted stainless steel and ceramic drills", *Clinical Oral Implants Research*, Vol. 23, No. 8, (2012), 963-969. <https://doi.org/10.1111/j.1600-0501.2011.02248.x>
4. Verma, R. P., "Titanium based biomaterial for bone implants: A mini review", *Materials Today: Proceedings*, Vol. 26, No. 2, (2020), 3148-3151. <https://doi.org/10.1016/j.matpr.2020.02.649>
5. Zhang, X., Huang, Y., Wang, B., Chang, X., Yang, H., Lan, J., Wang, S., Qiao, H., Lin, H., Han, S., Guo, Y., "A functionalized Sm/Sr doped TiO₂ nanotube array on titanium implant enables exceptional bone-implant integration and also self-antibacterial activity", *Ceramics International*, Vol. 46, No. 10, (2020), 14796-14807. <https://doi.org/10.1016/j.ceramint.2020.03.004>
6. Arcos, D., Vallet-Regí, M., "Substituted hydroxyapatite coatings of bone implants", *Journal of Materials Chemistry B*, Vol. 8, No. 9, (2020), 1781-1800. <https://doi.org/10.1039/C9TB02710F>
7. Prakash, C., Singh, S., Ramakrishna, S., Królczyk, G., Le, C. H., "Microwave sintering of porous Ti-Nb-HA composite with high strength and enhanced bioactivity for implant applications", *Journal of Alloys and Compounds*, Vol. 824, (2020), 153774. <https://doi.org/10.1016/j.jallcom.2020.153774>
8. Zhang, K., Van Le, Q., "Bioactive glass coated zirconia for dental implants: a review", *Journal of Composites and Compounds*, Vol. 2, No. 2, (2020), 10-17. <https://doi.org/10.29252/jcc.2.1.2>
9. Soltani, M., Yousefpour, M., Taherian, Z., "Porous fluorhydroxyapatite-magnesium-gelatin novel composite scaffold based on freeze-drying mechanism for bone tissue engineering application", *Materials Letters*, Vol. 244, (2019), 195-198. <https://doi.org/10.1016/j.matlet.2019.02.088>
10. Nayak, A. K., "Hydroxyapatite synthesis methodologies: an overview", *International Journal of ChemTech Research*, Vol.

- 2, No. 2, (2010), 903-907. [https://sphinxsai.com/s_v2_n2/CT_V.2No.2/ChemTech_Vol_2N o.2_pdf/CT=24%20\(903-907\).pdf](https://sphinxsai.com/s_v2_n2/CT_V.2No.2/ChemTech_Vol_2N o.2_pdf/CT=24%20(903-907).pdf)
11. Khandelwal, H, Prakash, S., "Synthesis and characterization of hydroxyapatite powder by eggshell", *Journal of Minerals and Materials Characterization and Engineering*, Vol. 4, No. 2, (2016), 119-126. <https://doi.org/10.4236/jmmce.2016.42011>
 12. Szatkowski, T., Kołodziejczak-Radzimska, A., Zdzarta, J., Szwarz-Rzepka, K., Paukszta, D., Wysokowski, M., Ehrlich, H., Jesionowski, T., "Synthesis and characterization of hydroxyapatite/chitosan composites", *Physicochemical Problems of Mineral Processing*, Vol. 51, (2015), 575-585. <https://doi.org/10.5277/ppmp150217>
 13. Jaafar, A., Hecker, C., Árki, P., Joseph, Y., "Sol-gel derived hydroxyapatite coatings for titanium implants: A review", *Bioengineering*, Vol. 7, No. 4, (2020), 127. <https://doi.org/10.3390/bioengineering7040127>
 14. Vu, A. A., Robertson, S. F., Ke, D., Bandyopadhyay, A., Bose, S., "Mechanical and biological properties of ZnO, SiO₂, and Ag₂O doped plasma sprayed hydroxyapatite coating for orthopaedic and dental applications", *Acta Biomaterialia*, Vol. 92, (2019), 325-335. <https://doi.org/10.1016/j.actbio.2019.05.020>
 15. Ke, D., Vu, A. A., Bandyopadhyay, A., Bose, S., "Compositionally graded doped hydroxyapatite coating on titanium using laser and plasma spray deposition for bone implants", *Acta Biomaterialia*, Vol. 84, (2019), 414-423. <https://doi.org/10.1016/j.actbio.2018.11.041>
 16. Wang, Y., Li, X., Chen, M., Zhao, Y., You, C., Li, Y., Chen, G., "In vitro and in vivo degradation behavior and biocompatibility evaluation of microarc oxidation-fluoridated hydroxyapatite-coated Mg-Zn-Zr-Sr alloy for bone application", *ACS Biomaterials Science & Engineering*, Vol. 5, No. 6, (2019), 2858-2876. <http://doi.org/10.1021/acsbiomaterials.9b00564>
 17. Sarkar, N., Bose, S., "Controlled delivery of curcumin and vitamin K2 from hydroxyapatite-coated titanium implant for enhanced in vitro chemoprevention, osteogenesis, and in vivo osseointegration", *ACS Applied Materials & Interfaces*, Vol. 12, No. 12, (2020), 13644-13656. <http://doi.org/10.1021/acsami.9b22474>
 18. Pitiot, V., Hermann, R., Coudert, A., Truy, E., "Lysis of the long process of the incus secondary to Vibrant SounBridge® middle ear implants, treated with hydroxyapatite bone cement", *Auris Nasus Larynx*, Vol. 46, No. 6, (2019), 952-955. <https://doi.org/10.1016/j.anl.2019.02.011>
 19. Muñoz, L. C., Silva, R. F., "Comparison of subcutaneous inflammatory response to commercial and engineered zinc hydroxyapatite implants in rabbits", *Arquivo Brasileiro de Medicina Veterinária e Zootecnia*, Vol. 71, (2019), 1873-1879. <http://doi.org/10.1590/1678-4162-11407>
 20. Sharifianjazi, F., Pakseresht, A. H., Shahedi Asl, M., Esmailkhanian, A., Jang, H. W., Shokouhimehr, M., "Hydroxyapatite consolidated by zirconia: applications for dental implant", *Journal of Composites and Compounds*, Vol. 2, No. 2, (2020), 26-34. <https://doi.org/10.29252/jcc.2.1.4>
 21. Nosrati, H., Sarraf-Mamoory, R., Le, D. Q. S., Bünger, C. E., "Enhanced fracture toughness of three dimensional graphene-hydroxyapatite nanocomposites by employing the Taguchi method", *Composites Part B: Engineering*, Vol. 190, (2020), 107928. <https://doi.org/10.1016/j.compositesb.2020.107928>
 22. Shahbaz, A. H., Esmailian, M., NasrAzadani, R., Gavanji, K., "The effect of MgF₂ addition on the mechanical properties of hydroxyapatite synthesized via powder metallurgy", *Journal of Composites and Compounds*, Vol. 1, No. 1, (2019) 16-21. <https://doi.org/10.29252/jcc.1.1.3>
 23. Bulut, B., Demirkol, N., Erkmen, Z., Kayali, E., "Comparison of microstructural and mechanical properties of hydroxyapatite-Al₂O₃ composites with commercial inert glass (CIG) addition", *Acta Phys Pol A*, Vol. 127, No. 4, (2015), 1094-1096. <http://doi.org/10.12693/APhysPolA.127.1094>
 24. Oktar, F. N., "Hydroxyapatite-TiO₂ composites", *Materials Letters*, Vol. 60, No. 17-18, (2006), 2207-2210. <https://doi.org/10.1016/j.matlet.2005.12.099>
 25. Parente, P., Sanchez-Herencia, A. J., Mesa-Galan, M. J., Ferrari, B., "Functionalizing Ti-surfaces through the EPD of hydroxyapatite/nanoY₂O₃", *The Journal of Physical Chemistry B*, Vol. 117, No. 6, (2013), 1600-1607. <https://doi.org/10.1021/jp305176h>
 26. Choi, J. W., Kong, Y. M., Kim, H. E. and Lee, I. S., "Reinforcement of hydroxyapatite bioceramic by addition of Ni₃Al and Al₂O₃", *Journal of the American Ceramic Society*, Vol. 81, No. 7, (1998), 1743-1748. <https://doi.org/10.1111/j.1151-2916.1998.tb02543.x>
 27. Khalid, P., Hussain, M. A., Rekha, P. D., Arun, A. B., "Synthesis and characterization of carbon nanotubes reinforced hydroxyapatite composite", *Indian Journal of Science and Technology*, Vol. 6, No. 12, (2013), 5546-5551. <https://doi.org/10.17485/ijst/2013/v6i12.7>
 28. Danks, A. E., Hall, S. R., Schnepf, Z., "The evolution of 'sol-gel' chemistry as a technique for materials synthesis", *Materials Horizons*, Vol. 3, No. 2, (2016), 91-112. <https://doi.org/10.1039/C5MH00260E>
 29. Dehghanghadikolaei, A., Ansary, J., Ghoreishi, R., "Sol-gel process applications: A mini-review", *Proceedings of the Nature Research Society*, Vol. 2, No. 1, (2018), 02008-02029. <https://doi.org/10.11605/j.pnrs.201802008>
 30. Sidane, D., Chicot, D., Yala, S., Ziani, S., Khireddine, H., Iost, A., Decoopman, X., "Study of the mechanical behavior and corrosion resistance of hydroxyapatite sol-gel thin coatings on 316 L stainless steel pre-coated with titania film", *Thin Solid Films*, Vol. 593, (2015), 71-80. <https://doi.org/10.1016/j.tsf.2015.09.037>
 31. Poinescu, A. A., Radulescu, C., Vasile, B. S., Ionita, I., "Research regarding sol-gel hydroxyapatite coating on 316L stainless steel", *Revista de Chimie*, Vol. 65, No. 10, (2014), 1245-1248. <https://citeseerx.ist.psu.edu/document?repid=rep1&type=pdf&doi=cbc0a3d48b90176468ca8339717a56c22815c394>
 32. Sidane, D., Rammal, H., Beljebbar, A., Gangloff, S. C., Chicot, D., Velard, F., Khireddine, H., Montagne, A., Kerdjoudj, H., "Biocompatibility of sol-gel hydroxyapatite-titania composite and bilayer coatings", *Materials Science and Engineering: C*, Vol. 72, (2017), 650-658. <https://doi.org/10.1016/j.msec.2016.11.129>
 33. Jafari, S., Taheri, M. M., Idris, J., "Bioactive coating on stainless steel 316 L through sol-gel method", In *Advanced Materials Research*, Trans Tech Publications Ltd., Vol. 383-390, (2012), 3944-3948. <https://doi.org/10.4028/www.scientific.net/AMR.383-390.3944>
 34. Baştan, F. E., Rehman, M. A. U., Avcu, Y. Y., Avcu, E., Üstel, F., Boccaccini, A. R., "Electrophoretic co-deposition of PEEK-hydroxyapatite composite coatings for biomedical applications", *Colloids and Surfaces B: Biointerfaces*, Vol. 169, (2018) 176-182. <https://doi.org/10.1016/j.colsurfb.2018.05.005>
 35. Chavez-Valdez, A. R. B. A., Shaffer, M. S., Boccaccini, A. R., "Applications of graphene electrophoretic deposition. A review", *Journal of Physical Chemistry B*, Vol. 117, No. 6, (2013), 1502-1515. <https://doi.org/10.1021/jp3064917>
 36. Frajkorová, F., Molero, E., Ferrari, B., "Electrophoretic deposition of gelatin/hydroxyapatite composite coatings onto a stainless steel substrate", In *Key Engineering Materials*, Trans Tech Publications Ltd., Vol. 654, (2015), 195-199. <https://doi.org/10.4028/www.scientific.net/kem.654.195>
 37. Amirnejad, M., Afshar, A., Salehi, S., "The effect of titanium dioxide (TiO₂) nanoparticles on hydroxyapatite (HA)/TiO₂ composite coating fabricated by electrophoretic deposition (EPD)", *Journal of Materials Engineering and Performance*, Vol. 27, No. 5, (2018), 2338-2344. <https://doi.org/10.1007/s11665-018-3342-6>
 38. Pang, X., Zhitomirsky, I., "Electrophoretic deposition of composite hydroxyapatite-chitosan coatings", *Materials Characterization*, Vol. 58, No. 4, (2007), 339-348. <https://doi.org/10.1016/j.matchar.2006.05.011>

39. Sorkhi, L., Farrokhi-Rad, M., Shahrabi, T., "Electrophoretic deposition of hydroxyapatite-chitosan-titania on stainless steel 316 L", *Surfaces*, Vol. 2, No. 3, (2019), 458-467. <https://doi.org/10.3390/surfaces2030034>
40. Azhar, N. H., Talari, M., Ramli, R., Koong, C. K., "Characterization of Thermal Sprayed Titanium/hydroxyapatite Composite Coating on Stainless Steel", In *Advanced Materials Research*, Trans Tech Publications Ltd., Vol. 974, (2014), 152-156. <https://doi.org/10.4028/www.scientific.net/amr.974.152>
41. Safavi, M. S., Walsh, F. C., Surmeneva, M. A., Surmenev, R. A., Khalil-Allafi, J., "Electrodeposited hydroxyapatite-based biocoatings: Recent progress and future challenges", *Coatings*, Vol. 11, No. 1, (2021), 110. <https://doi.org/10.3390/coatings11010110>
42. Qadir, M., Li, Y., Wen, C., "Ion-substituted calcium phosphate coatings by physical vapor deposition magnetron sputtering for biomedical applications: A review", *Acta Biomaterialia*, Vol. 89, (2019), 14-32. <https://doi.org/10.1016/j.actbio.2019.03.006>
43. Jeong, Y. H., Choe, H. C., Eun, S. W., "Hydroxyapatite coating on the Ti-35Nb-xZr alloy by electron beam-physical vapor deposition", *Thin Solid Films*, Vol. 519, No. 20, (2011), 7050-7056. <https://doi.org/10.1016/j.tsf.2011.04.086>
44. Nijhuis, A. W., Leeuwenburgh, S. C., Jansen, J. A., "Wet-chemical deposition of functional coatings for bone implantology", *Macromolecular Bioscience*, Vol. 10, No. 11, (2010), 1316-1329. <https://doi.org/10.1002/mabi.201000142>
45. Liu, Y., Wu, G., de Groot, K., "Biomimetic coatings for bone tissue engineering of critical-sized defects", *Journal of the Royal Society Interface*, Vol. 7, No. suppl_5, (2010), S631-S647. <https://doi.org/10.1098/rsif.2010.0115.focus>
46. Sureshbabu, S., Komath, M., Shibli, S. M. A., Varma, H. K., "Biomimetic deposition of hydroxyapatite on titanium with help of sol-gel grown calcium pyrophosphate prelayer", *Materials Research Innovations*, Vol. 15, No. 3, (2011), 178-184. <https://doi.org/10.1179/143307511x13018917925586>
47. Xia, W., Lindahl, C., Lausmaa, J., Engqvist, H., "Biomimetic hydroxyapatite deposition on titanium oxide surfaces for biomedical application", *Advances in Biomimetics*, Vol. 20, (2011), 429-452. <https://doi.org/10.5772/14900>
48. Nayar, S., Pramanick, A. K., Sharma, B. K., Mishra, R. K., Bansal, S. K., Prajapati, A., Sahu, K. K., Das, S. K., Pathak, L., Sinha, A., "Hydroxyapatite coating on stainless steel pre-coated with bovine serum albumin at ambient conditions", *Colloids and Surfaces B: Biointerfaces*, Vol. 48, No. 2, (2006), 183-187. <https://doi.org/10.1016/j.colsurfb.2005.09.006>
49. Ciobanu, G., Harja, M., Rusu, L., "Biomimetic hydroxyapatite/silver coatings on titanium surfaces", *Revue Roumaine De Chimie*, Vol. 62, No. 4-5, (2017), 449-454. <https://revroum.lew.ro/wp-content/uploads/2017/4/Art%2016.pdf>
50. Choudhary, R., Vecstaudza, J., Krishnamurthy, G., Raghavendran, H. R. B., Murali, M. R., Kamarul, T., Swamiappan, S., Locs, J., "In-vitro bioactivity, biocompatibility and dissolution studies of diopside prepared from biowaste by using sol-gel combustion method", *Materials Science and Engineering: C*, Vol. 68, (2016), 89-100. <https://doi.org/10.1016/j.msec.2016.04.110>
51. Chung, C., Kim, Y. K., Shin, D., Ryoo, S. R., Hong, B. H., Min, D. H., "Biomedical applications of graphene and graphene oxide", *Accounts of chemical research*, Vol. 46, No. 10, (2013), 2211-2224. <https://doi.org/10.1021/ar300159f>
52. Feng, L., Wu, L., Qu, X., "New horizons for diagnostics and therapeutic applications of graphene and graphene oxide", *Advanced Materials*, Vol. 25, No. 2, (2013), 168-186. <https://doi.org/10.1002/adma.2011203229>
53. Romero-Aburto, R., Narayanan, T. N., Nagaoka, Y., Hasumura, T., Mitcham, T. M., Fukuda, T., Cox, P. J., Bouchard, R. R., Maekawa, T., Kumar, D. S., Torti, S. V., "Fluorinated graphene oxide; a new multimodal material for biological applications", *Advanced Materials*, Vol. 25, No. 39, (2013), 5632-5637. <https://doi.org/10.1002/adma.201301804>
54. Li, M., Liu, Q., Jia, Z., Xu, X., Cheng, Y., Zheng, Y., Xi, T., Wei, S., "Graphene oxide/hydroxyapatite composite coatings fabricated by electrophoretic nanotechnology for biological applications", *Carbon*, Vol. 67, (2014), 185-197. <https://doi.org/10.1016/j.carbon.2013.09.080>
55. Sebastin, A. X. S., Uthirapathy, V., "In Vitro Electrochemical Behavior of Sol-Gel Derived Hydroxyapatite/Graphene Oxide Composite Coatings on 316L SS for Biomedical Applications", *ChemistrySelect*, Vol. 5, No. 39, (2020), 12140-12147. <https://doi.org/10.1002/slct.202003368>
56. Amaravathy, P., Sathyanarayanan, S., Sowndarya, S., Rajendran, N., "Bioactive HA/TiO₂ coating on magnesium alloy for biomedical applications", *Ceramics International*, Vol. 40, No. 5, (2014), 6617-6630. <https://doi.org/10.1016/j.ceramint.2013.11.119>
57. Drnovšek, N., Rade, K., Milačič, R., Štrancar, J., Novak, S., "The properties of bioactive TiO₂ coatings on Ti-based implants", *Surface and Coatings Technology*, Vol. 209, (2012), 177-183. <https://doi.org/10.1016/j.surfcoat.2012.08.037>
58. Mallakpour, S., Aalizadeh, R., "A simple and convenient method for the surface coating of TiO₂ nanoparticles with bioactive chiral diacids containing different amino acids as the coupling agent", *Progress in Organic Coatings*, Vol. 76, No. 4, (2013), 648-653. <https://doi.org/10.1016/j.porgcoat.2012.12.004>
59. Zhao, C., Ur Rehman, F., Yang, Y., Li, X., Zhang, D., Jiang, H., Selke, M., Wang, X., Liu, C., "Bio-imaging and photodynamic therapy with tetra sulphonatophenyl porphyrin (TSPP)-TiO₂ nanowhiskers: new approaches in rheumatoid arthritis theranostics", *Scientific Reports*, Vol. 5, No. 1, (2015), 1-11. <https://doi.org/10.1038/srep11518>
60. Chu, X., Mao, L., Johnson, O., Li, K., Phan, J., Yin, Q., Li, L., Zhang, J., Chen, W., Zhang, Y., "Exploration of TiO₂ nanoparticle mediated microdynamic therapy on cancer treatment", *Nanomedicine: Nanotechnology, Biology and Medicine*, Vol. 18, (2019), 272-281. <https://doi.org/10.1016/j.nano.2019.02.016>
61. Wang, T., Jiang, H., Wan, L., Zhao, Q., Jiang, T., Wang, B., Wang, S., "Potential application of functional porous TiO₂ nanoparticles in light-controlled drug release and targeted drug delivery", *Acta Biomaterialia*, Vol. 13, (2015), 354-363. <https://doi.org/10.1016/j.actbio.2014.11.010>
62. Nathanael, A. J., Arul, N. S., Ponpandian, N., Mangalaraj, D., Chen, P. C., "Nanostructured leaf like hydroxyapatite/TiO₂ composite coatings by simple sol-gel method", *Thin Solid Films*, Vol. 518, No. 24, (2010), 7333-7338. <https://doi.org/10.1016/j.tsf.2010.04.105>
63. Henaio, J., Cruz-Bautista, M., Hincapie-Bedoya, J., Ortega-Bautista, B., Corona-Castuera, J., Giraldo-Betancur, A. L., Espinosa-Arbelaez, D. G., Alvarado-Orozco, J. M., Clavijo-Mejia, G. A., Trapaga-Martínez, L. G., Poblano-Salas, C. A., "HVOF hydroxyapatite/titania-graded coatings: microstructural, mechanical, and in vitro characterization", *Journal of Thermal Spray Technology*, Vol. 27, No. 8, (2018), 1302-1321. <https://doi.org/10.1007/s11666-018-0811-2>
64. Soltani, M., Yousefpour, M., Taherian, Z., "Synthesis and Characterization Properties of Gelatin-Fluorhydroxyapatite Composite Scaffold for Application in Bone Tissue Engineering and Investigation of Cellular Attachment", *Journal of Mashhad Dental School*, Vol. 43, No. 2, (2019), 131-147. <https://doi.org/10.22038/jmds.2019.13122>
65. Soltani, M., Alizadeh, P., "Aloe vera incorporated starch-64S bioactive glass-quail egg shell scaffold for promotion of bone regeneration", *International Journal of Biological Macromolecules*, Vol. 217, (2022), 203-218. <https://doi.org/10.1016/j.ijbiomac.2022.07.054>
66. Saleem, O., Wahaj, M., Akhtar, M. A., Ur Rehman, M. A., "Fabrication and Characterization of Ag-Sr-Substituted Hydroxyapatite/Chitosan Coatings Deposited via Electrophoretic Deposition: A Design of Experiment Study", *ACS Omega*, Vol. 5, No. 36, (2020), 22984-22992. <https://doi.org/10.1021/acsomega.0c02582>

67. Nikpour, M. R., Rabiee, S. M., Jahanshahi, M. J. C. P. B. E., "Synthesis and characterization of hydroxyapatite/chitosan nanocomposite materials for medical engineering applications", *Composites Part B: Engineering*, Vol. 43, No. 4, (2012), 1881-1886. <https://doi.org/10.1016/j.compositesb.2012.01.056>
68. Sutha, S., Dhineshabu, N. R., Prabhu, M., Rajendran, V., "Mg-doped hydroxyapatite/chitosan composite coated 316L stainless steel implants for biomedical applications", *Journal of Nanoscience and Nanotechnology*, Vol. 15, No. 6, (2015), 4178-4187. <https://doi.org/10.1166/jnn.2015.9753>
69. Bi, Q., Song, X., Chen, Y., Zheng, Y., Yin, P., Lei, T., "Zn-HA/Bi-HA biphasic coatings on Titanium: Fabrication, characterization, antibacterial and biological activity", *Colloids and Surfaces B: Biointerfaces*, Vol. 189, (2020), 110813. <https://doi.org/10.1016/j.colsurfb.2020.110813>
70. Yao, H. L., Yi, Z. H., Yao, C., Zhang, M. X., Wang, H. T., Li, S. B., Ji, G. C., "Improved corrosion resistance of AZ91D magnesium alloy coated by novel cold-sprayed Zn-HA/Zn double-layer coatings", *Ceramics International*, Vol. 46, No. 6, (2020), 7687-7693. <https://doi.org/10.1016/j.ceramint.2019.11.271>
71. Behera, D. R., Nayak, P., Rautray, T. R., "Phosphatidylethanolamine impregnated Zn-HA coated on titanium for enhanced bone growth with antibacterial properties", *Journal of King Saud University-Science*, Vol. 32, No. 1, (2020), 848-852. <https://doi.org/10.1016/j.jksus.2019.03.004>
72. Sivaraj, D., Vijayalakshmi, K., "Enhanced corrosion resistance and antibacterial activity of Zn-HA decorated MWCNTs film coated on medical grade 316L SS implant by novel spray pyrolysis technique", *Journal of Analytical and Applied Pyrolysis*, Vol. 134, (2018), 176-182. <https://doi.org/10.1016/j.jaap.2018.06.006>
73. Ullah, I., Siddiqui, M. A., Liu, H., Kolawole, S. K., Zhang, J., Zhang, S., Ren, L., Yang, K., "Mechanical, biological, and antibacterial characteristics of plasma-sprayed (Sr, Zn) substituted hydroxyapatite coating", *ACS Biomaterials Science & Engineering*, Vol. 6, No. 3, (2020), 1355-1366. <https://doi.org/10.1021/acsbomaterials.9b01396>
74. Kumar, R., Thanigaivelan, R., Rajanikant, G. K., Jagadeesha, T., Das, J., "Evaluation of hydroxyapatite-and zinc-coated Ti-6Al-4V surface for biomedical application using electrochemical process", *Journal of the Australian Ceramic Society*, Vol. 57, No. 1, (2021), 107-116. <https://doi.org/10.1007/s41779-020-00517-6>
75. Yılmaz, E., Çakıroğlu, B., Gökçe, A., Findik, F., Gulsoy, H. O., Gulsoy, N., Mutlu, Ö., Özacar, M., "Novel hydroxyapatite/graphene oxide/collagen bioactive composite coating on Ti6Nb alloys by electrodeposition", *Materials Science and Engineering: C*, Vol. 101, (2019), 292-305. <https://doi.org/10.1016/j.msec.2019.03.078>
76. Peng, F., Zhang, D., Wang, D., Liu, L., Zhang, Y., Liu, X., "Enhanced corrosion resistance and biocompatibility of magnesium alloy by hydroxyapatite/graphene oxide bilayer coating", *Materials Letters*, Vol. 264, (2020), 127322. <https://doi.org/10.1016/j.matlet.2020.127322>
77. Fathyunes, L., Khalil-Allafi, J., Sheykholeslami, S. O. R., Moosavifar, M., "Biocompatibility assessment of graphene oxide-hydroxyapatite coating applied on TiO₂ nanotubes by ultrasound-assisted pulse electrodeposition", *Materials Science and Engineering: C*, Vol. 87, (2018), 10-21. <https://doi.org/10.1016/j.msec.2018.02.012>
78. Nizami, M. Z. I., Campéon, B. D. L., Nishina, Y., "Electrodeposition of hydroxyapatite and graphene oxide improves the bioactivity of medical grade stainless steel", *Materials Today Sustainability*, Vol. 19, (2022), 100193. <https://doi.org/10.1016/j.mtsust.2022.100193>
79. Yuan, B., Chen, H., Zhao, R., Deng, X., Chen, G., Yang, X., Xiao, Z., Aurora, A., Iulia, B. A., Zhang, K., Zhu, X., Iulian, A. V., Hai, S., Zhang, X., "Construction of a magnesium hydroxide/graphene oxide/hydroxyapatite composite coating on Mg-Ca-Zn-Ag alloy to inhibit bacterial infection and promote bone regeneration", *Bioactive Materials*, Vol. 18, (2022), 354-367. <https://doi.org/10.1016/j.bioactmat.2022.02.030>
80. Sivaraj, D., Vijayalakshmi, K., "Novel synthesis of bioactive hydroxyapatite/f-multiwalled carbon nanotube composite coating on 316L SS implant for substantial corrosion resistance and antibacterial activity", *Journal of Alloys and Compounds*, Vol. 777, (2019), 1340-1346. <https://doi.org/10.1016/j.jallcom.2018.10.341>
81. Sonekar, M. M., Rathod, W. S., "Tribological Behavior of Atmospheric Plasma Sprayed HA-CNT Coatings of Biomaterials", In *Tribology of Machine Elements: Fundamentals and Applications*, IntechOpen, (2022), 237. <https://doi.org/10.5772/intechopen.103860>
82. Al-Amin, M., Abdul-Rani, A. M., Rao, T. V. V. L. N., Danish, M., Rubaiee, S., bin Mahfouz, A., Parameswari, R. P., Wani, M. F., "Investigation of machining and modified surface features of 316L steel through novel hybrid of HA/CNT added-EDM process", *Materials Chemistry and Physics*, Vol. 276, (2022), 125320. <https://doi.org/10.1016/j.matchemphys.2021.125320>
83. Naseri, H., Ghatee, M., Yazdani, A., Mohammadi, M., Manafi, S., "Characterization of the 3YSZ/CNT/HAP coating on the Ti6Al4V alloy by electrophoretic deposition", *Journal of Biomedical Materials Research Part B: Applied Biomaterials*, Vol. 109, No. 10, (2021), 1395-1406. <https://doi.org/10.1002/jbm.b.34799>
84. Stevanović, M., Djošić, M., Janković, A., Kojić, V., Vukašinović-Sekulić, M., Stojanović, J., Odović, J., Crevar Sakač, M., Kyong Yop, R., Mišković-Stanković, V., "Antibacterial graphene-based hydroxyapatite/chitosan coating with gentamicin for potential applications in bone tissue engineering", *Journal of Biomedical Materials Research Part A*, Vol. 108, No. 11, (2020), 2175-2189. <https://doi.org/10.1002/jbm.a.36974>
85. Khanmohammadi, S., Aghajani, H., Farrokhi-Rad, M., "Vancomycin loaded-mesoporous bioglass/hydroxyapatite/chitosan coatings by electrophoretic deposition", *Ceramics International*, Vol. 48, No. 14, (2022), 20176-20186. <https://doi.org/10.1016/j.ceramint.2022.03.296>
86. Louvier-Hernández, J. F., García, E., Mendoza-Leal, G., Flores-Flores, T., Flores-Martínez, M., Rodríguez de Anda, E., Hernández-Navarro, C., "Effect of the variation of the electrodeposition time of hydroxyapatite/chitosan coatings on AISI 316L SS", *Journal of Composite Materials*, Vol. 55, No. 29, (2021), 4421-4430. <https://doi.org/10.1177/00219983211038621>
87. Kocak, F. Z., Yar, M., Rehman, I. U., "Hydroxyapatite-Integrated, Heparin-and Glycerol-Functionalized Chitosan-Based Injectable Hydrogels with Improved Mechanical and Proangiogenic Performance", *International Journal of Molecular Sciences*, Vol. 23, No. 10, (2022), 5370. <https://doi.org/10.3390/ijms23105370>
88. Reina, S. A., Tito, B. J. E., Malini, M. H., Iqrimatien, F. G., Sa'diyah, E., "Porosity and compressive strength of PLA-based scaffold coated with hydroxyapatite-gelatin to reconstruct mandibula: a literature review", In *Journal of Physics: Conference Series*, Indonesia, 20-22 November 2020, IOP Publishing, Vol. 1816, No. 1, (2021), 012085. <https://doi.org/10.1088/1742-6596/1816/1/012085>
89. Yan, Z. H. A. N. G., Yinsheng, D. O. N. G., Bin, L. I. U., PingHua, L. I. N., Chenglin, C. H. U., Xiaobo, S. H. E. N. G., Chao, G. U. O., "Preparation of Hydroxyapatite/gelatin Composite Coating on Porous Calcium Phosphate Ceramic by Dipping Method", *Journal of Tissue Engineering and Reconstructive Surgery*, Vol. 4, No. 6, (2008), 301. <https://doi.org/10.3969/j.issn.1673-0364.2008.06.001>
90. Dizaj, S. M., Mokhtarpour, M., Shekaari, H., Sharifi, S., "Hydroxyapatite-gelatin nanocomposite films; production and evaluation of the physicochemical properties", *Journal of Advanced Chemical and Pharmaceutical Materials (JACPM)*, Vol. 2, No. 2, (2019), 111-115. <http://advchempharm.ir/journal/index.php/JACPM/article/view/70>

91. Ciobanu, G., Harja, M., "Cerium-doped hydroxyapatite/collagen coatings on titanium for bone implants", *Ceramics International*, Vol. 45, No. 2, (2019), 2852-2857. <https://doi.org/10.1016/j.ceramint.2018.07.290>
92. Yang, X., Li, Y., He, W., Huang, Q., Zhang, R., Feng, Q., "Hydroxyapatite/collagen coating on PLGA electrospun fibers for osteogenic differentiation of bone marrow mesenchymal stem cells", *Journal of Biomedical Materials Research Part A*, Vol. 106, No. 11, (2018), 2863-2870. <https://doi.org/10.1002/jbm.a.36475>
93. Shyam, R., Hameed, P., Suya Prem Anand, P., Rangasamy, L., Palaniappan, A., Manivasagam, G., "3D Printing Technology for Fighting COVID-19 Pandemic", In Sandhu, K., Singh, S., Prakash, C., Sharma, N.R., Subburaj, K. (Eds.), *Emerging Applications of 3D Printing During CoVID 19 Pandemic*, Lecture Notes in Bioengineering, Springer, Singapore, (2022), 81-109. https://doi.org/10.1007/978-981-33-6703-6_5
94. Tapsir, Z., Jamaludin, F. H., Pinguan-Murphy, B., Saidin, S., "Immobilisation of hydroxyapatite-collagen on polydopamine grafted stainless steel 316L: Coating adhesion and in vitro cells evaluation", *Journal of Biomaterials Applications*, Vol. 32, No. 7, (2018), 987-995. <https://doi.org/10.1177/0885328217744081>
95. Liu, C., Zhang, W., Xu, T., Li, H., Jiang, B., Miao, X., "Preparation and corrosion resistance of a self-sealing hydroxyapatite-MgO coating on magnesium alloy by microarc oxidation", *Ceramics International*, Vol. 48, No. 10, (2022), 13676-13683. <https://doi.org/10.1016/j.ceramint.2022.01.249>
96. Zhang, X., Yin, H., Xiao, L., Li, Z., Ma, C., Xu, W., Wang, Y., "Chitosan regulated electrochemistry for dense hydroxyapatite/MgO nanocomposite coating with antibiosis and osteogenesis on titanium alloy", *Colloid and Interface Science Communications*, Vol. 48, (2022), 100616. <https://doi.org/10.1016/j.colcom.2022.100616>
97. Azari, R., Rezaie, H. R., Khavandi, A., "Investigation of functionally graded HA-TiO₂ coating on Ti-6Al-4V substrate fabricated by sol-gel method", *Ceramics International*, Vol. 45, No. 14, (2019), 17545-17555. <https://doi.org/10.1016/j.ceramint.2019.05.317>
98. Tahmasebi, M., Hajisafari, M., "Investigation of Microstructure and Corrosion Resistance of HA/TiO₂ Coating Fabricated by Sol-Gel Method", *Iranian Journal of Surface Science and Engineering*, Vol. 16, No. 44, (2020), 1-14. http://www.surfacejournal.ir/article_44919_3ff72d6693316b44ba406f5fee21389a.pdf
99. Mehrvarz, A., Ghazanfar-Ahari, Y., Khalil-Allafi, J., Mahdavi, S., Etmannfar, M., "The microstructural features and corrosion behavior of Hydroxyapatite/ZnO nanocomposite electrodeposit on NiTi alloy: Effect of current density", *Ceramics International*, Vol. 48, No. 2, (2022), 2191-2202. <https://doi.org/10.1016/j.ceramint.2021.09.311>
100. Geuli, O., Lewinsein, I., Mandler, D., "Composition-tailoring of ZnO-hydroxyapatite nanocomposite as bioactive and antibacterial coating", *ACS Applied Nano Materials*, Vol. 2, No. 5, (2019), 2946-2957. <https://doi.org/10.1021/acsanm.9b00369>
101. Ananth, K. P., Sun, J., Bai, J., "An innovative approach to manganese-substituted hydroxyapatite coating on zinc oxide-coated 316L SS for implant application", *International Journal of Molecular Sciences*, Vol. 19, No. 8, (2018), 2340. <https://doi.org/10.3390/ijms19082340>
102. Bansal, P., Singh, G., Sidhu, H. S., "Investigation of surface properties and corrosion behavior of plasma sprayed HA/ZnO coatings prepared on AZ31 Mg alloy", *Surface and Coatings Technology*, Vol. 401, (2020), 126241. <https://doi.org/10.1016/j.surfcoat.2020.126241>
103. Nabipour, M., Rasouli, S., Gardeshzadeh, A. R., "Preparation of nanohydroxyapatite-carbon nanotube composite coatings on 316L stainless steel using electrophoretic deposition", *Progress in Color, Colorants and Coatings*, Vol. 5, No. 1, (2012), 47-53. https://pccc.icrc.ac.ir/article_77113.html
104. Manso, M., Jimenez, C., Morant, C., Herrero, P., Martinez-Duart, J. M., "Electrodeposition of hydroxyapatite coatings in basic conditions", *Biomaterials*, Vol. 21, No. 17, (2000), 1755-1761. [https://doi.org/10.1016/S0142-9612\(00\)00061-2](https://doi.org/10.1016/S0142-9612(00)00061-2)
105. Sadat-Shojai, M., Khorasani, M. T., Dinpanah-Khoshdargi, E., Jamshidi, A., "Synthesis methods for nanosized hydroxyapatite with diverse structures", *Acta Biomaterialia*, Vol. 9, No. 8, (2013), 7591-7621. <https://doi.org/10.1016/j.actbio.2013.04.012>
106. Fathi, M. H., Hanifi, A., Mortazavi, V., "Preparation and bioactivity evaluation of bone-like hydroxyapatite nanopowder", *Journal of Materials Processing Technology*, Vol. 202, No. 1-3, (2008), 536-542. <https://doi.org/10.1016/j.jmatprotec.2007.10.004>
107. Wang, H., *Hydroxyapatite Degradation and Biocompatibility*, Doctoral dissertation, The Ohio State University, (2004). https://etd.ohiolink.edu/apexprod/rws_etd/send_file/send?accession=osu1087238429&disposition=inline
108. Sharma, C., Dinda, A. K., Potdar, P. D., Chou, C. F., Mishra, N. C., "Fabrication and characterization of novel nano-biocomposite scaffold of chitosan-gelatin-alginate-hydroxyapatite for bone tissue engineering", *Materials Science and Engineering: C*, Vol. 64, (2016), 416-427. <https://doi.org/10.1016/j.msec.2016.03.060>
109. Lee, J. S., Baek, S. D., Venkatesan, J., Bhatnagar, I., Chang, H. K., Kim, H. T., Kim, S. K., "In vivo study of chitosan-natural nano hydroxyapatite scaffolds for bone tissue regeneration", *International Journal of Biological Macromolecules*, Vol. 67, (2014), 360-366. <https://doi.org/10.1016/j.ijbiomac.2014.03.053>
110. Kwok, C. T., Wong, P. K., Cheng, F. T., Man, H. C., "Characterization and corrosion behavior of hydroxyapatite coatings on Ti6Al4V fabricated by electrophoretic deposition", *Applied Surface Science*, Vol. 255, No. 13-14, (2009), 6736-6744. <https://doi.org/10.1016/j.apsusc.2009.02.086>
111. Khor, E., Lim, L. Y., "Implantable applications of chitin and chitosan", *Biomaterials*, Vol. 24, No. 13, (2003), 2339-2349. [https://doi.org/10.1016/S0142-9612\(03\)00026-7](https://doi.org/10.1016/S0142-9612(03)00026-7)
112. Ragetly, G., Griffon, D. J., Chung, Y. S., "The effect of type II collagen coating of chitosan fibrous scaffolds on mesenchymal stem cell adhesion and chondrogenesis", *Acta Biomaterialia*, Vol. 6, No. 10, (2010), 3988-3997. <https://doi.org/10.1016/j.actbio.2010.05.016>
113. Kumar, M. N. R., "A review of chitin and chitosan applications", *Reactive and Functional Polymers*, Vol. 46, No. 1, (2000), 1-27. [https://doi.org/10.1016/S1381-5148\(00\)00038-9](https://doi.org/10.1016/S1381-5148(00)00038-9)



Materials and Energy Research Center

MERC

Contents lists available at [ACERP](#)

Advanced Ceramics Progress

Journal Homepage: www.acerp.ir

Advanced Ceramics Progress

Original Research Article

Investigation of the Impact of Graphene Nanostructure on the Mechanical Properties of Tires Compounds

Kazem Jeddi ^a, Farhad Sattari ^{b,*}, Seyede Zahra Mortazavi ^c, Soghra Mirershadi ^d^a MSc, Department of Physics, Faculty of Sciences, University of Mohaghegh Ardabili, Ardabil, Ardabil, Iran^b Associate Professor, Department of Physics, Faculty of Sciences, University of Mohaghegh Ardabili, Ardabil, Ardabil, Iran^c Associate Professor, Department of Physics, Faculty of Sciences, Imam Khomeini International University, Qazvin, Qazvin, Iran^d Associate Professor, Department of Engineering Sciences, Faculty of Advanced Technologies, University of Mohaghegh Ardabili, Namin, Ardabil, Iran* Corresponding Author Email: f_sattari@uma.ac.ir (F. Sattari)URL: https://www.acerp.ir/article_161861.html

ARTICLE INFO

ABSTRACT

Article History:

Received 14 November 2022
 Received in revised form 21 November 2022
 Accepted 29 November 2022

Keywords:

Graphene
 Tensile Strength
 Rubber Compound
 Stress and Strain

Numerous researchers have shown interest in the new technique of adding various nanoparticles to elastic materials in an attempt to improve their properties. Physical qualities such as wear resistance, strength, thermal properties, tear limit, and elastic fracture were improved as a result of the atomic scale bonds between the nanoparticles and elastic compounds. These characteristics will in turn lead to high-quality and market-friendly products that can compete in international markets. According to the literature, various nanoscale materials including graphene, calcium carbonate (CaCO₃) nanoparticles, aluminum nanoparticles, diamond nanoparticles, nanoclays, and zinc oxide nanoparticles have been widely used in the rubber industry. Development of significant CaCO₃ nanoparticle structures has continued to date. Carbon nanotubes are another type of nanoscale that can be employed in the rubber industry. In this paper, the effect of graphene on the mechanical properties of rubber compounds was studied due to the significance of incorporation of graphene into the composites, especially into the rubber compounds. The obtained results demonstrated that mechanical properties including tensile strength, wear resistance, and elongation percentage could be easily enhanced by adding graphene to rubber materials. The authors hope that these enhanced compounds will be applicable to the industrial production.


<https://doi.org/10.30501/acp.2022.369482.1111>

1. INTRODUCTION

The tire industry manufactures a wide variety of tires, including various sized riding tires, motorcycle tires, truck tires, tractor tires, and bicycle tires. Tire tread, grooves, ridges, layers, tire collars, etc. are the basic parts of a tire. Each part of the tire (rubber) is manufactured for a particular purpose with unique properties. In recent

years, the characteristics of tires have been significantly improved by adding various nanoparticle combinations. Due to the atomic-scale bonds that exist between the nanoparticles and elastic compounds, the presence of nanoparticles not only enhances the physical properties of the rubber compounds but also increases their wear resistance, strength (improves mechanical properties), thermal properties, and tear and fracture limits [1-3].

Please cite this article as: Jeddi, K., Sattari F., Mortazavi S. Z., Mirershadi, S., "Investigation of the Impact of Graphene Nanostructure on the Mechanical Properties of Tires Compounds", *Advanced Ceramics Progress*, Vol. 8, No. 4, (2022), 42-47. <https://doi.org/10.30501/acp.2022.369482.1111>

2423-7485/© 2022 The Author(s). Published by MERC.

This is an open access article under the CC BY license (<https://creativecommons.org/licenses/by/4.0/>).

These factors come together to produce a high-quality marketable product that can compete on international markets. Numerous nanometer materials such as calcium carbonate (CaCO_3) nanoparticles, calcium oxide nanoparticles, alumina nanoparticles, diamond nanoparticles, nanoclays, and fullerenes have reportedly found widespread applications in the rubber industry. However, according to the literature, CaCO_3 nanoparticles have recently gained in popularity [4]. Due to the atomic-scale bonds that exist between the nanoparticles and elastic compounds, the presence of nanoparticles enhances the physical properties of rubber compounds. Carbon nanotubes and graphene are two more significant nanostructures that can be used in the rubber industry. In the following, some of the characteristics of graphene will be examined.

Pure carbon and graphene atoms are arranged in a regular hexagonal structure, much like graphite but with one-atom thickness, to form graphene. Graphene, one of the carbon allotropes, has a single-sheet structure composed of atoms joined together by strong bonds to form a honeycomb-like crystal network. Graphene is the thinnest, yet strongest, known material discovered so far [5-9]. In this structure, the carbon-carbon bond is 1.42 Å long. One square meter plate of graphene weighs just 0.77 g, making it a lightweight substance. A graphite sheet or crystal is formed of several graphene sheets that are bonded together and are arranged on top of one another at the distance of 3.35 Å. Theoretical physicist Philip Wallace first investigated the theory of graphene in 1947. He made attempts to comprehend the complex electrical characteristics of the three-dimensional graphite at a time when graphene had not yet been given a name. The term graphene, first coined in 1962 by Hans-Peter Boehm, is a combination of the words graphite and its suffix. They employed a transmission electron microscope to examine the single-layer carbon plates; however, graphene had not been yet produced until the 21st century when Professor Andre Geim and Konstantin Novoselov in cooperation with their research group from the University of Manchester succeeded in separating single layers of graphene using adhesive tape in 2004 and won the Nobel Prize in Physics in 2010. The Massachusetts Institute of Technology selected graphene as one of the top ten technologies owing to its unique features and the extensive studies conducted on it. Additionally, a scientific journal named it the top-notch scientific achievement of 2009. Graphene is currently the thinnest yet most resistant material in the world. Although it is highly transparent due to its thinness, the smallest gas atom, helium, cannot pass through it due to its high density [10-12].

Single-layer, double-layer, and multi-layer graphene have potential applications in different industries. The hardest and thinnest material ever created by humans is called graphene. Its thinness, which is equal to the thickness of a carbon atom, allows light to pass through

it despite its dense structure. Additionally, ease of preparation, conductivity (it is even more conductive than copper), and capacity of graphene to transmit heat and electricity make it a new option to be used in optical screens and computer components. This substance is even harder than diamond with considerable resistance to pressure that causes a disintegration 200 to 300 times greater than that of steel. Owing to its highly desirable lightness and flexibility, graphene is described as a super material which is expected to bring about a revolution in the electronics sector in the future [13]. One of the characteristics that distinguishes graphene from other materials and makes it particularly effective as a reinforcing component in composites is its impressive mechanical properties. The stability of the Sp^2 bonds that make up the hexagonal network and resist all types of in-plane deformations are other outstanding mechanical characteristics of graphene [14-16].

2. MATERIALS AND METHODS

A variety of techniques have been employed so far to analyze the investigated graphene including Scanning Electron Microscopy (SEM), Diffusion Reflectance Spectroscopy (DRS), and X-Ray Diffraction (XRD), to name a few, and to evaluate the properties of the crystal structure and determine the network parameters. The following procedure was considered to create the principal compound of 980 KN (2 kg) in a laboratory tank with a nominal capacity of 2.5 liters using a combination of rubber, carbon black, chemicals, oil, and other materials (Table 1). A ram used for pressurization and consist mixing was employed in conjunction with a laboratory mixer with a volume of 5.2 liters that was made by Samak Iran. The ram is pneumatically operated that works at the pressure of 5 bar. The task of pressurizer is to provide uniform mixing in the mixer chamber. The chemicals, oil, and soot are loaded into the hopper after being weighed and then, the feed door located above the hopper is utilized to feed the materials. The rubbers are poured into the funnel in the first step. Chemicals, carbon, and oil are introduced to the funnel once the temperature reaches 100 °C, with the exception of the chemical curing agents. The temperature serves as the decisive factor of the test. Once the compound was thoroughly mixed and the temperature reached 140 °C, KN compound was discharged until the compound age (rest) time was passed.

Once the compound reached its age period, the curing chemical agents were added. Since there was not enough graphene in the lab, 100 g of the initial compound was used. A relatively small laboratory mill was utilized because it was unable to produce 100 g of the chemical in a 2.5-liter beaker. Then, KN compound was softened on the mill as the working technique. Then, in accordance with the instructions given in Table 2, graphene was

added to the compound in varying amounts (in the first step, 0.5 g of graphene), and the mixture was thoroughly mixed on a mill (two mills). Next, the curing agents were added to the nano compound, and after 24 hours of aging

time, 70 g of the nano compound was baked in a special mold in a laboratory baking press for 30 minutes at the temperature of 155 °C.

TABLE 1. Quantities of chemicals required to produce master batch compound or KN

Trade name of chemical substances	Chemical name	The amount of substances (g)	The amount of substances (wt. %)
SBR1500	Butadiene Starene Rubber	377.2	12.041
PBR1220	Poly Butadiene Rubber	506.5	6.592
SBR1712	Oily Rubber Butadiene Styrene	474.7	15.153
CARBONN375	Carbon	718.4	22.932
AROMATIC OIL	Aromatic oil	188.5	6.017
ZNO	Zinc Oxide	359.2	11.466
IPPD Antioxidant	N-Diparaphenylene isopropyl amine	269.4	8.600
STEARIC ACID	Stearic acid	359.2	11.466
TMQ Antioxidant	Polymerized 2,2,4-Trimethyl – 1,2- Dihydroquinoline	269.4	5.733

TABLE 2. The fraction of chemicals required to produce the final composition of graphene

Baking Factors and Graphene	Weight of chemical compounds, Graphene			
Master Batch (MB)	98.665	98.181	97.701	96.756
CBS Accelerator	0.632	0.629	0.626	0.620
Sulfur	0.637	0.634	0.631	0.625
PVI Anti scorch	0.065	0.065	0.064	0.064
Graphene	0	0.491	0.977	1.935

Following the compound baking step, four samples were created using a punch machine in the shape of dumbbell-shaped strips so that the tests could be performed on the strips. The tensile, wear, and hardness tests are considered the necessary mechanical testing.

3. RESULTS AND DISCUSSION

The XRD method was employed to characterize the synthesized graphene and examine the crystal structure properties and establish their lattice parameters. Figure 1 displays the X-ray diffraction spectrum of the synthetic graphene.

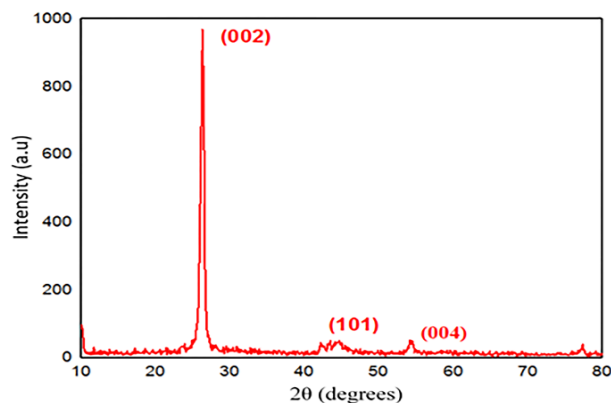


Figure 1. Graphene's X-ray diffraction spectrum

According to the data analysis, the peaks that appear at the angles of 26.3, 43.5, and 54.3 degrees, respectively, refer to the plates with the Miller indices (002), (101), and (004). The observed results, which are consistent with the findings supported by reliable scientific journals, demonstrate that a graphene structure with a lattice constant of 3.34 Å has formed [17–18].

Figure 2 depicts the images captured from the surface of the created graphene samples at different magnifications by scanning electron microscopy that helps examine the surface morphology of the graphene thin layer sample and confirm the creation of graphene nanosheets. As observed in the images, the surface of the created graphene is quite wide, and the folds and bends suggest that the graphene is single-layered.

The energy gap of the graphene nanosheets was calculated using the diffusion reflection method. As a result, to determine the energy gap, first, diffuse reflection spectroscopy, capable of measuring the powder samples, was used to determine the reflection spectrum in terms of the wavelength of light.

In the diffusion reflectance spectroscopy, the spectrophotometer measures the intensity of the light reflected from the sample and compares it with the that of the light reflected from the surface of the reference sample.

The spectrum in Figure 3 depicts the transition of electrons from the valence band to the conduction band as a result of incident photon energy, the cause of light intensity at the relevant wavelength to drop. In other

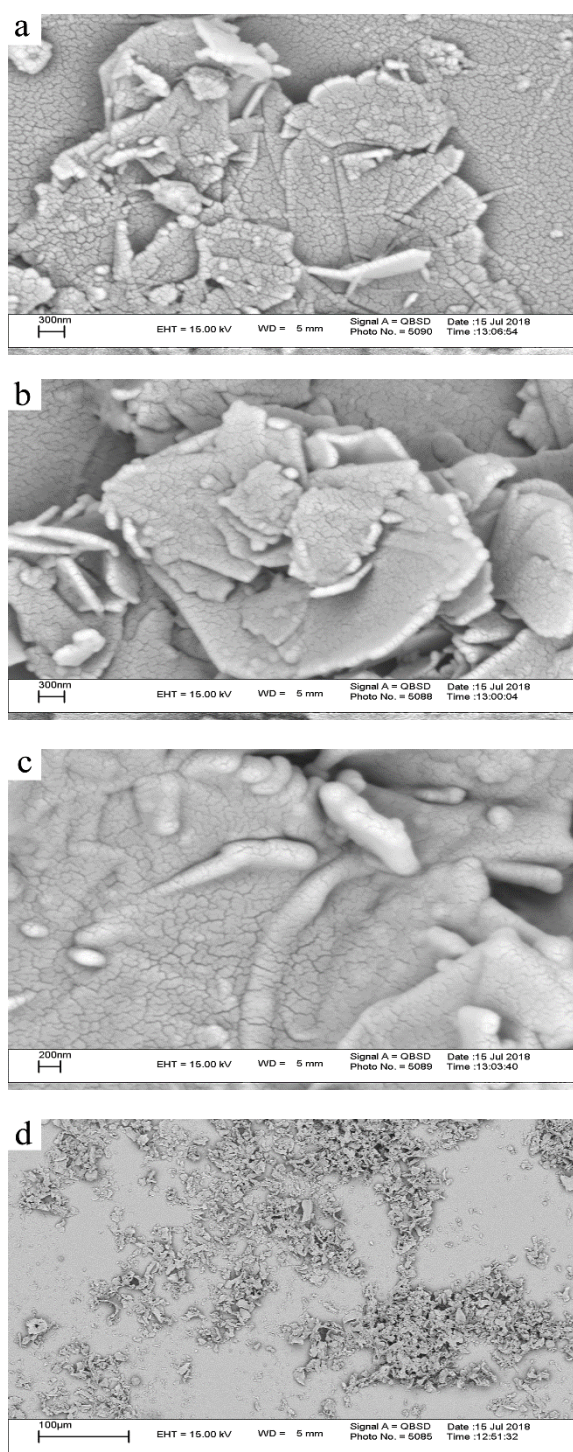


Figure 2. Scanning electron microscope images of graphene nanoparticles magnified by 300 nm in (a), 300 nm in (b), 200 nm in (c), and 100 micrometers in (d)

words, there is a decrease in the ratio of the transmitted to the reflected light. As shown in the graphene sample, the amount of light reflection decreased with a decrease in the wavelength of the incident photon from 500 nm to 320 nm.

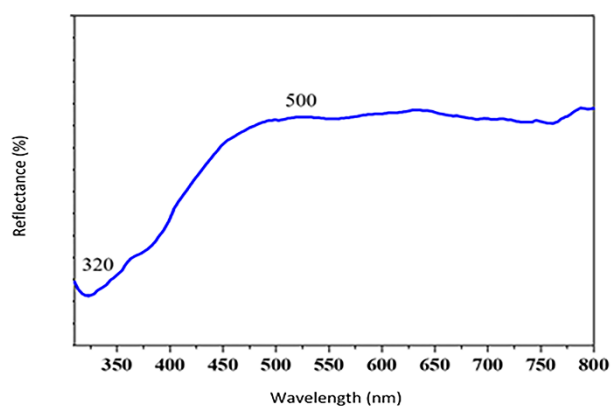


Figure 3. The graphene nanostructure's reflection spectrum as a function of the light's incident wavelength

Graphene thin layer energy gap was calculated using Mott and Davis's theory, where the $(\alpha h\nu)^2$ curve was drawn in terms of photon energy ($h\nu$). To be specific, the reflection coefficient $R(\lambda)$ is considered to derive the absorption coefficient $\alpha(\nu) = (1 - R)^2 / 2R$, and the energy gap was then simply calculated by drawing a tangent line on the linear portion of the graph produced from $(\alpha h\nu)^2$ in terms of energy [19]. Based on Figure 4, the energy gap for this two-dimensional structure was calculated as approximately 0.8 eV by drawing the tangent line on the graph in the linear region.

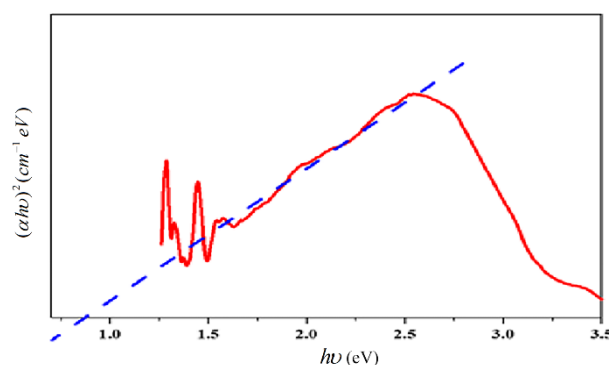


Figure 4. The curve of changes of $(\alpha h\nu)^2$ in the two-dimensional graphene nanostructure in terms of photon energy ($h\nu$)

Following that, the impact of graphene on the mechanical characteristics of the compound was examined in terms of its tensile strength, tearing force, and elongation. This examination in turn had a positive impact on the compound, as shown in Figure 5.

Particularly, an increase in the length, tearing force, and tensile strength were all greatly improved by graphene, which accounts for 1.935 wt. % of the material. As the graphene weight increased, the tear force roughly increased proportionally. In diagram (a) attributed to the compound without graphene, the sample is subjected to

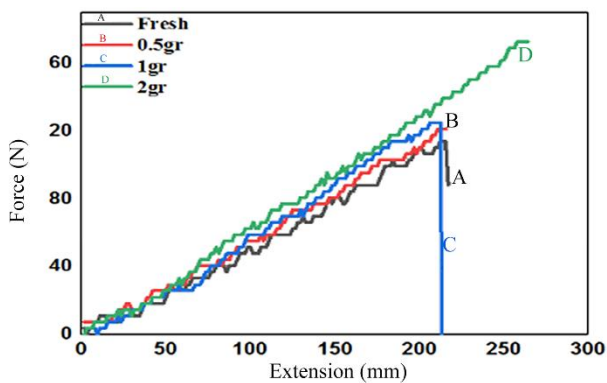


Figure 5. Compound tension diagram with different amounts of graphene in terms of force-tension

the maximum force of 114 N; in other words, the force imposed at the point of rupture was 114 N, and the displacement was 215.54 mm. In addition, the values of stress, strain, and length increase were obtained as 11.4 MPa, 7.18 dimensionless, and 718 %, respectively. Diagram (b) shows a compound containing 0.491 % graphene by weight and the relevant applied force, displacement or stretching, stress, strain, and length increase. In this diagram, the values of the applied force, displacement or stretching, stress, strain, and length increase were obtained as 121.4 N, 215.56 mm, 12.14 MPa, 7.18, and 718.53 %, respectively.

The applied force in diagram (c), which represents the compound containing 0.977 % by weight of graphene, is 125.1 N, and the values of displacement or stretching, tension, strain, length increase, and modulus are 212.46 mm, 12.51 MPa, 7.08, 708 %, and 1.69 N/mm², respectively. In diagram (d), the values of the applied force, displacement, stress, strain, elongation, and modulus in the compound containing 1.935 g of graphene were obtained as 172.9 N, 264.06 mm, 17.29 MPa, 8.88, 880.2 %, and 1.96 N/mm², respectively. The obtained results are presented in Table 3.

TABLE 3. The values obtained from the graph of compound tension with different amounts of graphene in terms of weight percentage

Graphene in weight (%)	0	0.491	0.977	1.935
Force (N)	114.0	121.4	125.1	172.9
Tensile (mm)	215.5	215.5	212.4	264.1
Tension (MPa)	11.4	12.1	12.5	17.2
Strain	7.2	7.2	7.1	8.8
Increased length (%)	718.04	718.5	708.0	880.2
Modulus (MPa)	1.5	1.6	1.7	1.9

The A SHORE equipment from Bareiss, Germany, was used to conduct the hardness test, the results of which are given in the following. The reference sample, containing no graphene, yielded 62 ShoreA. In addition, 2, 1, and 0.5 g of graphene yielded ShoreA64.5, ShoreA65, and

ShoreA64, respectively, in the samples constructed at various levels of graphene presence.

The wear test was completed in two minutes using a wear instrument developed by Bareiss in Germany. The results for the rubber compound containing the nanographene substance are reported in Table 4, and the wear test samples are displayed in Figure 6. The wear test result for graphene with the weight percentages of 0.491 and 0.977 is 80 %, while that for the graphene with the weight percentage of 1.935 is 65 %. Finally, for the reference sample, which is our initial compound without graphene, the result is 145 %

TABLE 4. The degree of wear in compounds with a graphene weight fraction

The amount of Graphene in compound	The amount of wear (%)
Without nano	145
0.491	80
0.977	80
1.935	65



Figure 6. Examples of baked mixtures for a hardness test

4. CONCLUSION

The current research aims to examine the impact of graphene nanostructure on the elastic compounds, and a summary of the obtained results will be given in the following. The tensile strength, tearing force, and elongation were examined to determine the impact of graphene on the mechanical properties of the compound, and the results showed that graphene had a positive impact on the compound, which was also confirmed in the relevant diagram. Particularly, an increase in the length, tearing force, and tensile strength were all greatly intensified by the presence of graphene, especially the one with the weight percentage of 1.935 %. As graphene weight increased, the tear force was proportionally raised. In the reference compound that contained no graphene, the greatest force imposed on the sample, the amount of force applied at the moment of rupture, was 114 N, and displacement was 215.54 mm. In addition, the values of stress, strain, and length increase were obtained as 11.4 MPa, 7.18 without dimension, and 718 %, respectively. The displacement or amount of tension in the compound with the weight percentage of 0.491 was measured as 215.56 mm, applied force as 121.4 N, stress

as 12.14 MPa, strain as 7.18, and length increase as 718.53 %. The modulus of the compound with the weight percentage of 0.977 was 1.76 N/mm². The values of the applied force, displacement or amount of tension, stress, strain, was and length increase were measured as 125.1 N, 212.46 mm, 12.51 MPa, 7.08, and 708 %, respectively. In the compound with an applied force of 172.9 N and the displacement or tension of 264.06 mm, the stress value of was obtained as 17.29 MPa, strain as 8.88, length increase as 880.2 %, and modulus as 1.96 N/mm², respectively. The results from wear and hardness tests showed that the strength of the elastic compound could be greatly enhanced by adding graphene nanostructure.

ACKNOWLEDGEMENTS

The authors would like to express their gratitude to the management and personnel of the Artaville Tire Ardabil factory for their cooperation and assistance.

REFERENCES

- Wang, W., Wang, S., Ma, X., Gong, J., "Recent advances in catalytic hydrogenation of carbon dioxide", *Chemical Society Reviews*, Vol. 40, No. 7, (2011), 3703-3727. <https://doi.org/10.1039/C1CS15008A>
- Yan, L., Wang, J., Han, X., Ren, Y., Liu, Q., Li, F., "Enhanced microwave absorption of Fe nanoflakes after coating with SiO₂ nanoshell", *Nanotechnology*, Vol. 21, No. 9, (2010), 095708. <https://doi.org/10.1088/0957-4484/21/9/095708>
- Lehman, K., "Reviews of science for science Librarians: Graphene", *Science & Technology Libraries*, Vol. 30, No. 2, (2011), 132-142. <https://doi.org/10.1080/0194262X.2011.575628>
- Shao, H. Q., Wei, H., He, J. H., "Dynamic properties and tire performances of composites filled with carbon nanotubes", *Rubber Chemistry and Technology*, Vol. 91, No. 3, (2018), 609-620. <https://doi.org/10.5254/ret.18.82599>
- Novoselov, K. S., Geim, A. K., Morozov, S. V., Jiang, D., Katsnelson, M. I., Grigorieva, I. V., Dubonos, S. V., Firsov, A. A., "Two-dimensional gas of massless Dirac fermions in graphene", *Nature*, Vol. 438, No. 7065, (2005), 197-200. <https://doi.org/10.1038/nature04233>
- Sawangphruk, M., Srimuk, P., Chiochan, P., Sangsri, T., Siwayaprahm, P., "Synthesis and antifungal activity of reduced graphene oxide nanosheets", *Carbon*, Vol. 50, No. 14, (2012), 5156-5161. <https://doi.org/10.1016/j.carbon.2012.06.056>
- Meyer, J. C., Geim, A. K., Katsnelson, M. I., Novoselov, K. S., Oberfell, D., Roth, S., Girit, C., Zettl, A., "On the roughness of single- and bi-layer graphene membranes", *Solid State Communications*, Vol. 143, No. 1-2, (2007), 101-109. <https://doi.org/10.1016/j.ssc.2007.02.047>
- Raadi, Z., Rahimi, A., Ghanbari, H., Sarpoolaky, H., "2D Materials; Introduction, Classifications, Properties, and Applications", *Journal of Advanced Materials and Technologies*, Vol. 10, No. 4, (2022), 37-75. <https://doi.org/10.30501/jamt.2021.260205.1145>
- Moniri Javadhesari, S., Jabraili, M., Koohi, M., "A Review on the Application of Nanoparticles for Targeted Gene Delivery", *Advanced Ceramics Progress*, Vol. 8, No. 1, (2022), 44-55. <https://doi.org/10.30501/acp.2022.345741.1091>
- Selvam, J. D. R., Smart, D. R., Dinaharan, I., "Microstructure and some mechanical properties of fly ash particulate reinforced AA6061 aluminum alloy composites prepared by compositing", *Materials and Design*, Vol. 49, (2013), 28-34. <https://doi.org/10.1016/j.matdes.2013.01.053>
- Reyhani, A., Mortazavi, S. Z., NozadGolikand, A., Moshfegh, A. Z., Mirershadi, S., "The effect of various acids treatment on the purification and electrochemical hydrogen storage of multi-walled carbon nanotubes", *Journal of Power Sources*, Vol. 183, No. 2, (2008), 539-543. <https://doi.org/10.1016/j.jpowsour.2008.05.039>
- Liu, W. W., Xia, B. Y., Wang, X. X., Wang, J. N., "Exfoliation and dispersion of graphene in ethanol-water mixtures", *Frontiers of Materials Science*, Vol. 6, (2012), 176-182. <https://doi.org/10.1007/s11706-012-0166-4>
- Ibrahim, K. S., "Carbon nanotubes-properties and applications: a review", *Carbon Letters*, Vol. 14, No. 3, (2013), 131-144. <http://doi.org/10.5714/CL.2013.14.3.131>
- Dresselhaus, M. S., Lin, Y. M., Rabin, O., Jorio, A., Souza Filho, A. G., Pimenta, M. A., Saito, R., Samsonidze, G., Dresselhaus, G., "Nanowires and nanotubes", *Materials Science and Engineering: C*, Vol. 23, No. 1-2, (2003), 129-140. [https://doi.org/10.1016/S0928-4931\(02\)00240-0](https://doi.org/10.1016/S0928-4931(02)00240-0)
- Sheshmani, S., Ashori, A., Fashapoyeh, M. A., "Wood plastic composite using graphene nanoplatelets", *International Journal of Biological Macromolecules*, Vol. 58, (2013), 1-6. <https://doi.org/10.1016/j.ijbiomac.2013.03.047>
- Papageorgiou, D. G., Kinloch, I. A. Young, R. J., "Mechanical properties of graphene and graphene-based nanocomposites", *Progress in Materials Science*, Vol. 90, (2017), 75-127. <https://doi.org/10.1016/j.pmatsci.2017.07.004>
- Mirershadi, S., Mortazavi, S. Z., Reyhani, A., Moniri, N., Novinrooz, A. J., "Effective condition for purification of multi-walled carbon nanotubes by nitric acid", *Synthesis and Reactivity in Inorganic, Metal-Organic, and Nano-Metal Chemistry*, Vol. 39, No. 6, (2009), 312-316. <https://doi.org/10.1080/15533170902858104>
- Vozmediano, M. A., "Renormalization group aspects of graphene", *Philosophical Transactions of the Royal Society A : Mathematical, Physical and Engineering Sciences*, Vol. 369, No. 1946, (2011), 2625-2642. <https://doi.org/10.1098/rsta.2010.0383>
- Novoselov, K. S., Geim, A. K., Morozov, S. V., Jiang, D., Katsnelson, M. I., Grigorieva, I. V., Dubonos, S., Firsov, A. A., "Two-dimensional gas of massless Dirac fermions in graphene", *Nature*, Vol. 438, No. 7065, (2005), 197-200. <https://doi.org/10.1038/nature04233>



Materials and Energy Research Center

MERC

Contents lists available at [ACERP](#)

Advanced Ceramics Progress

Journal Homepage: www.acerp.ir

Advanced Ceramics Progress

Original Research Article

Characterization and Stability Study of Polyurethane / Magnetic Strontium Hexaferrite / Clinoptilolite Nanocomposite

Komeil Azadikhah ^a, Mehran Davallo ^{b,*}, Vahid Kiarostami ^b, Saeid Mortazavi Nik ^c^a PhD Candidate, Department of Chemistry, North Tehran Branch, Islamic Azad University, Tehran, Tehran, Iran^b Associate Professor, Department of Chemistry, North Tehran Branch, Islamic Azad University, Tehran, Tehran, Iran^c Assistant Professor, Department of Chemistry, North Tehran Branch, Islamic Azad University, Tehran, Tehran, Iran* Corresponding Author Email: m_davallo@yahoo.com (M. Davallo)URL: https://www.acerp.ir/article_165206.html

ARTICLE INFO

A B S T R A C T

Article History:

Received 26 November 2022

Received in revised form 16 January 2023

Accepted 18 January 2023

Keywords:

Nanocomposite
 pH_{pzc}
 Chemical Stability
 Thermal Stability
 Surface Characterization

In this research, a new polyurethane / strontium hexaferrite / clinoptilolite (PU/SrM/CLP) nanocomposite was synthesized through the in-situ polymerization method, and its chemical stability in both acidic and alkaline solutions was assessed. It was found that the incorporation of CLP and SrM into the PU matrix would enhance the thermal stability of the nanomaterial. The thermal stability of the composite ingredients against the thermal events up to the temperature of 700 °C in an ascending order includes PU, strontium hexaferrite, and CLP zeolite, respectively. As a result, the formed nanocomposite exhibited more thermal stability than PU. Several analytical techniques such as XRF, XRD, FTIR, SEM-EDX, and BET were employed to characterize the physicochemical properties of the nanocomposite. The presence of FTIR peaks at the wavelengths of 1700 cm⁻¹ and 3400 cm⁻¹ confirms the C=O and N-H groups due to the formation of PU in the composite structure, respectively. The pore volume and specific surface area of the Nano sorbent using BET were obtained as 0.5978 cm³/g and 2.60 m²/g, respectively. Based on the Scherrer equation, the adsorbent crystallite size was measured as 12.76 nm at the highest peak (100 %). In addition, The chemical stability of the prepared nanocomposite was assessed in both acidic and alkaline solutions which showed about a 12 % reduction. The point of zero charge (pH_{pzc}) for nano sorbent was 7.4. According to the obtained results, the PU/SrM/CLP nanocomposite can be utilized as a stable and magnetic sorbent in aqueous harsh media, especially in wastewater samples.

<https://doi.org/10.30501/acp.2023.369331.1112>

1. INTRODUCTION

A composite material is a combination of various constituents which differ in terms of their physical and chemical properties. When these constituents are combined, they produce a material that is tailored to do a specific job.

Owing to the various properties of the composite materials, they are used in different fields such as wastewater treatment, aerospace, automobile, electronics, construction, energy, biomedical, and other industrial applications [1]. Owing to their excellent physical properties and high adaptability to a chemical structure, polyurethanes (PUs) are extensively applied in

Please cite this article as: Azadikhah, K., Davallo, M., Kiarostami, V., Mortazavi Nik, S., "Characterization and Stability Study of Polyurethane / Magnetic Strontium Hexaferrite / Clinoptilolite Nanocomposite", *Advanced Ceramics Progress*, Vol. 8, No. 4, (2022), 48-56. <https://doi.org/10.30501/acp.2023.369331.1112>

2423-7485/© 2022 The Author(s). Published by MERC.

This is an open access article under the CC BY license (<https://creativecommons.org/licenses/by/4.0/>).

different industrial sectors such as coatings, adhesives, fibers, thermoplastic elastomers, and also the production of porous foams. The PUs are generally formed from the reaction of an isocyanate component with polyol [2]. The fragmented PUs are multi-block copolymers-(X-Y)-which are thermodynamically composed of soft (X) and hard (Y) parts, respectively. At high temperatures, the hard part acts as an efficient reinforcement filler, providing the dimensional stability of the PU by creating a bridge connecting the soft part and elastomeric matrix. Due to the thermodynamic differences, the soft and hard parts in hard use conditions (acidic and strong base and hot solutions) are usually separated by forming a cumulative two-phase network [3]. Despite of excellent properties that PUs have, these compounds are characterized by low thermal stability and mechanical strength. To overcome these drawbacks, some fillers such as heat and impact modifiers can be incorporated into the polymer matrix to enhance their properties. To improve the biodegradability properties of the PUs, biocompatible components such as the hydroxyl group of ricin oleic acid and triglycerides with 90 % C18 fatty acid were introduced into the PU chains. Depending on the nature of the diol and isocyanate fractions, a thermoset or thermoplastic PU can be formed. In case a diol (OHR-OH) forms the soft part and a di inosinate (NCOR-NCO) the hard part, a linear thermoplastic PU will be formed. However, if the ratio of polyisocyanate to polyhydroxy segment is relatively high, the formation of a PU thermostat is quite likely [4]. The structure and properties of the PUs, in addition to the choice of raw materials, depending on the polymerization method, degree of phase separation, hydrogen bonding, morphology, and crystallization rate [5]. PU foam is a new type of organic polymeric material with interesting properties such as low thermal conductivity, chemical inertness, high energy adsorption capacity, and good mechanical strength. There are several reports about the addition of filler particles such as silica to PU, which in turn affects the mechanical and physical properties of these polymers.

In addition, the presence of Magnetic Nanoparticles (MNPs) facilitated control of foam structures, increased mechanical and thermal properties, and improved insulation properties due to its high mechanical, thermal, and magnetic properties in PU foams. Nowadays, the synthesis of new magnetic materials and their composition in polymer matrices has drawn many researchers' attention due to their widespread applications in various fields such as carriers to stabilize microorganisms in water and absorb electromagnetic waves. Despite these advantages, magnetic compounds have at least two major limitations: the limited number of functional groups on the surface and their low dispersion in the polymer matrix. To overcome these limitations and prevent the accumulation of particles in the polymer matrix and increase the interaction chance between the

components at the interface, it is suggested that functionalized silages be used for surface modification of the magnetic nanoparticles [6]. Of note, the use of magnetic adsorbents due to their easier separation from the solution with minerals rich in active adsorption sites such as natural zeolite especially Clinoptilolite (CLP) in a polymeric substrate is one of the effective and low-cost methods in dye wastewater treatment [7,8]. The CLP was used in some fields to solve several problems [9-13]. In addition, the application of these mineral particles in harsh conditions such as hot solutions as well as acidic and alkaline environments can change the properties of these minerals and greatly reduce their adsorption properties [14].

In our previous works, several adsorbents including polypyrrole/SrFe₁₂O₁₉/graphene oxide [15,16] carbon nanotubes [17], and copper oxide nanoparticles immobilized on activated carbon [18] were fabricated and their characteristics were investigated. In addition, the fabrication of a new composite of ternary components including PU, CLP, and Strontium hexaferrite (SrM) was synthesized in our research group and then employed to adsorb malachite green dye from aqueous solutions and wastewater [19].

This research is the continuation of the previous project that aims to fully characterize the PU/SrM/CLP nanocomposite. The first objective of this project was to determine the chemical stability of the composite material in harsh media using high and low pH_s. Moreover, it assessed the thermal stability of the nanocomposite and compared it with other composite materials.

2. EXPERIMENTAL PROCEDURE

2.1. Materials and Instruments

The Semnan natural zeolite (CLP) powder (Afrand Touska Company, Isfahan, Iran) used in this work with granulation of less than 100×10^{-6} m was provided by the Ministry of Industries and Mines of the Mineralogy Department (Tehran, Iran) as a gift. In addition, Sr(NO₃)₂.9H₂O, Fe(NO₃)₃.9H₂O, ammonia, citric acid, and other reagents and chemicals with analytical grade were purchased from Merck and Sigma companies. The cationic surfactant of hexadecyl trimethyl ammonium bromide (HDTMA-Br, Merck) with a laboratory grade and purity of 99.99 % (Merck) was provided by the Research Institute of Paint and Coating Science and Technology (Tehran, Iran). The commercial urethane resin (Rokopol RF551, PCC Rokita, Poland) with a viscosity of 4.52 pa.s and average molecular weight of 600 g/mol at 25 °C was also used for the fabrication of rigid PU foams. The 4,4'-Methylene Diphenyl Isocyanate (MDI) hardener with 36 % of NCO groups and a density of 1.57 g/cm³ at 25 °C was obtained from Yantai Wanhua PUs Group Co (China). Malachite Green Standard (MG)

with a density of $1100 \times 10^3 \text{ g/m}^3$ and a percentage purity greater than 99 % at 20 °C was obtained from Sinopharm chemical reagent company (Shanghai, China).

A Nicolet 8700, Thermo FT-IR spectrometer (USA), A DR-5000–Hach UV-Vis spectrometer (USA), a Scanning Electron Microscopy (SEM, (SIGMA VP-500, ZEISS SEM, Germany)), an RHB2, IKA Centrifuge system (Germany), a Q600 Waters thermogravimetric analyzer (USA), an X-Ray Diffractometer (STADI MP, STOE XRD, Germany) were utilized in this experiment.

2.2. Synthesis and Preparation

2.2.1. Synthesis of Strontium Hexaferrite

The SrM was fabricated through the self-ignition process [20]. First, a mixture of strontium and ferric nitrates with a weight ratio of 2:3 was dissolved in deionized water at 60 °C. The complex of strontium and iron ions was prepared using citric acid and metal ions solution. The solution pH was adjusted at 7 by adding 1:1 water-ammonia solution and stirring it at 80 °C to form a viscous brown gel. Then, the prepared brown gel was placed in a furnace and allowed to reach its combustion temperature. The resulting gel caught fire spontaneously to obtain a compound with a tree-like shape. Subsequently, the collected ash sample was pulverized using an agate mortar and calcined at 450 °C for 1.5 h in the muffle furnace (Nabertherm, LT3/11). Finally, the resulting powder was annealed at 900 °C for 1.5 h to produce SrM.

2.2.2. Preparation of Modified Clinoptilolite

Modification of CLP with HDTMABr was carried out, as reported by Jin and coworkers [21]. Briefly, CLP (60 g) was added into the HDTMABr solution (300 mL, 0.4 % (w/v)), and the solution was shaken at 200 rpm for 23 h at 25 °C on the orbital shaker (GFL3005). Then, centrifugation was performed, and the washing steps were carried out on the final material several times with deionized water. Next, the HDTMABr-modified CLP was placed in an air oven (Binder ED53) at 100 °C for 12 h. The dried material was then pulverized in a vibratory ball mill and was screened through a US 120 mesh screen. The final powder was used for the composite fabrication.

2.2.3. Preparation of Composite

The PU/SrM/CLP nanocomposite was prepared by in-situ polymerization of urethan resin [22] in the presence of SrM and CLP particles using Methylene Diphenyl diisocyanate (MDI), as reported in our previous work [19].

2.3. Characterization

X-Ray Fluorescence (XRF) was utilized to determine the elemental composition of the CLP powders before and followed by surface modification. SEM was employed to study the morphology of the samples.

Energy Dispersive X-ray Spectroscopy (EDS) was then used to determine the molar percentage of the elements in the strontium hexaferrite compound. Infrared spectrometers (FT-IR) were subsequently utilized to determine the type of functional groups as well as new bonds formed in the samples. Further, Thermal Gravimetric Analysis (TGA) was used to investigate the thermal behavior of the samples, and X-Ray Diffraction (XRD) analysis to identify the crystal properties of the synthesized nanocomposite. Brunauer-Emmett-Teller (BET) and Langmuir models were developed to study the surface area of the nanocomposite. Brunauer-Joyner-Halenda (BJH) and t-Plot techniques were employed to estimate the pore size distribution, microporous volume, and specific surface area of the nanocomposite, respectively.

2.4. Adsorbent Stability

2.4.1. Thermal Stability

TGA analysis is a method for studying how a substance behaves as a function of temperature. In this work, 5.31 mg of each sample was used and their thermal behavior was evaluated in the temperature range of 25-1350 °C at a rate of 20 °C/min [23,24].

2.4.2. Chemical Stability

The chemical stability of the PU/SrM/CLP composite was studied at both low and high pH values using HCl and NaOH (1 M). First, 0.1 g of the composite was added to 50 ml of NaOH or HCl solution and stored for one week. Then, each sample was filtered and rinsed with double distilled water to achieve a neutral pH. The adsorbent was then dried in an air oven, and its weight losses were recorded during this period. Finally, the adsorption efficiencies of the malachite green dye for the nanocomposite were compared in solutions with and without acid and alkaline [25].

2.5. The pH of Point Zero Charge

The pH of the point of zero charge (pH_{PZC}) was computed for the nanocomposite to identify the pH impacts. First, several aliquots of 50 mL of 0.01 M NaCl solution were prepared, and their pH values were adjusted in the range of 2-12 by adding 0.1 M HCl or 0.1 M NaOH solutions dropwise. Then, 0.1 g of adsorbent was added to each flask containing 50 ml of NaCl solution, whose solution pH values had been previously adjusted, and shaken for six hours in airtight conditions at 200 rpm at 25 °C. The pH values of the solution were recorded before and after adding the composite during the processing period. In the next step, the secondary pH values were plotted against the initial pH values. Finally, the pH_{PZC} was determined from the intersection of the curve (The straight line of initial pH_s) and the line with the slope of 45° (The line of final pH_s) [26].

3. RESULTS AND DISCUSSION

3.1. Acid Washing

Acid washing was performed in a 250 mL flask containing the specific amount of the CLP in 60 min.

Table 1. Elemental composition in clinoptilolite before and after acid washing

Sample Percentage	SiO ₂ %	Al ₂ O ₃ %	Fe ₂ O ₃ %	CaO %	Na ₂ O %	MgO %	K ₂ O %	TiO ₂ %	MnO %	P ₂ O ₅ %	L.O.I. ¹ %
Before Acid Washing	67.191	11.66	1.205	1.999	1.92	1.428	1.524	0.216	0.014	0.022	12.14
After Acid Washing	68.696	11.81	1.337	1.588	1.231	1.343	1.525	0.219	0.014	0.019	12.16

1- Loss of Ignition

3.2. FTIR Spectra

The FT-IR spectra of the SrM at the three-temperature modes including < 450 °C, > 450 °C, and 900 °C are shown in the wavelength range of 500-4000 cm⁻¹. While no peaks of metal-oxygen bonds were formed (Figure 1a) at temperatures below 450 °C, there is no evidence of hexaferrite formation (Figure 1b) at temperatures above 450 °C. The FT-IR spectrum at temperatures above 900 °C has been determined previously in our published paper [19]. Briefly, at the wavelengths of 435 cm⁻¹ and 595 cm⁻¹ confirmed the presence of Fe-O stretching vibrations in octagonal and quadrilateral cavities, respectively, indicating the formation of the M-type SrM hexaferrite compound [20]. The observed peaks at about 3500 and 1400 cm⁻¹ are attributed to the vibrations of the water molecules present in samples [27].

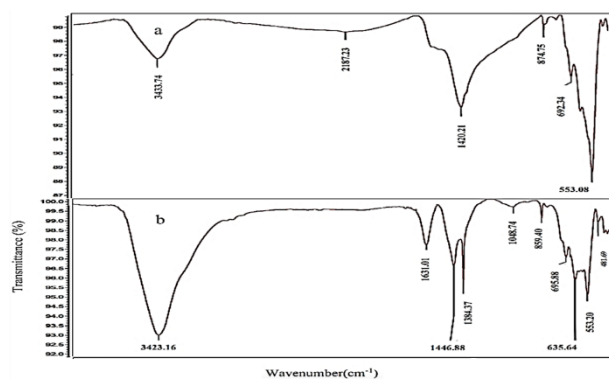


Figure 1. FT-IR spectra of the strontium Hexaferrite at temperatures a) below 450 °C AND b) above 450 °C

The FT-IR spectra of the CLP particles in three states including before acid washing, after acid washing, and after surface modification with HDTMA-Br surfactant are shown in Figure 2. As shown in Figure 2a, the main zeolitic vibrations are located in the ranges of 1069-1077 cm⁻¹ (related to Si-O-Si asymmetric stretching vibration) which can be covered by the stretching vibration of (Al-O-Si) and (Al-O), 603-794 cm⁻¹ and 496-600 cm⁻¹ (related to the stretching vibrations of tetrahedra). The located peak at about 1069 cm⁻¹ is present in all zeolitic

structures and sensitive to the framework Si/Al ratio. The located band at about 3400 cm⁻¹ for CLP corresponds to the bridging OH groups in Al-OH-Si [28]. Followed by acid washing, the presence of peaks of acidic groups is not significantly different from those of pre-acid washing (Figure 2b). However, after the surface modification of the CLP with a surfactant, the presence of the peaks around 1236 cm⁻¹ and 1373 cm⁻¹ represents the C-N groups and symmetric bending vibrations of CH₃ group of HDTMA-Br surfactant, respectively. The intensive peak at 1752 cm⁻¹ is indicative of the stretching vibrational bond of C=O between the surfactant and CLP (Figure 2c) [7].

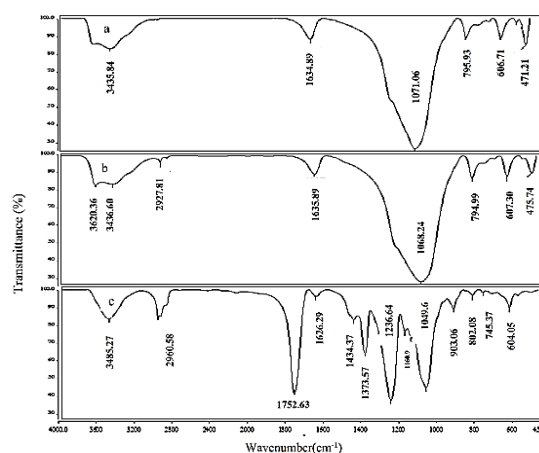


Figure 2. FTIR spectra of clinoptilolite particles in three different states: a) before acid washing, b) after acid washing, and c) after surface modification

3.3. X-Ray Diffraction

The XRD patterns of PU/CLP/SrM composite, SrM, and Modified CLP have been investigated in our published work [19]. Briefly, the presence of PU and hexaferrite reduced the intensity of the XRD peaks of CLP in the nanocomposite. The hexagonal structure of SrM pretreated at a temperature above 900 °C was identified using three characteristic indices (No. 01-080-1198). The characteristic reflection peaks at

about 2θ values of 9.88° , 11.18° , 12.96° , 16.96° , 19.50° , 22.36° , 25.19° , 26.04° , and 30.15° are in good agreement with the CLP crystalline structure data file [JCPDS No. 39–1383] [29]. The peaks at about $2\theta = 24$ and 32 degrees prove the presence of CLP. As observed, the crystallite size depends on different factors such as intensity, peak broadening, sharpness, dislocation density, and strain, which can be calculated through Equation (1) [30].

$$\text{Crystallite Size } (D) = \frac{K\lambda}{\beta \cos \theta} \quad (1)$$

where D is the crystallite size in nm, K is the shape factor which is equal to 0.94, λ the wavelength of X-ray radiation Cu $k_{\alpha 1}$ ($\lambda = 1.5406 \text{ \AA}$), β the Full-Width Half Maximum (FWHM) intensity, and θ the Bragg's angle. The dislocation density (δ), lattice constants (a and c), interplanar spacing (d), and unit cell volume (V) were calculated by Equations (2-4). The calculated values are listed in Table 2.

Based on Equation (1) as well as the indices, we have:

$$\text{Dislocation density } (\delta) = \frac{1}{D^2} \quad (2)$$

$$\text{Inter - planner spacing } \frac{1}{d^2} = \frac{4(h^2+hk+k^2)}{3a^2} + \frac{1}{c^2} \quad (3)$$

$$\text{Volume } (V) = a^2c \quad (4)$$

3.4. SEM Studies

The SEM images of strontium hexaferrite is shown in Figure 3. The SEM image of the pretreated SrM below 450°C indicates an almost uniform distribution of the SrM particles (Figure 3a). Upon increasing the temperature up to above 450°C , the size of the particles will decrease with a relatively more uniform dispersion of nanoparticles (Figure 3b). The SEM images of PU/SrM/CLP nanocomposite has been shown in our published paper [19]. Briefly, increasing the temperature up to above 900°C , the morphology of nanoparticles generally changed to more irregular shapes, and the size of the SrM nanoparticles reduced to below 100 nanometers. The SrM nanoparticles were aggregated because of the magnetic interaction [31].

3.5. The Surface Characterization

The surface characteristics were compared with those of other methods such as Langmuir, T-Plot, and BJH isotherms, each having specific parameters. The surface characteristics of the synthesized nano sorbent per gram unit such as pore volume and specific surface area according to the Langmuir method were $1.198 \text{ (cm}^3\text{g}^{-1}\text{)}$ and $5.21 \text{ (m}^2\text{g}^{-1}\text{)}$, respectively, which is more satisfactory compared to other methods and adsorbents (Figure 4, Table 3) [32].

Table 2. The obtained crystallographic parameters for strontium hexaferrite crystals

Rel. Int. (%)	2θ (degree)	(hkl)	FWHM Left [2 θ] β (degree)	d – Spacing [\AA]	Crystallite Size D ($\times 10^{-9}\text{m}$)	Dislocation Density $\delta \times 10^{-3}$	Unit Cell Volume [\AA^3]
42.57	28.1719	203	0.2666	2.412	5.583	31.169	2.49
65.90	30.4004	110	0.2362	2.94	6.515	42.44	
76.67	32.4399	107	0.1476	2.75	10.212	104.284	
100	34.1528	114	0.1181	2.62	12.76	162.817	

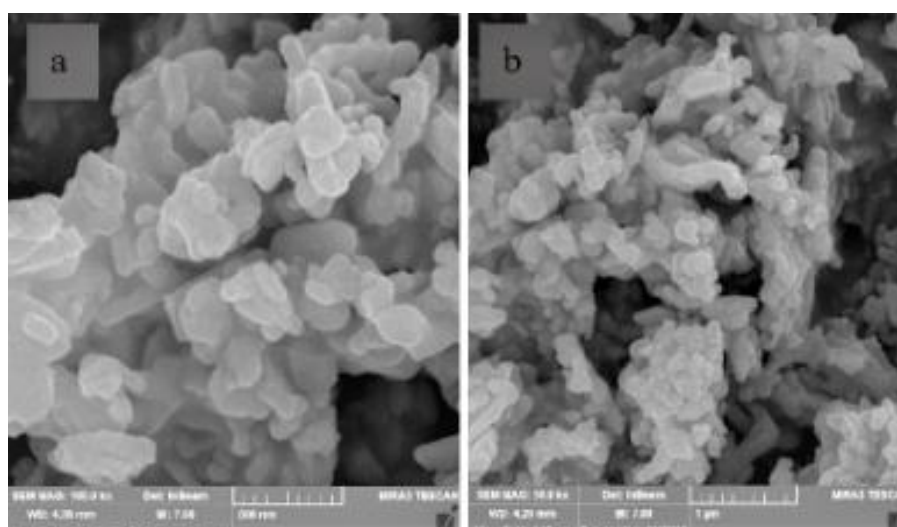


Figure 3. The SEM images of SrM nanoparticles for two conditions including a) below 450°C and b) above 450°C

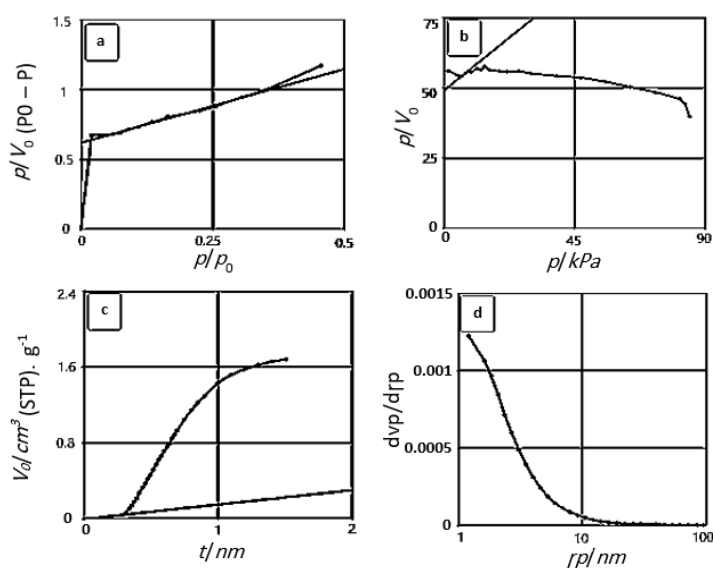


Figure 4. The plots of surface characterization methods include a) BET, b) Langmuir, c) T-Plot, and d) BJH

Table 3. Comparison of the surface parameters of the fabricated nanocomposite with other adsorbents

Samples	Measurement Methods	Surface Features					Ref.
		Pore Volume (cm ³ g ⁻¹)	Special Surface Area (m ² g ⁻¹)	BET Constant (C)	The Average Diameter of the Cavities (×10 ⁻⁹ m)	Hole Radius (×10 ⁻⁹ m)	
PU/SrM/CLP	Langmuir	1.198	5.21	-	-	-	This work
	T-Plot	-	0.237	-	-	-	
	BET	0.5978	2.60	2.69	4.908	-	
	BJH	0.0039	2.93	-	-	1.21	
Pristine Zeolite	Langmuir	1.12	4.9	-	-	-	[23]
CLP Treated by HCl		0.061	20.24	-	-	-	[24]
SBA-15-oz		1.16	711	-	-	-	[25]
ms-OTMS-oz		0.73	945	-	-	-	

3.6. Estimation of Adsorption Mechanism Based on Isothermal Model

The mechanism of the synthesized nanoparticle adsorption is consistent with isotherm type III, in which the graph is convex relative to the P/P₀ axis (Figure 5).

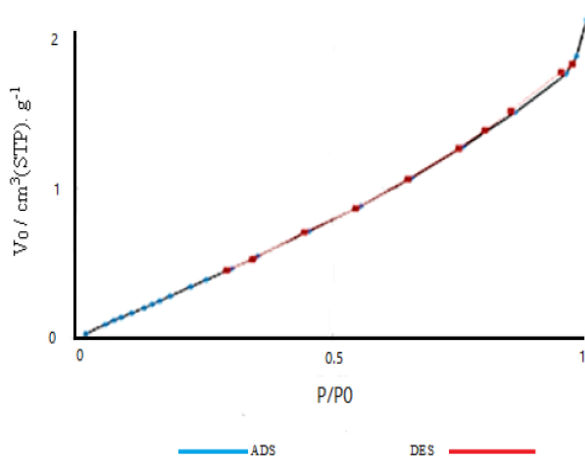


Figure 5. Isothermal Adsorption Diagram of Synthesized Nanocomposite

In this type of adsorption, interactions will occur between the adsorbent molecules in which the adsorption heat is less than the adsorbent heat, indicating that the adsorption process is more interactive between the adsorbent and adsorbed layer than the interaction with the adsorbent surfaces.

This diagram is related to the period when low adsorption occurred on non-porous powders or powders with a diameter greater than the micro size. The swelling point near the end of the adsorption is indicative of the occurrence of adsorption in one layer [32].

3.7. Composite Stability Evaluation

3.7.1. Thermal Stability

The weight loss diagram of the synthesized nanocomposite along with its components versus temperature during the thermal gravimetric method is shown in Figure 6.

The synthesized nanocomposite undergoes a slight weight loss (2 %) during the thermal phenomenon of about 260 °C, which can be attributed to the decomposition of the hard parts of the PU base matrix

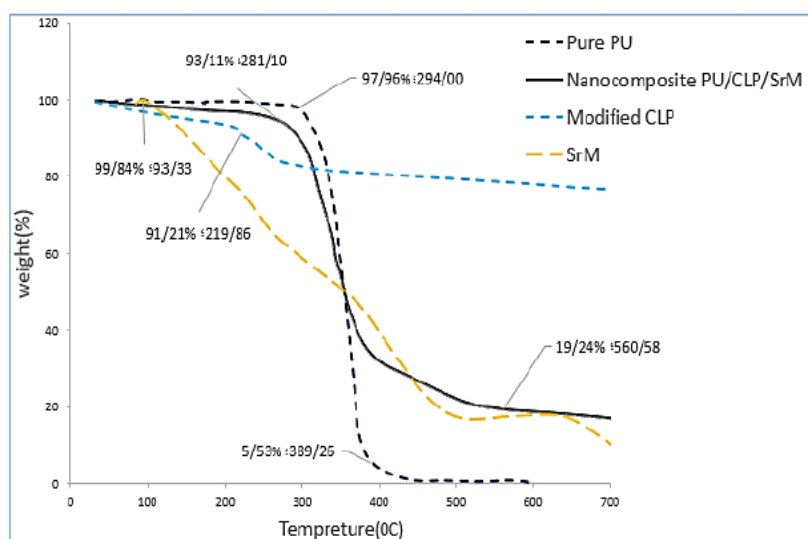


Figure 6. TGA Thermograms of pure PU, Modified CLP, SrM, and PU/SrM/CLP nanocomposite

The greatest weight loss of this nano sorbent (65 %) at the temperature of about 337 °C is due to the removal of the soft parts of the base matrix. This weight loss, however, is less than that of pure PU losing most of its weight (approximately 98 %) at the temperature of 360 °C.

The presence of fillers such as strontium hexaferrite and CLP in the nano sorbent with PU base matrix revealed better thermal stability with less weight loss of 23 % and 18 % at 440 °C and 220 °C, respectively.

The results of the thermal stability of the prepared nanocomposite compared with other adsorbents are shown in Table 4 [31].

Table 4. Thermogravimetric analysis of PU/CLP/SrM nanocomposite in comparison with other adsorbents

Adsorbent	stages (°C)	T max (°C)	Mass Loss (%)	Ref.
Pure PU	I 202 - 351	294	2.04	[28]
	II 351 - 535	389	94.47	
Modified CLP	I 202 - 225	219.86	8.79	[27]
SrM Particle	I 60 - 100	93.33	0.16	[31]
PU/Polyglycerol/Bentonite	-	392	50	[26]
PUR/PSO	I 225 - 300	285	3	[17]
	II 300 - 420	358	53	
PU/CLP/SrM	I 240 - 345	281.10	6.89	This Work
	II 345 - 500	470	80.76	

3.7.2. Chemical Stability

The stability of the PU/SrM/CLP nanocomposite was examined by its immersion in a concentrated HCl and also NaOH solution (1 M) for one week. The

nanocomposite showed a percentage of weight loss, indicating that the nanocomposite was stable enough in harsh environments. Of note, a comparison of the changes in their adsorption efficiency under the standard malachite green dye solution and the composite without harsh environment showed little difference in their performance when exposed to strong acidic and alkaline environments (Table 5) [25].

Table 5. The chemical stability of the PU/SrM/CLP nanocomposite and comparison of the adsorption efficiency of malachite green (MG) dye in harsh environment

Measured Parameter	Exposed to NaOH	Exposed to HCl	Not exposed to Harsh Environment
Weight Loss (%)	10	12	-
Adsorption Efficiency (%)	86	76.67	99.62
Standard Deviation	2.1	1.35	2.87

3.8. The pH of the Point of Zero Charge

The pH_{PZC} for the nanocomposite was determined in the pH range of 2-12. In the presence of adsorbent, the initial pH of 4 was converted to the final pH of 6.2. However, in alkaline media, the initial pH of 12 was converted to the final pH of 10.3 in the presence of an adsorbent (Figure 7), indicating that in an acidic environment, the adsorbent surface had a positive charge, thus electrostatically adsorbing anion samples. Conversely, if the pH value exceeds the pH_{PZC} value, the surface charge will be negative so that the cations can be adsorbed.

As shown in Figure 7, pH_{PZC} is equal to 7.4, obtained from the intersection of the regression line of the final pH values in presence of the nanocomposite and the line with a slope of 45° degrees (The regression line of the initial pH value in absence of the nanocomposite).

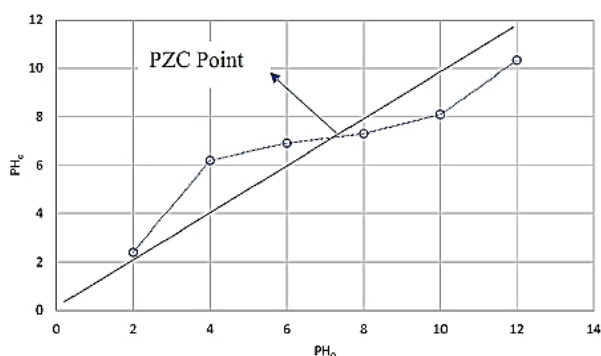


Figure 7. The plot of final pH (pH_f) against the initial pH (pH_0)

To obtain the neutral charge pH point and also find at which point the adsorbent has a neutral charge and tends to change the acidic pH to an alkaline pH, a line between pH 8 and pH 6 with a straight line and slope degree of 45° line was assumed. The line collision with the curve was identified as a point without load or pH_{PZC} equal to 7.4 (Figure 7). At this point, the adsorbent surface charge is zero while at the point above 7.4, the adsorbent tends to remove the positive charge and cationic contaminants. However, at the point below 7.4, the adsorbent tends to remove the negative charge and anionic contaminants [20].

4. CONCLUSION

The thermal analysis showed that the nanocomposite exhibited more thermal stability than polyurethane in the overall temperature range due to its less weight loss percentage. The synthesized nano sorbent mechanism was consistent with isotherm type III, where the diagram was convex relative to the P/P0 axis. This type of adsorption occurred interactively between the adsorbent and the adsorbed layer which was greater than the interaction with the adsorbent surfaces. The point of inflection near the end of the adsorption indicated that the adsorption took place in a single layer. The results obtained from the chemical stability study revealed that the nanocomposite was characterized by suitable thermal stability. In terms of costs, CLP additive as a low-cost natural zeolite is economically viable. Strontium hexaferrite is certainly cost-effective in special applications that require magnetizing the adsorbent and adding proper stability characteristics. Hence, from the results obtained, the PU/SrM/CLP nanocomposite can be utilized as a stable sorbent in aqueous harsh media, especially in wastewater samples.

ACKNOWLEDGMENTS

The authors acknowledge Chemistry Faculty, North

Tehran Branch, Islamic Azad University for their support of this research.

”

REFERENCES

1. Chung, D. D. L., *Composite Materials: Science and Applications*, 2nd ed., Springer Science & Business Media, London, (2010). <https://doi.org/10.1007/978-1-84882-831-5>
2. Alaa, M. A., Yusoh, K., Hasany, S. F., “Pure polyurethane and castor oil based polyurethane: synthesis and characterization”, *Journal of Mechanical Engineering and Sciences*, Vol. 8, (2015), 1507-1515. <http://doi.org/10.15282/jmes.8.2015.25.014>
3. Lan, P. N., Corneillie, S., Schacht, E., Davies, M., Shard, A., “Synthesis and characterization of segmented polyurethanes based on amphiphilic polyether diols”, *Biomaterials*, Vol. 17, No. 23, (1996), 2273-2280. [https://doi.org/10.1016/0142-9612\(96\)00056-7](https://doi.org/10.1016/0142-9612(96)00056-7)
4. Emrani, J., Benrashid, R., Mohtarami, S., Fini, E. H., Abu-Lebdeh, T., “Synthesis and characterization of bio-based polyurethane polymers”, *American Journal of Engineering and Applied Sciences*, Vol. 11, No. 4, (2018), 1298-1309. <https://doi.org/10.3844/ajeassp.2018.1298.1309>
5. Jiang, L., Ren, Z., Zhao, W., Liu, W., Liu, H., Zhu, C., “Synthesis and structure/properties characterizations of four polyurethane model hard segments”, *Royal Society Open Science*, Vol. 5, No. 7, (2018), 180536. <https://doi.org/10.1098/rsos.180536>
6. Nikje, M. M. A., Akbar, R., Ghavidel, R., Vakili, M., “Preparation and characterization of magnetic rigid polyurethane foam reinforced with dipodal silane iron oxide nanoparticles $Fe_3O_4@APTS/GPTS$ ”, *Cellular Polymer*, Vol. 34, No. 3, (2015), 137-156. <https://doi.org/10.1177/026248931503400302>
7. Ebrahimi, R., Maleki, A., Shahmoradi, B., Rezaee, R., Daraei, H., Safari, M., Zandsalimi, Y., Bahmani, P., Harkaranahalli Puttaiah, S., “Organic dye removal from aqueous media by using acid modified Clinoptilolite”, *Journal of Advances in Environmental Health Research*, Vol. 6, No. 2, (2018), 118-127. <https://doi.org/10.22102/jaehr.2018.132980.1080>
8. Armağan, B., Özdemir, O., Turan, M., Celik, M. S., “The removal of reactive azo dyes by natural and modified zeolites”, *Journal of Chemical Technology & Biotechnology: International Research in Process, Environmental & Clean Technology*, Vol. 78, No. 7, (2003), 725-732. <https://doi.org/10.1002/jctb.844>
9. Pourtaheri, A., Nezamzadeh-Ejehieh, A., “Enhancement in photocatalytic activity of NiO by supporting onto an Iranian clinoptilolite nano-particles of aqueous solution of cefuroxime pharmaceutical capsule”, *Spectrochimica Acta Part A: Molecular and Biomolecular Spectroscopy*, Vol. 137, (2015), 338-344. <https://doi.org/10.1016/j.saa.2014.08.058>
10. Nezamzadeh-Ejehieh, A., Tavakoli-Ghinani, S., “Effect of a nano-sized natural clinoptilolite modified by the hexadecyltrimethyl ammonium surfactant on cephalixin drug delivery”, *Comptes Rendus Chimie*, Vol. 17, No. 1, (2014), 49-61. <https://doi.org/10.1016/j.crci.2013.07.009>
11. Sharifian, S., Nezamzadeh-Ejehieh, A., “Modification of carbon paste electrode with Fe (III)-clinoptilolite nano-particles for simultaneous voltammetric determination of acetaminophen and ascorbic acid”, *Materials Science and Engineering: C*, Vol. 58, (2016), 510-520. <https://doi.org/10.1016/j.msec.2015.08.071>
12. Nezamzadeh-Ejehieh, A., Afshari, E., “Modification of a PVC-membrane electrode by surfactant modified clinoptilolite zeolite towards potentiometric determination of sulfide”, *Microporous and Mesoporous Materials*, Vol. 153, (2012), 267-274. <https://doi.org/10.1016/j.micromeso.2011.12.054>
13. Tamiji, T., Nezamzadeh-Ejehieh, A., “Sensitive voltammetric determination of bromate by using ion-exchange property of a Sn (II)-clinoptilolite-modified carbon paste electrode”, *Journal of Solid State Electrochemistry*, Vol. 23, No. 1, (2019), 143-157. <https://doi.org/10.1007/s10008-018-4119-4>

14. Heard, C. J., Grajciar, L., Uhlík, F., Shamzhy, M., Opanasenko, M., Čejka, J., Nachtigall, P., “Zeolite (in) stability under aqueous or steaming conditions”, *Advanced Materials*, Vol. 32, No. 44, (2020), 2003264. <https://doi.org/10.1002/adma.202003264>
15. Ebrahimipour, S., Kiarostami, V., Khosravi, M., Davallo, M., Ghaedi, A., “Bees metaheuristic algorithm with the aid of artificial neural networks for optimization of acid red 27 dye adsorption onto novel polypyrrole/SrFe₁₂O₁₉/graphene oxide nanocomposite”, *Polymer Bulletin*, Vol. 76, (2019), 6529-6553. <https://doi.org/10.1007/s00289-019-02700-7>
16. Ebrahimipour, S., Kiarostami, V., Khosravi, M., Davallo, M., Ghaedi, A., “Optimization of tartrazine adsorption onto polypyrrole/SrFe₁₂O₁₉/graphene oxide nanocomposite using central composite design and bat-inspired algorithm with the aid of artificial neural networks”, *Fibers and Polymers*, Vol. 22, (2021), 159-170. <https://doi.org/10.1007/s12221-021-8163-9>
17. Vafaei, A., Ghaedi, A. M., Avazzadeh, Z., Kiarostami, V., Agarwal, S., Gupta, V. K., “Removal of hydrochlorothiazide from molecular liquids using carbon nanotubes: Radial basis function neural network modeling and culture algorithm optimization”, *Journal of Molecular Liquids*, Vol. 324, (2021), 114766. <https://doi.org/10.1016/j.molliq.2020.114766>
18. Ghaedi, A. M., Karamipour, S., Vafaei, A., Baneshi, M. M., Kiarostami, V., “Optimization and modeling of simultaneous ultrasound-assisted adsorption of ternary dyes using copper oxide nanoparticles immobilized on activated carbon using response surface methodology and artificial neural network”, *Ultrasonics Sonochemistry*, Vol. 5, (2019), 264-280. <https://doi.org/10.1016/j.ultsonch.2018.10.007>
19. Azadikhah, K., Davallo, M., Kiarostami, V., Mortazavinik, S., “Modeling of malachite green adsorption onto novel polyurethane/SrFe₁₂O₁₉/clinoptilolite nanocomposite using response surface methodology and biogeography-based optimization-assisted multilayer neural network”, *Environmental Science and Pollution Research*, Vol. 29, No. 24, (2022), 36040-36056. <https://doi.org/10.1007/s11356-021-18249-w>
20. Masoudpanah, S. M., Ebrahimi, S. S., “Synthesis and characterization of nanostructured strontium hexaferrite thin films by the sol-gel method”, *Journal of Magnetism and Magnetic Materials*, Vol. 324, No. 14, (2012), 2239-2244. <https://doi.org/10.1016/j.jmmm.2012.02.109>
21. Jin, X., Yu, B., Chen, Z., Arocena, J. M., Thring, R. W., “Adsorption of Orange II dye in aqueous solution onto surfactant-coated zeolite: Characterization, kinetic and thermodynamic studies”, *Journal of Colloid and Interface Science*, Vol. 435, (2014), 15-20. <https://doi.org/10.1016/j.jcis.2014.08.011>
22. Peng, H. K., Wang, X. X., Li, T. T., Huang, S. Y., Lin, Q., Shiu, B. C., Lou, C. W., Lin, J. H., “Effects of hydrotalcite on rigid polyurethane foam composites containing a fire retarding agent: compressive stress, combustion resistance, sound adsorption, and electromagnetic shielding effectiveness”, *RSC Advances*, Vol. 8, No. 58, (2018), 33542-33550. <https://doi.org/10.1039/C8RA06361C>
23. Filip, D., Macocinschi, D., “Thermogravimetric analysis of polyurethane – polysulfone blends”, *Polymer International*, Vol. 51, No. 8, (2002), 699-706. <https://doi.org/10.1002/pi.972>
24. Filip, D., Macocinschi, D., Vlad, S., “Thermogravimetric study for polyurethane materials for biomedical applications”, *Composites Part B: Engineering*, Vol. 42, No. 6, (2011), 1474-1479. <https://doi.org/10.1016/j.compositesb.2011.04.050>
25. Talley, K., Alexov, E., “On the pH-optimum of activity and stability of proteins”, *Proteins: Structure, Function, and Bioinformatics*, Vol. 78, No. 12, (2010), 2699-2706. <https://doi.org/10.1002/prot.22786>
26. Fiol, N., Villaescusa, I., “Determination of sorbent point zero charge: usefulness in sorption studies”, *Environmental Chemistry Letters*, Vol. 7, (2009), 79-84. <https://doi.org/10.1007/s10311-008-0139-0>
27. Iazdani, F., Nezamzadeh-Ejhieh, A., “FeO-Clinoptilolite nanoparticles: Brief characterization and its photocatalytic kinetics towards 2,4-dichloroaniline”, *Chemical Physics*, Vol. 550, (2021), 111305. <https://doi.org/10.1016/j.chemphys.2021.111305>
28. Nezamzadeh-Ejhieh, A., Shirzadi, A., “Enhancement of the photocatalytic activity of Ferrous Oxide by doping onto the nanoclinoptilolite particles towards photodegradation of tetracycline”, *Chemosphere*, Vol. 107, (2014), 136-144. <https://doi.org/10.1016/j.chemosphere.2014.02.015>
29. Manikandan, B., Murali, K. R., John, R., “Optical, Morphological and Microstructural Investigation of TiO₂ nanoparticles for Photocatalytic application”, *Iranian Journal of Catalysis*, Vol. 11, No. 1, (2021), 1-11. https://ijc.shahreza.iau.ir/article_680810.html
30. Samandari, M., Taghva Manesh, A., Hosseini, S. A., Mansouri, S., “Process Optimization and Kinetic study of Wet Peroxide Oxidation of Phenol in Wastewater over Mg-Al Nano Mixed Oxide”, *Iranian Journal of Catalysis*, Vol. 11, No. 2, (2021), 175-180. https://ijc.shahreza.iau.ir/article_682697.html
31. Trovati, G., Sanches, E. A., Neto, S. C., Mascarenhas, Y. P., Chierice, G. O., “Characterization of polyurethane resins by FTIR, TGA, and XRD”, *Journal of Applied Polymer Science*, Vol. 115, No. 1, (2010), 263-268. <https://doi.org/10.1002/app.31096>
32. Bardestani, R., Patience, G. S., Kaliaguine, S., “Experimental methods in chemical engineering: specific surface area and pore size distribution measurements-BET, BJH, and DFT”, *The Canadian Journal of Chemical Engineering*, Vol. 97, No. 11, (2019), 2781-2791. <https://doi.org/10.1002/cjce.23632>

AIMS AND SCOPE

Advanced Ceramics Progress (ACERP) as an ISC international journal is devoted to elucidating the fundamental aspects of chemistry and physics occurring at a wide range of oxide and nonoxide ceramics and composite materials and their processing, microstructure, properties, and applications. The journal provides a unique venue for publishing new exciting research, focusing on dynamic growth areas in this field.

INSTRUCTIONS FOR AUTHORS

Submission of manuscript represents that it has neither been published nor submitted for publication elsewhere and is result of research carried out by author(s).

Authors are required to include a list describing all the symbols and abbreviations in the manuscript. Use of the international system of measurement units is mandatory.

- On-line submission of manuscripts results in faster publication process and is recommended. Instructions are given in the ACERP web site: www.acerp.ir
- References should be numbered in brackets and appear in sequence through the text. List of references should be given at the end of the manuscript.
- Figures' captions are to be indicated under the illustrations. They should sufficiently explain the figures.
- Illustrations should appear in their appropriate places in the text.
- Tables and diagrams should be submitted in a form suitable for reproduction.
- Photographs and figures should be of high quality saved as jpg files (resolution > 600 dpi).
- Tables, illustrations, figures and diagrams will be normally printed in single column width (8 cm). Exceptionally large ones may be printed across two columns (17 cm).

PAGE CHARGES AND REPRINTS

ACERP subscribers do not need to make any payment for publication and reprints.

AUTHORS CHECKLIST

- Author(s), bio-data including academic degree, affiliation(s), ORCID(s), and e-mail addresses.
- Manuscript including title, abstract, key words, illustrations, tables with tables' captions, figures with figures' captions, acknowledgement, and list of references.
- MS Word files of the manuscript in the ACERP template and all figures (resolution > 600 dpi).
- Similarity check of the manuscript, copyright forms, and conflict of interest forms

Advanced Ceramics Progress,
P.O. Box 31787-316, Meshkin Dasht, Alborz, I. R. Iran
Materials and Energy Research Center, Imam Khomeini Blvd, Meshkin Dasht, Alborz, I. R. of Iran
P.O. Box 14155-4777, Tehran, I. R. Iran
No. 5, Ahuramazda St., Alvand Ave., Argentine Sq., Tehran, I. R. of Iran

Advanced Ceramics Progress

Volume 8, Number 4, Autumn 2022

CONTENTS

Solmaz Moniri Javadhesari Mohaddeseh Koochi Masoud Jabraili	Nanomaterials: Applications in Regeneration of Damaged Tissues	1-14
Nazli Aharipour Ali Nemati Adrine Malek Khachatourian	Green Synthesis of Silica Extracted from Rice Husk Ash	15-20
Behnaz Hamrahi Benyamin Yarmand Abouzar Massoudi	Tailoring Bioactivity and Corrosion Properties of Plasma Electrolytic Oxidized Titanium Using GO-Silane Particles	21-31
Behnam Doudkanlouy Milan Hurieh Mohammadzadeh Robabeh Jafari Mohammad Soltani	Investigation of the Coating Methods and Types of Coatings Containing Hydroxyapatite for Applications in Tissue Engineering	32-41
Kazem Jeddi Farhad Sattari Seyedeh Zahra Mortazavi Soghra Mirershadi	Investigation of the Impact of Graphene Nanostructure on the Mechanical Properties of Tires Compounds	42-47
Komeil Azadikhah Mehran Davallo Vahid Kiarostami Saeid Mortazavi Nik	Characterization and Stability Study of Polyurethane / Magnetic Strontium Hexaferrite / Clinoptilolite Nanocomposite	48-56



Journal Home Page: www.acerp.ir